Polypropylene/filler nanocomposites by melt compounding and in situ polymerization of propylene with metallocene/MAO catalysts

by

Omar Soltan

Dissertation presented for the degree of Doctor of Philosophy (Polymer Science)

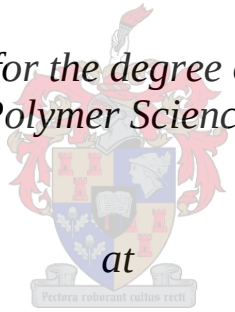

at

Stellenbosch University

Promoter: Prof. A.J. van Reenen

Stellenbosch
December 2010

DECLARATION

By submitting this dissertation electronically, I declare that the entirety of the work contained therein is my own, original work, that I am the owner of the copyright thereof (unless to the extent explicitly otherwise stated) and that I have not previously in its entirety or in part submitted it for obtaining any qualification.

Signature: ..... Date: .....

Abstract

The properties of polymer nanocomposites depend greatly on the chemistry of the polymer matrices, the nature of the nanofillers, and the way in which they are prepared. Understanding the synthesis–structure–property relationship of nanocomposites is vital for the development of advanced polymer nanocomposites with enhanced mechanical strength, stiffness and toughness for structural engineering applications. To this end, the primary aim of this study was to determine the impact that the preparation methods have on the properties of PP/filler nanocomposites, with specific focus on the in situ polymerization of propylene via the methylaluminoxane (MAO) activated metallocene catalyst technique.

Two different fillers (Silica and Calcium carbonate) were used as support for the metallocene catalysts. Different supporting methodologies for the synthesis of the supported catalyst were examined. A C_2 symmetric metallocene catalyst *ansa* dimethylsilylbis(2-methyl benzoindenyl) zirconium dichloride (MBI) was used in this study. The catalyst systems were then evaluated for propylene polymerization.

The early observation shows that a direct adsorption of the metallocene onto the filler has a diminishing effect on the catalyst productivity and the fillers had to be treated with MAO in order to avoid catalyst deactivation by the filler surface. Due to the low productivity of the supported active species, the presence of soluble catalyst active species, besides the supported active species is required in the synthesis of PP nanocomposites via in situ polymerizations.

The syntheses of PP nanocomposites were carried out via in situ polymerization in which different quantities of MAO treated fillers were reacted with pre-activated catalyst solution. The effect of the addition of MAO-filler on the polymerization kinetics and consequently on PP matrix microstructure was investigated. Changes in the in situ polymerization kinetics, compared to kinetics of homogeneous polymerization, were observed. Therefore, the

microstructure of the polymer matrix was also influenced by the presence of nanofillers in the polymerization media.

The influence of the different synthesis methods on the performance of the nanocomposites was investigated using melt-mixed PP/filler nanocomposites obtained using PP homopolymer. The dispersed phase morphologies of the different nanocomposites were investigated by transmission electron microscopy (TEM). Results show that PP nanocomposites with improved filler dispersion were achieved by in situ polymerization compared to melt-mixed nanocomposites.

The influence of the synthesis method on the crystallization behaviour of PP nanocomposites was also investigated. It was found that, for the in situ prepared nanocomposites the tacticity of the PP matrix plays the major role in determining the degree of crystallinity. Results also show that when nanocomposites with comparable PP matrices are compared, the overall crystallization rate of the in situ polymerized nanocomposites is higher than that of the melt mixed nanocomposites.

The mechanical properties of in situ polymerized PP and melt mixed PP nanocomposite were also investigated and compared. Due to improved nanoparticle dispersion in the PP matrix, in situ polymerized nanocomposites show enhanced mechanical properties, especially tensile and impact properties, compared to pure PP and melt mixed prepared nanocomposites when a PP matrix of equivalent microstructure was used.

Finally, the melt compounding method was further investigated using different fillers and commercial PP as a matrix. The effect of filler type, size and applied surface coating on the flow and mechanical properties of PP nanocomposites was studied. The aim of this part of this study is to obtain a good trade-off between the processability and the mechanical properties and to gain insight into the cause of the emergence of different properties for nanocomposites prepared by melt compounding.

Opsomming

Die eienskappe van polimeer nanokomposiete hang grotendeels af van die chemie van die polimeer matriks, die wese van die nano-vullers, en die manier waarop hierdie materiale berei word. Om die sintese-struktuur-eienskap verwantskap te verstaan is noodsaaklik vir die ontwikkeling van gevorderde nanokomposiete met beter meganiese eienskappe, styfheid en taaiheid vir strukturele ingenieurstoepassings Die primêre doelstelling van hierdie studie was dus om die impak van voorbereidingsmetodes op die eienskappe van PP/vuller nanokomposiete te bestudeer, met spesifieke fokus op die in-situ polimerisasie van propileen met metiel alumoksaan-geativeerde metalloseen kataliste.

Twee verskillende vullers (silika en kalsium karbonaat) is gebruik as ondersteuning vir die metalloseen kataliste. Verskillende metodiek is gebruik om die ondersteunde kataliste te berei. ‘n C_2 simmetriese metalloseen katalis ansa-dimetielsiliel(2-metiel bensoindeniel) sirkonium dichloride (MBI) is in die studie gebruik. Die katalissisteme is daarna evalueer vir propileen polimerisasie.

Daar is oorspronklik vasgestel dat direkte adsorpsie van die metalloseen op die vuller ‘n negatiewe effek op die katalis aktiwiteit gehad het, en dat die vuller oppervlak eers met MAO behandel moes word om deaktivering van die katalis deur die vuller-oppervlak te vermy. As gevolg van die lae aktiwiteit van die ondersteunde aktiwe katalisspesies, is die teenwoordigheid van opgeloste aktiewe katalis nodig vir die voorbereiding van PP nanokomposiete via in situ polimerisasie-reaksies.

Die sintese van PP nanokomposiete is uitgevoer deur in –situ polimersiasie waartydens verskillende hoeveelhede MAO-behandelde vullers gereageer is met vooraf-geaktiveerde katalis oplossings. Die effek van die byvoeging van MAO-vuller op die polimerisasie-kinetika en gevolglik op die PP matriks mikrostruktuur is ondersoek. Dit is gevind dat die mikrostruktuur van die polimeer-matriks beinvloed word deur die teenwoordigheid van nanovullers in die polimerisasie-medium.

Die invloed van verskillende bereidingsmetodes op die eienskappe van die nanokomposiete is ondersoek deur smelt-vermengde PP/vuller nanokomposiete te maak. Die dispersie-fase morfologie van verskillende nanokomposiete is ondersoek deur transmissie elektron mikroskopie (TEM). Resultate wys dat PP nanokomposiete met verbeterde vuller-dispersie berkry is deur in situ polimerisasie in vergelyking met die smelt-vermengde materiale.

Die effek van die sintese-metode op die kristallisasie van die PP nanokomposiete is ook ondersoek. Daar is gevind dat, vir die in situ bereide nanokomposiete, die taktisiteit van die PP matriks die grootste rol speel in die bepaling van die persentasie kristalliniteit. Resultate het ook gewys dat, wanneer nanokomposiete met soortgelyke PP matrikse vergelyk word met die in situ nanokomposiete, die laasgenoemde se tempo van kristallisasie hoer is as vir die smelt-vermengde nanokomposiete.

Die meganiese eienskappe van die in situ bereide en smelt-vermengde PP nanokomposiete is ook ondersoek en vergelyk. As gevolg van verbeterde nano-partikel dispersie in die PP matriks, het die in situ bereide nanokomposiete beter meganiese eienskappe openbaar, in vergelyking met die smelt-vermenge nanokomposiete, veral trek- en slagsterkte. .

Laastens is die smelt-vermengings metode verder ondersoek deur gebruik te maak van verskillende vullers en kommersiële PP as matriks. Die effek van die tipe vuller, die grootte en die oppervlakbedekking van die vullerpartikels op die vloei en meganiese eienskappe van die PP nanokomposiete is ondersoek. Die doel van hierdie studie was om ‘n balans te kry tussen prosesseerbaarheid en meganiese eienskappe en om insig te verkry oor die verskille in eienskappe wat openbaar word wanneer smelt-vermengde nanokomposiete bereie word.

“I would like to praise and thank Allah for giving me the strength, health, and opportunity to carry out this study in a proper way”

I dedicate this thesis to my mother and father, for their praying and love, to my wife, my brothers, my sisters and my friend for their support.

ACKNOWLEDGMENTS

I would like to thank Prof. A.J. van Reenen, my study leader, for his advice, guidance and financial support.

I would also like to thank the following people for their contributions to this study: Dr. M.J. Hurndall, for her assistance and advice on the proofreading of this thesis, Dr. G. Harding for HT-GPC analysis, Elsa Malherbe for NMR analysis, Madalen from department of Geology for SEM analysis and Mohamed Jaffer from the University of Cape Town for TEM.

I also would like to express my thanks to all member of our polyolefin's research group at Institute of Polymer science in Stellenbosch University for their friendship, assistance, helpful suggestions.

I would also like to thank the staff, friends and students at Polymer Science for their help.

I would also like to thank the Libyan International Centre of Macromolecular and Material Science for their financial support and giving me the opportunity to study in this field.

TABLE OF CONTENT

List of Figures

List of Tables

List of Schemes

List of Abbreviations

^{13}C NMR	Carbon thirteen nuclear magnetic resonance
CRYSTAF	Crystallization analysis fractionation
DMA	Dynamic mechanical analysis
DSC	Differential scanning calorimetry
$\Delta\Delta E‡$	Difference in activation energy
EDX	Energy dispersive X-ray analysis
FTIR	Fourier transform infrared (spectroscopy)
G	Rate of crystallization
G’	Storage modulus
G’’	Loss modulus
GPC	Gel permeation chromatography
ΔHc	Enthalpy of fusion
HT-GPC	High temperature gel permeation chromatography
i-PP	Isotactic polypropylene
MAO	Methylaluminoxane
MBI	Dimethylsilyl bis(2-methyl-4,5-benzo-indenyl)zirconium dichloride (rac-$Me_2Si(2\text{-}Me\text{-}4,5\text{-}benzoind)_2]ZrCl_2$)
MFI	Melt flow index
MH	Microhardness

mmmm (%)	Isotacticity pentad content
Mn	Number average molecular weight
Mw	Weight average molecular weight
MWD	Molecular weight distribution
NMR	Nuclear magnetic resonance spectroscopy
OM	Polarized optical microscope
PP	Polypropylene
R_p	Polymerization rate
SEM	Scanning electron microscopy
t	Time
T	Temperature
$t_{1/2}$	Half-time of crystallization
Tc	Crystallization temperature
TEM	Transmission electron microscopy
Tg	Glass transition temperature
TGA	Thermogravimetric analysis
Tm	Melting temperature
Tp	Polymerization temperature
UV	Ultraviolet/visible spectroscopy
WAXD	Wide-angle X-ray diffraction
Xc	Relative crystallinity
Xt	Degree of crystallinity

Chapter 1: Introduction and objectives

1.1 Introduction

Polypropylene (PP) is a semicrystalline thermoplastic polymer that has been widely used because of its attractive combination of good processability, mechanical properties, chemical resistance, and low cost. However, owing to its low modulus, high notch sensitivity, and poor impact resistance, especially under extreme conditions such as low temperatures or high strain rates, the usefulness of PP as an engineering thermoplastic is still limited.

Blending PP with rubber is an efficient way to increase its toughness, but one drawback of rubber toughening is the significant loss of both tensile strength and stiffness of PP [1]. Incorporation of particulate mineral fillers, on the other hand, enhances stiffness but reduces the strength and toughness of PP.

The challenge of obtaining an ideal balance between stiffness and toughness has prompted considerable interest. Polymer nanocomposites comprise a new class of materials in which nanoscale particulates are finely dispersed within the matrices. In comparison with neat polymers and microparticulate composites, these materials have been reported to exhibit markedly improved properties [2-5].

The large interfacial area of the nanosized fillers in a polymer nanocomposite helps to influence the properties of the nanocomposite to a great extent, even at rather low filler loading [6]. In order to achieve the optimum properties, it is generally believed that a homogeneous dispersion of the particles in the polymer matrix is a prerequisite. The presence of loosely agglomerated nanoparticles results in failure of the nanocomposites without approaching the desirable properties.

From a practical point of view a homogeneous dispersion of nanoparticles is very difficult to achieve, mainly because nanoparticles with high surface energy agglomerate easily. Thus, polymer nanocomposites are very difficult to make by the use of processing techniques common to conventional plastics because the shear force during compounding is not sufficient to overcome the strong agglomeration tendency of nanoparticles.

Surface modification of these nanoparticles becomes a key issue to break the agglomerated nanoparticles and produce nanostructured composites [7].

Several routes to obtain a homogeneous dispersion of particles in PP matrix are described in the literature. In situ polymerization has been considered to be most effective for the preparation of PP nanocomposites [8].

The interest in the synthesis of PP nanocomposites by in situ polymerization with methylaluminoxane (MAO) activated metallocene catalysts, has primarily been driven by the advances in heterogenization of single-site metallocene catalysts for olefin polymerization.

The in situ polymerization approach should lead to a better dispersion of nanoparticles in the polymer matrix because the active sites are linked directly or adjacent to the surface of the particles.

The catalyst systems and polymerization conditions determine the microstructure of the polymer matrix which, in turn determines the properties of these polymer nanocomposites. Unlike during the melt-compounding method, where the addition of filler may change only the kinetics of nucleation and the crystalline content, during the in situ polymerization the presence of filler particles may affect both the characteristics of the available active sites as well as the polymerization conditions, thus changing the polymerization kinetics, which results in new materials with different microstructures and properties.

The study of the effects of the in situ polymerization approach on the microstructures, and consequently on the properties, of PP nanocomposite is essential. In order to also gain insight into the cause of the emergence of different properties of nanocomposites prepared by different methods (melt-blending and in situ polymerization), a comparative study of the different methods by which to prepare nanocomposites is also considered essential.

This study specifically addresses the effect of the in situ polymerization approach on the microstructures, and consequently on the properties, of PP nanocomposites. A comparative study of the different methods by which to

prepare nanocomposites was also carried out in order to gain insight into the cause of the emergence of different properties of nanocomposites prepared by melt-blending and by in situ polymerization.

1.1 Objectives

The overall objective of this study was to determine the effect of different preparation methods of PP nanocomposites. Specifically, this study addresses the effect of the in situ polymerization approach on the microstructures and consequently on the properties of PP nanocomposites.

In order to accomplish this, the project was divided into a number of individual objectives.

(1) First the evaluation of different fillers as carriers for a metallocene catalyst was investigated. This included the study of their functional groups using Fourier Transform Infrared Spectroscopy (FTIR). The effect that the thermal treatment has on the surface characteristics of the different fillers was also to be investigated.

(2) Different heterogenization methods for supporting the catalyst on the fillers were examined. The different fillers were treated at various temperatures in order to control the concentration of the hydroxyl groups on their surface. The effect of the concentration of hydroxyl groups on the catalyst loading on the fillers surface and subsequently on the supported catalyst performance was investigated. The treatment of the different fillers with MAO was also examined and optimized. Energy dispersive X-ray analysis (EDX) and ultraviolet/visible spectroscopy (UV-Vis) were used to quantify the Al and Zr loading on the filler.

(3) These different catalyst systems were tested in propylene polymerization in order to obtain a suitable supporting method as well as optimize the parameters of this method.

(4) The supported catalyst was then be used for the synthesis of PP nanocomposites. Different polymerization conditions (e.g. initial filler feeds) was used in order to control the final filler load of the in situ polymerized PP

nanocomposites. The effect of the presence of nanofillers on the polymerization kinetics and on the polymer matrix microstructure was investigated. Various analytical techniques, such as high-temperature gel permeation chromatography (HT-GPC), carbon thirteen nuclear magnetic resonance spectroscopy (^{13}C-NMR) and crystallization analysis fractionation (CRYSTAF) were used to study the microstructure of the PP obtained.

(5) PP homopolymers were prepared and used for the preparation of PP nanocomposites via melt-mixing. The dispersed phase morphologies of the different nanocomposites were studied using transmission electron microscopy (TEM) and scanning electron microscopy (SEM).

(6) In conclusion, the crystallization behaviour of the different PP nanocomposites were studied using differential scanning calorimetry (DSC). Wide-angle X-ray diffraction (WAXD) and optical microscopy (OM) wre used to examine the effect of the filler and the synthesis method on the crystal morphology. Thermogravimetric analyses (TGA) was also used to investigate the thermal stability of the various nanocomposites.

(7) The influence of the preparation routes, filler loads, as well as matrix microstructures on the viscoelastic and mechanical properties of the different PP nanocomposites was also investigated utilizing the following mechanical tests: dynamic mechanical analysis (DMA), microhardness (MH), tensile tests and impact tests.

Part of the study was devoted to the preparation and characterization of PP nanocomposites using commercial PP. The influence of the characteristic of the filler on the mechanical properties and processability of the nanocomposites was investigated.

1.2 References

1. Liang, J.; Li, R., *J. Appl. Polym. Sci.*, 2000. **77**: p. 409.
2. Yu, Yiu-Wing Mai.; Zhong-Zhen, *Polymer nanocomposites*. 2006, Boca Raton: Woodhead Publishing Limited.
3. Kawasumi, M.; Hasegawa, N.; Kato, M.; Usuki, A.; Okada, A., *Macromolecules*, 1997. **30**: p. 6333.
4. Yuan, Q.; Misra, R., *Mater. Sci. Technol.*, 2006. **22**: p. 742.
5. Moussaif, N.; Groeninckx, G., *Polymer*, 2003. **44**: p. 7899.
6. Rong, M.; Zhang, M.; Zheng,Y.; Zeng, H.; Friedrich, K., *Polymer*, 2001. **42**: p. 167.
7. Cai, L.; Huang, X.; Rong, M.; Ruan, W.; Zhang, M, *Polymer*, 2006. **47**: p. 7043.
8. Scharlach, K.; Kaminsky, W., *Macromol. Symp.*, 2008. **261**: p. 10.

Chapter 2: Background and literature review

2.1 PP homopolymer

PP is one of the most important commercial polymers. It is a highly versatile polymer with an outstanding combination of low cost and excellent physical properties. It is therefore widely used in various applications, including packaging, houseware, textiles, carpets, artificial turf, and rope. The structure and properties of PP can be tailored to suit specific requirements. Modification of PP can be performed in different ways: during the polymerization [1], by reactor blending [2], compounding [3] or during the processing step.

2.1.1 PP microstructure

The general repeat unit of PP is shown in Figure 2.1. The way in which the monomer inserts into the polymer backbone (primary or secondary and the enantioface selectivity) determines the polymer's regioregularity and stereoregularity, respectively.

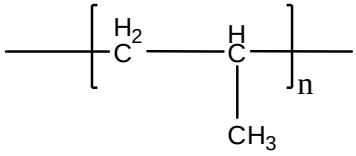

Figure 2.1: General structure of PP.

Depending on the enantioface selectivity three different PP structures can be produced [4].

Isotactic polypropylene (i-PP) results from the head-to-tail or primary addition of propylene monomer units, where the methyl groups always have the same configuration with respect to the polymer backbone (Figure 2.2 A). The first i-PP with high stereoregularity was produced in 1955 by Natta et al. [5]. IR spectroscopy was then the only technique used to determine the degree of isotacticity.

Atactic PP results from head-to-tail addition of monomer units, where the methyl groups have a random configuration with respect to the polymer backbone (Figure 2.2 B).

Syndiotactic PP results from the same head-to-tail addition of monomer units, but where the methyl groups have an alternating configuration with respect to the polymer backbone (Figure 2.2 C).

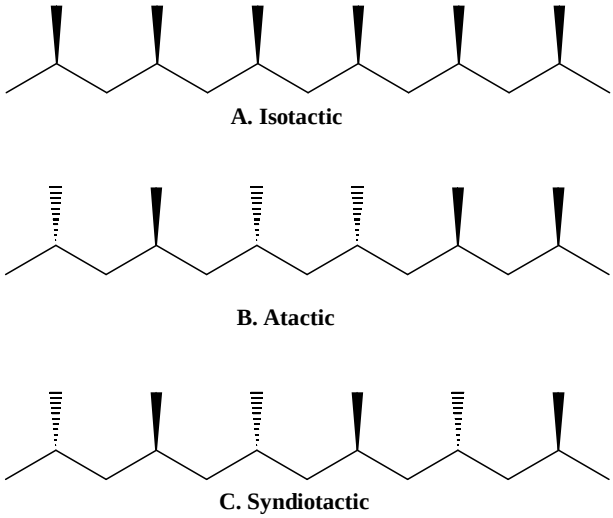

Figure 2.2: The different stereoregularities of PP.

Despite the fact that primary propylene insertion is clearly favoured by electronic factors, isolated secondary propylene units are often detectable in i-PP samples and their presence is the signature of a metallocene catalyst. Tail-to-tail propylene insertion, normally referred to as secondary or 2,1 insertion, occurs in i-PP prepared using isospecific metallocene catalysts with high, but opposite (with respect to primary insertions) enantioface selectivity (Figure 2.3).

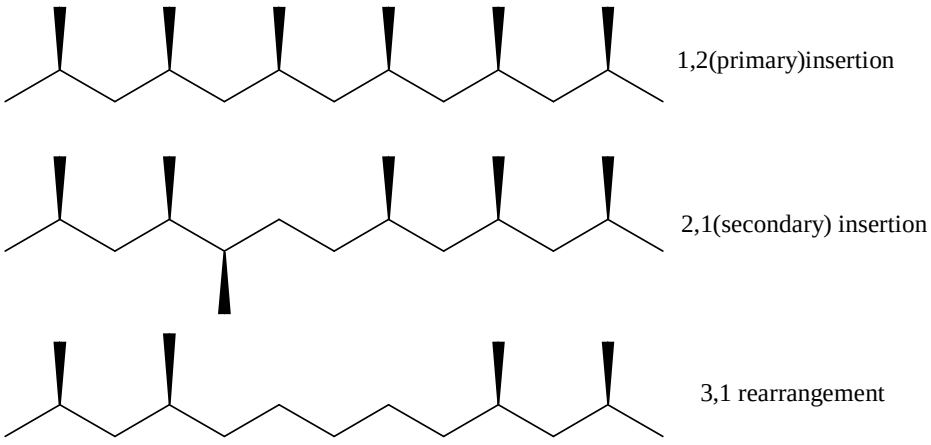

Figure 2.3: Regiochemistry of PP: primary and secondary insertion.

Regiodefects have a strong effect in terms of reducing the crystallinity and melting point of i-PP. There is also a close correlation between catalyst regioselectivity on one hand and catalyst activity and polymer molecular weight on the other, due to the lower monomer insertion rate after 2,1 insertion, and the competing H-transfer to the monomer after a secondary insertion [6, 7].

Two types of regioirregular units are formed in PP chains when metallocene catalysts are used: 2,1 insertions and 3,1 insertions. Rieger et al. [8], Schupfner and Kaminsky [9] and Prosenc and Brintzinger [10] suggest that 3,1 units are formed via isomerization of secondary Zr-alkyl units, resulting from 2,1 monomer insertion to primary Zr-alkyl units before the next monomer insertion [6].

2.1.1.1 ^{13}C NMR analysis

^{13}C NMR spectroscopy is the technique that provides the most information on the stereochemistry and regiochemistry of metallocene and related transition metal catalyzed propylene polymerizations.

A polymer chain is a permanent record of the statistical chain of events that makes up the polymerization process. From the polymer microstructure it is possible to identify the different reaction modes and to measure their relative rates. For instance, the most significant chain transfer reactions occurring in propylene polymerization with metallocene catalysts can be determined by analyzing the polymer end groups [11, 12].

In this respect, ^{13}C NMR has proved to be a most valuable analytical technique, particularly in the field of Ziegler-Natta and related transition metal catalyzed olefin polymerizations [13-18].

The chemical shift of the methyl groups in PP is highly sensitive to the relative stereochemistry of neighbouring monomer units. Each methyl carbon has a different chemical shift depending on the configuration of the adjacent methynes, which up to five on each side (a sequence length of 11 consecutive monomer units). The degree of isotacticity can be given as the pentad, triad,

or diad content (*mmmm*, *mm*, or *m*, respectively). The most commonly quoted stereosequence is at the pentad level, where the methyl resonance is split into nine or ten major peaks, assigned as *mmmm, mmrr, rrrr, mmmr, mmrm, mrrr, rmmr, rmrr, mrrm, rmrm* (see Figure 2.4).

End groups of the polymer chains provide information about the mechanism of termination, chain transfer and polymerization and can be detected using ^{1}H NMR and ^{13}C NMR spectroscopy. ^{13}C NMR analysis also gives information about 2,1 and 3,1 units.

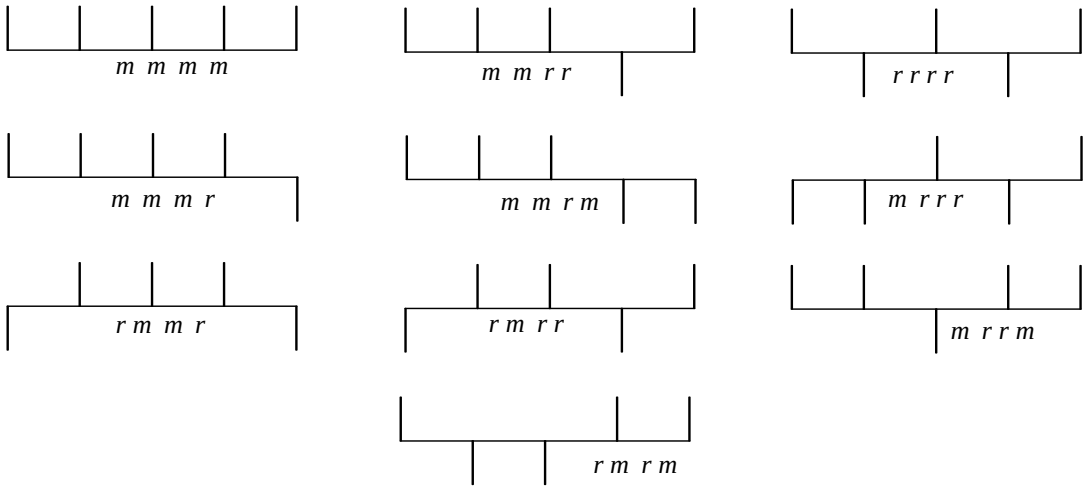

Figure 2.4: Pentad stereosequences in PP.

2.1.2 Crystallinity

Both the crystallization behaviour and crystal form of PP are strongly affected by the configuration (tacticity) and conformational structure of the polymer chain. Isotactic and syndiotactic PP can crystallize. The degree of crystallinity depends on the level of the tacticity of the polymer [19-21]. A 100% isotactic polymer has a crystallinity of 68% [22] and heat of fusion of a 100% crystalline PP is given as 163 J/g or 209 J/g [23]. Atactic PP is considered uncrystallizable, because the chain structure lacks regularity.

As with any semicrystalline polymer, PP shows different crystalline structures at three different levels: chain folding structure (or unit cell), lamellar structures, and spherulitic structures [24].

Isotactic PP can crystallize in three different crystal forms depending on the polymer structure and the crystallization conditions: the α-form with a monoclinic unit cell, the γ-form with an orthorhombic unit cell, and the β-form with a hexagonal unit cell [25-27].

The α-form is predominant in commercial i-PP prepared with traditional Ziegler-Natta catalyst [28, 29], while the γ and β modifications can form under special conditions [30, 31]. The most common method of qualifying the presence of these crystal forms is through the use WAXD analysis.

All of the different crystalline forms are composed of chains in helical conformation, with a common repeat distance 6.5 A^{o}, but differ in unit cell symmetry, and lamellar and spherulitic morphology [32]. For example, the α-form is characterized by its monoclinic unit cell and the coexistence of radial lamellae with tangential lamellae (cross-hatched). The α-phase is the most common crystalline form of i-PP. It is observed for both melt-crystallized and solution-crystallized samples prepared under atmospheric pressure. The pure β-form can be obtained with the aid of nucleating agents. The γ-form can be induced by adding a small quantity of comonomer (e.g. ethylene) or by decreasing the isotactic segment length. The optical clarity of the γ-form is significantly better than that of the α-form. The growth rate of β-form spherulites is up to 70% faster than that of the α-form spherulites [33].

2.1.3 Physical properties

Many PP homopolymer grades with different properties are produced and are commercially available worldwide. These include PP with varying molecular weights or melt flow index (MFI) and tacticities, filled grades, and grades with different levels of stabilization. Properties of various PP homopolymer grades are given in Table 2.1.

Table 2.1: Typical property ranges of commercial i-PP grades [34]

Property	Value
Melt flow index (g/10 min)	0.4 – 35
Density (g/cm^3)	0.90 – 0.91
Tensile strength (MPa)	29 – 39
Elongation at yield (%)	11 – 15
Elongation at break (%)	500 – 900
Young's modulus (MPa)	1000 –1700
Notched IZOD (J/m)	20 –120

In practical application, the polymer molecular weight (Mw) and the molecular weight distribution (MWD) are tailored to give the specific properties with the best processing characteristics for each fabrication process [34].

2.1.4 Relationship between structure, morphology and properties

The mechanical properties of PP are determined by its structures at different stages. The polymer structure is directly related to the catalyst, polymerization, and compounding technologies used in preparation.

Figure 2.5 is a representation of the relationship between structure, morphology, and end-use properties. The microstructure of PP strongly determines the crystallization behaviour and physical properties [35-41]. The crystallization behaviour in turn determines the properties of the final products [42-44].

The figure shows that polymer morphology provides a "bridge" between polymer structure, processing, fabrication history, and end-use properties. Understanding the effect of the structure variables on PP morphology is essential because it is the morphology that most directly determines the polymer properties.

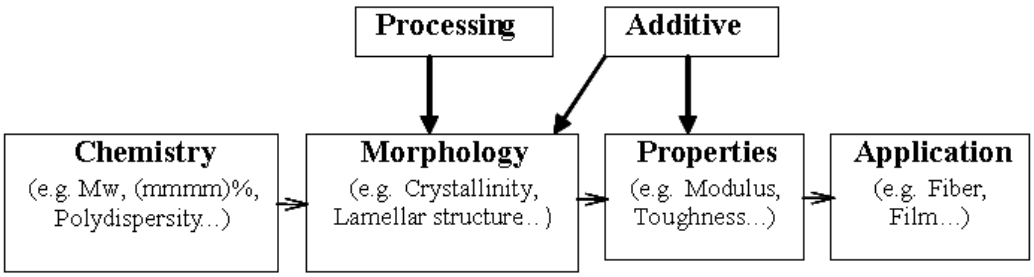

Figure 2.5: Polymer structure, morphology, properties, and end-use relationship of PP.

Depending on the tacticity, PP polymers with different percentages of crystallinity can be obtained. Tacticity, or regularity of the chain, greatly influences higher order levels of morphology, e.g. at the lamellar level and the spherulitic level [45, 46]. The changes on the higher structural levels obviously have an influence on the deformation behaviour. Table 2.2 shows the influence of the degree of crystallinity on various properties [34].

Table 2.2: Effect of crystallinity on PP properties [34]

Property	Increasing crystallinity
flexural modulus	↑
tensile yield strength	↑
elongation at break	↓
Izod impact	↓
hardness	↑

Molecular weight also has a significant impact in determining the morphology and consequently on the thermal and mechanical properties. In general, an increase in Mw strongly enhances the impact properties of the polymer. For example, the brittle-to-ductile transition temperature decreases with increasing Mw [47, 48]. The Mw also influences the maximum obtainable degree of crystallinity. Increasing the Mw of the polymer causes a larger amount of entanglements and amorphous tie chains in the inter-lamellar and inter-spherulitic regions [49]. This leads to enhanced stabilization and extension of a crazed network, resulting in higher toughness [50, 51].

The molecular weight distribution and the intra-chain architecture, which includes comonomer distribution in random copolymers, also play a significant role in determining the end-use of the polymer [45].

Polymer microstructure can be influenced by catalyst structure, polymerization conditions, the technology used for the polymerization, and the type and percentage of the comonomer used (see Figure 2.6).

During the polymerization of propylene monomer any change in the catalyst structure or reduction in catalyst concentration will lead to changes in the structure of the formed polymer.

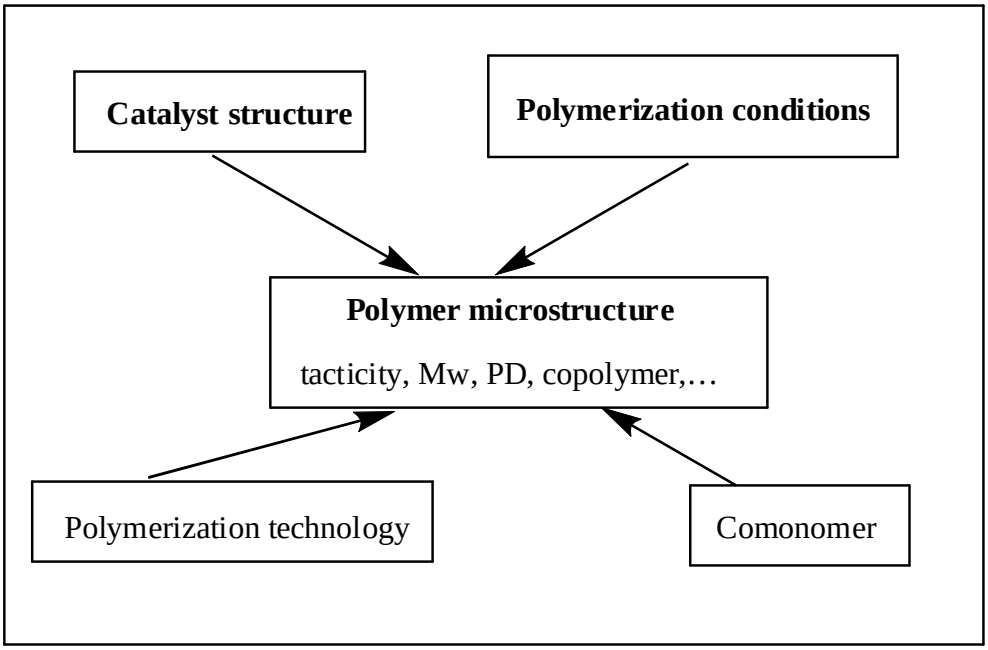

Figure 2.6: Factors that influence the microstructure of PP.

Besides the polymer microstructure, it is worth mentioning that different processing parameters and different types of additives can be used to manipulate the morphology and the final properties of the polymer. For example, injection-moulded i-PP samples display distinct skin-core morphologies as a result of processing [45, 52]. Furthermore, the incorporation of soft or rigid fillers can be used to adjust the morphology, and consequently the properties, of PP.

2.1.5 Filled and reinforced PP

PP containing filler has been widely used in many different applications for many years [53, 54]. Fillers are inert substances added to reduce the polymer cost and/or improve its physical properties (e.g. hardness, stiffness and impact strength) [55, 56]. Commonly used fillers are calcium carbonate, silica, talc, clay, mica, glass fiber and others. Only fillers that are relevant to this study are now discussed.

2.1.5.1 Calcium carbonate

Calcium carbonate is the most widely used inorganic filler. It is available in a variety of particle sizes and treatments, especially for composite applications. It assists in reducing shrinkage of moulded parts. Most common grades of calcium carbonate filler are derived from limestone or marble.

Calcium carbonate occurs in three crystalline polymorphs: calcite, aragonite and vaterite, with calcite being the most stable. The surface properties play a very important role in the final product. Under ambient atmospheric conditions in the presence of CO_2 and H_2O, the surface of $CaCO_3$ contains hydroxyl groups that persist even under ultrahigh-vacuum conditions [57-59]. Studies have shown that Ca^{2+} and CO_3^{2-} are the most important surface ions in $CaCO_3$ dispersed in aqueous solutions [59]. It has been suggested that H^+, OH^-, HCO_3^-, S^- and $[Ca(HCO_3)]^+$ species are also present on the surface and influence the properties of the calcite surface.

Owing to its hydrophilic surface properties, calcium carbonate has a poor dispersion in organic polymers. In order to improve its application performance, the surface of calcium carbonate needs to be modified.

2.1.5.2 Silica

Silica is one of the most abundant oxide materials in the earth. It can exist in an amorphous form (vitreous silica) or in a variety of crystalline forms. Silica particles have hydrophilic properties because of the presence of hydroxyl groups on the particle surface. At ambient atmospheric conditions silica contains physisorbed water, surface hydroxyl groups, and siloxane [60].

The hydroxyl groups appear in several forms: single (isolated), geminal, and hydrogen-bonded. Varying the calcination temperature varies the surface functionalities and their concentrations. Reactive hydroxyl groups on the surface of silica nanoparticles are of great importance because they are used in the modification of the surface, thus imparting the desired characteristics for specific applications [61-63].

2.2 Propylene polymerization catalysts

2.2.1 Heterogeneous catalysts

Heterogeneous olefin polymerization catalysts, the so-called Ziegler-Natta catalysts, are used for the production of more than two-thirds of the commodity polyolefins consumed worldwide [64]. Since the discovery of $TiCl_4/AlR_3$ catalyst [65], heterogeneous Ziegler-Natta catalysts have been improved through several generations of catalysts. This has been widely reviewed in literature [66-68]. The first-generation catalysts, based on $TiCl_3/Al(Et_2)Cl$, afforded PP containing 90 wt% of boiling heptane insoluble fractions (Isotactic Index) but low catalyst productivity.

The introduction of a Lewis base (electron donors) into the catalyst system gave rise to the second-generation catalysts, which are more active and stereospecific. However, most of the titanium salt involved in the catalyst was inactive and remaining as a polluting residue in the polymer, which then needed to be removed.

The third-generation of catalysts was composed of $TiCl_3$ supported on $MgCl_2$, with trialkylaluminum as a cocatalyst and one or two Lewis bases as electron donors. These catalyst systems showed high activity and stereoselectivity (activity >2400 kg PP/g Ti, tacticity index > 98%), which eliminated the requirement of catalyst removal.

The fourth-generation catalysts emerged from the introduction of a new combination of electron donors, which are able to afford a much better productivity and isotacticity. Since the catalyst morphology replicates the morphology of the polymer particles produced, the polymer can now be made spherical, with a controlled diameter, particle-size distribution, and with

controlled microporosity according to the specific architectures of the catalysts.

2.2.2 Homogeneous catalysts (metallocene catalysts)

2.2.2.1 Historical overview

Metallocenes are well-known organometallic complexes that were discovered as early as 1951. The first compound discovered was ferrocene [69], a simple complex consisting of an iron centre and two cyclopentadienyl (CP) rings surrounding the metal.

The term metallocene was used to describe any complex with a metal centre and CP ligands surrounding it. Today, the term is used to describe a wide variety of organometallic complexes including those with altered structures such as substituted CP rings and bridging atoms.

In 1957 Breslow and Newburg reported the polymerization of ethylene with the titanocene catalyst, Cp_2TiCl_2 (Figure 2.7) [70, 71]. This was accomplished with the cocatalyst trimethyl aluminium. The activity of the metallocene was however very low, and hence of little commercial use.

In the mid 1970s, during experiments involving a metallocene catalyst of the form Cp_2ZrCl_2 and the cocatalyst $Al(CH_3)_3$, water was accidentally introduced into the system [72]. It was noted that the activity of the metallocene/alkylaluminum catalysts could be significantly increased by the controlled addition of water to the polymerization reactor. After further research it was postulated that the high activity was a result of the hydrolysis of the cocatalyst trimethyl aluminum, to form MAO [72, 73].

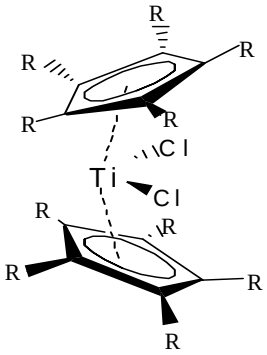

Figure 2.7: Titanocene catalyst.

In 1982 Wild et al. [74] reported the synthesis of the ansa C_2-symmetric metallocene catalyst rac-Et(Ind)$_2$ZrCl_2. The use of this catalyst allowed for the stereospecific polymerization of propylene. In 1988 Ewen et al. [75] reported a Cs-symmetric zirconocene ([Me_2C(Flu)(Cp)]ZrCl_2) which allowed for the production of syndiotactic PP in high quantities.

Since then a considerable amount of research has been conducted in the area of metallocenes. The structure of metallocenes has also received much attention in efforts to optimize them for the polymerization of α-olefins. Metallocenes can be substituted, bridged, unbridged, or of the half-sandwich type. Ligands such as indenyl (Ind) and flourenyl (Flu) have also been used instead of cyclopentadienyl (Cp) (Figure 2.8).

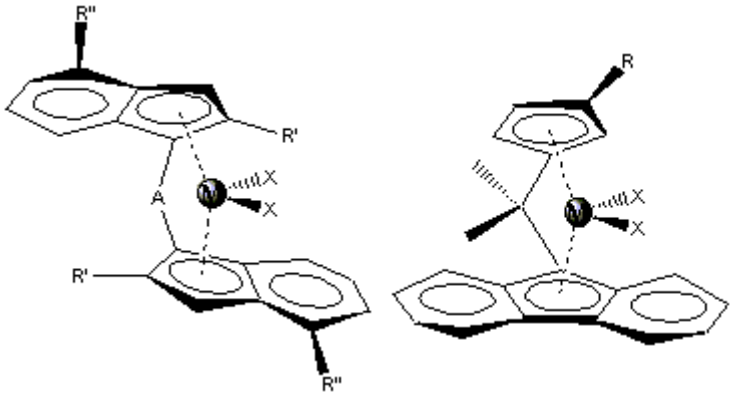

(R=H, Me, iPr, iPr$_2$, nBu)
(X=Cl)

Figure 2.8: Examples of different structures of metallocene catalysts.

2.2.2.2 The role of the cocatalyst

The cocatalysts are the key to the activity of the metallocenes. MAO is the cocatalyst most commonly used. Other bulky anionic complexes that show weak coordination, such as borates [76-79], are also increasingly used as cocatalysts.

MAO is an oligomeric compound with a molecular weight of 1000–1500 g/mol, obtained by the controlled hydrolysis of trimethylaluminum [80, 81]. Studies have shown that MAO is a mixture of several different compounds, including residual (coordinated) $AlMe_3$ and possibly AlO_3 units, in dynamic equilibrium [82].

The exact structure of MAO has not yet been determined. It supposedly exists as a mixture of different cyclic or linear oligomers with degrees of oligomerization commonly varying from 6 to 20. MAO may have the structures shown in Figure 2.9 [83].

Some recent experimental studies have suggested that MAO can also have a three-dimensional open cage structure [80].

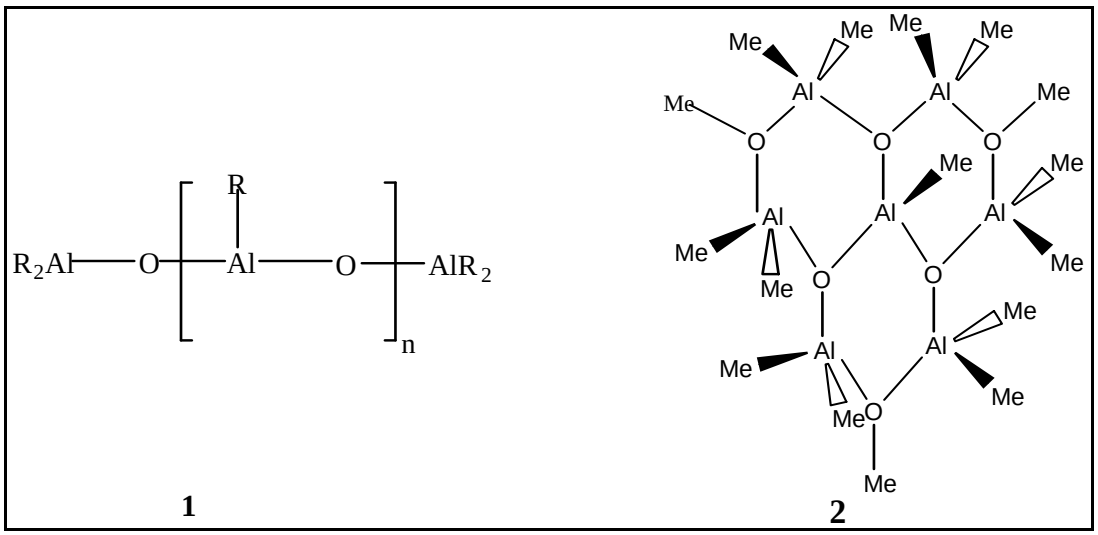

Figure 2.9: Proposed structures of MAO [83].

The first function of the MAO is the alkylation of the halogenated metallocene complex. Monomethylation takes place within seconds, and an excess of MAO leads to dialkylated species [84]. The generally accepted

mechanism of metallocene activation by MAO is shown schematically in Scheme 2.1.

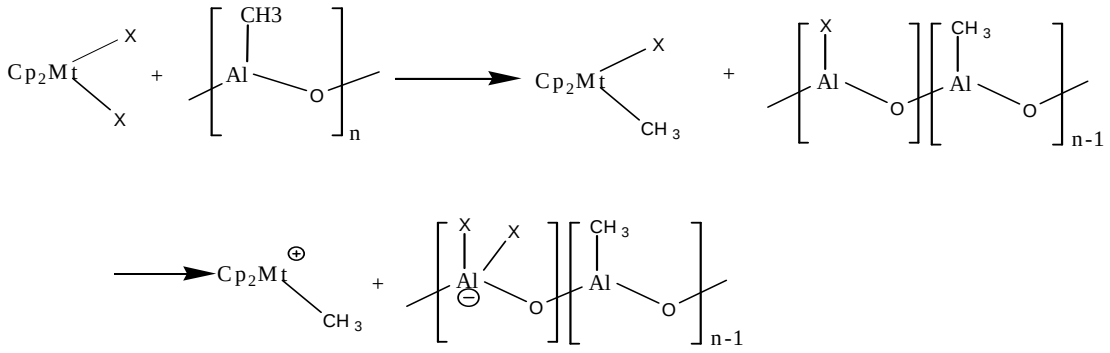

Scheme 2.1: The mechanism of metallocene activation by MAO [6].

2.2.2.3 Mechanism of olefin polymerization with metallocenes

In order for the polymerization to take place, the active metal atom centre bearing the growing alkyl chain must have a site for coordination. Insertion occurs via chain migration to the closest carbon of the olefin double bond, which undergoes cis opening with formation of the new Mt–C and C–C bonds.

Four mechanisms for olefin polymerization have been proposed. The first mechanism is the so-called Cossee mechanism [85], which essentially involves two steps: (i) olefin coordination and (ii) alkyl migration of the σ-coordinated growing chain to the π-coordinated olefin. This results in a net migration of the Mt-chain σ-bond to the coordination position previously occupied by the coordinated olefin (Scheme 2.2).

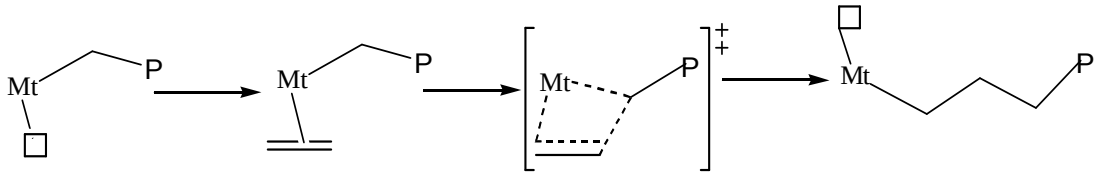

Scheme 2.2: Cossee mechanism.

The second mechanism is the so-called Green and Rooney mechanism [86], which involves an oxidative 1,2 hydrogen shift from the first C atom of the growing chain to the metal, giving rise to an alkylidene hydride species bonded to the metal. A four-center metallacycle is then generated by

reaction of the alkylidene moiety with a coordinated monomer molecule. The final step is a reductive elimination reaction between the hydride species bonded to the metal and the metallacycle.

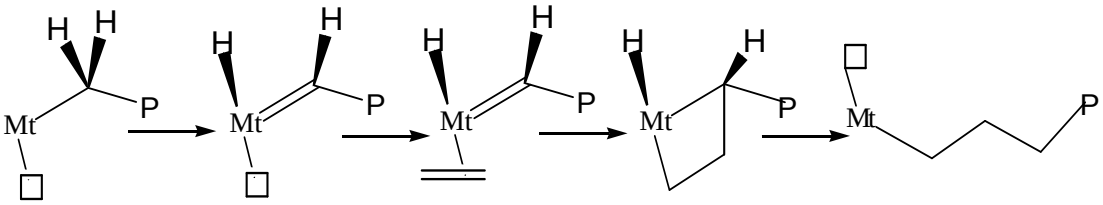

Scheme 2.3: Green and Rooney mechanism.

The third mechanism was also developed by Green, Rooney, and Brookhart [87]; it is known as the “modified Green-Rooney mechanism” and requires a stabilizing α-agostic interaction in various stages of the reaction.

The fourth mechanism (Scheme 2.5), which is very similar to the modified Cossee mechanism, also requires the presence of an α-agostic interaction.

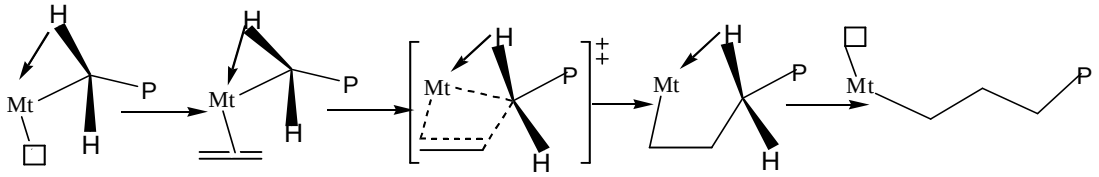

Scheme 2.4: Ground and transition state α-agostic mechanism.

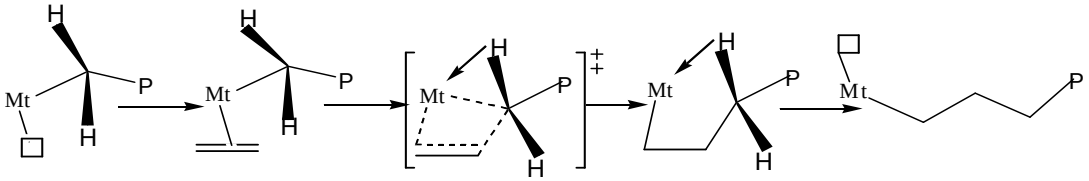

Scheme 2.5: Transition state α-agostic mechanism.

All the mechanisms presented show that the olefin insertion occurs by cis opening of the double bond and with chain migratory insertion. In metallocene catalysts each metal atom is regarded as an active centre and each active centre has two active sites in which coordination can take place. Because of the two sites, and the mechanism of chain migratory insertion with site switching, metallocene catalysts allow for the formation of different olefin

structures. This can be predicted by knowing the relationship between metallocene site symmetry and polymer stereochemistry.

2.2.2.4 Mechanisms of stereocontrol in propylene polymerization

Stereoselectivity or enantioface selectivity of the olefin insertion can be due to two mechanisms. The most effective one is that which is generally called enantiomorphic site control, that is, the chirality arises from the catalytic site. This is due to the spatial arrangement of the 2 η^5-coordinated Cp ligands, the growing polymer chain and the coordinated monomer itself. The arrangement is largely determined by energy considerations, and the lowest energy state will determine the preferred monomer coordination. If the last coordinated monomer is able to influence the coordination of the next monomer, then the mechanism is called chain-end control.

a) Mechanism of enantiomorphic site control (isospecific catalysts)

If we assume that 1,2 or primary insertion of the monomer is prevalent, then there are two ways for a prochiral monomer like propylene to coordinate. These two stereospecific processes can have a difference in activation energy ($\Delta\Delta E^{\ddagger}$) of up to 5 kcal/mol [88], so the possibility for stereoerror to occur is theoretically very low.

In C_2-symmetric catalysts, such as rac-Et$(Ind)_2MtCl_2$, the two active sites available for the incoming monomer and the growing chain are the same (homotopic), and therefore the configuration of the central metal atom does not change after the chain migratory insertion of the coordination monomer (see Scheme 2.6).

b) Lack of control (aspecific catalyst)

In achiral Cs-symmetric catalysts, such as meso-Et$(Ind)_2MtCl_2$, the positions of the coordinated olefin and the alkyl ligands are not chirotopic (fixed by energy considerations), and therefore the catalyst control is completely lacking (see Scheme 2.7).

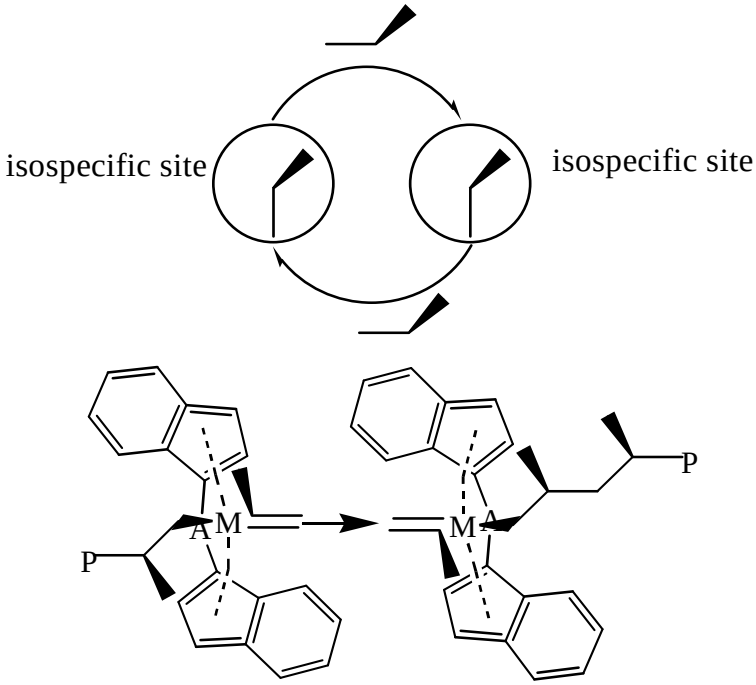

Scheme 2.6: Propylene polymerization mechanism with C_2-symmetric metallocene catalysts.

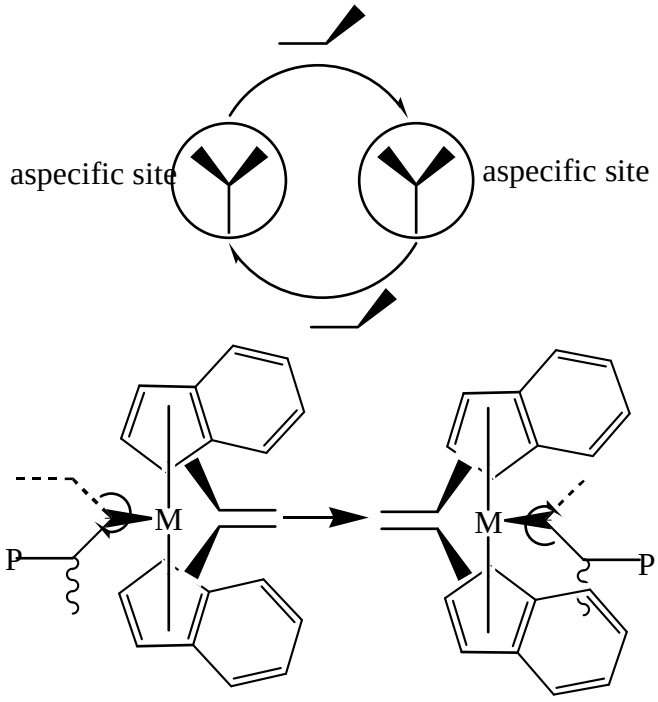

Scheme 2.7: Propylene polymerization mechanism with achiral Cs-symmetric metallocenes (meso isomers of C_2 symmetry).

Chain-end control could be functional here, and is less effective than site control. The $\Delta\Delta E^{\ddagger}$ between the insertions of the two enantiofaces is about 2 kcal/mol, so the stereoerror is more likely than in the case of enantiomorphic

site control. The types of stereoerrors arising from chain-end control (or a lack of site control) are diagnostic of this state of affairs and can be clearly seen in ^{13}C NMR spectra [88].

2.2.3 Kinetic models

Many kinetic models have been developed to characterize the homogeneous polymerization of propylene using metallocene catalyst systems [6, 88-96].

Generally, in analogy to heterogeneous Ziegler-Natta catalysis, a first-order polymerization rate (R_p) with respect to monomer concentration [M] and catalyst concentration is also assumed for metallocene-based catalysts:

$$Rp = KpCp[M] \tag{2.1}$$

where Kp is the propagation rate constant. Cp is the number of propagating active centres correlated to the total number of active sites (Co), by the expression:

$$Co = Cp + CA \tag{2.2}$$

where CA is temporarily inactive centres.

The Al/Zr ratio has a remarkable effect on the reaction rate in propylene polymerization with metallocene catalysts [6,97]. The polymerization activity reaches a maximum at a specific Al/Zr ratio for various metallocenes. At an optimum Al/Zr ratio the metallocene is converted to cationic complexes with weakly coordinating MAO-complexed counterions. At higher Al/Zr ratios the excess of MAO and olefin can compete for vacant coordination sites. The polymerization temperature (Tp) also plays a role in controlling the polymerization rate [8, 98].

2.3 Supported metallocene catalysts

The advantage of metallocene catalysts over Ziegler-Natta catalysts is the “single-centre” character of the active catalytic species, which leads to the production of polymers that have narrow MWDs, and uniform and tuneable

microstructures. However, there are some problems associated with metallocene catalysts, including the very large quantity of expensive MAO required to achieve high catalyst activity and that current PP production technologies (gas-phase and slurry reactors) can only be used for heterogeneous catalyst systems.

One solution that has been fairly successful entails heterogenization of the metallocene complex on a support [99-101]. Amorphous SiO_2 is currently regarded as the best support for metallocenes with MAO as cocatalyst because SiO_2 has a high surface area and porosity, good mechanical properties, and is stable and inert under reaction and processing conditions [102-104]. A typical example of a metallocene supported on silica is shown in Figure 2.10 (Ind = Indene ligands).

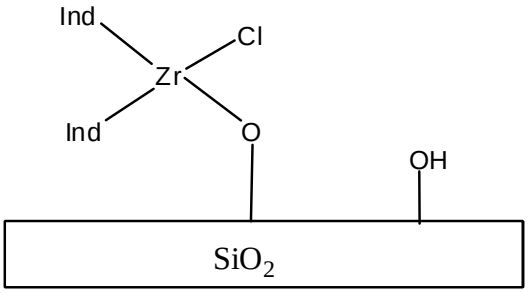

Figure 2.10: Silica-supported metallocene catalyst.

2.3.1 Supporting methods and procedures

Three main methods have been developed to support homogeneous systems [99, 102], and they are reviewed here.

2.3.1.1 Direct immobilization of the metallocene

This method involves first supporting the metal complex on the carrier, and then reacting with alumoxane. This method is more common for the in situ synthesis of a metallocene on a support [105-107], and the reaction of metallocene complexes having functional anchors with the support surface [108-110]. Metallocenes react with silica surfaces to form Si–metallocene

bonds, which are converted to catalytic species on reaction with MAO (Scheme 2.8).

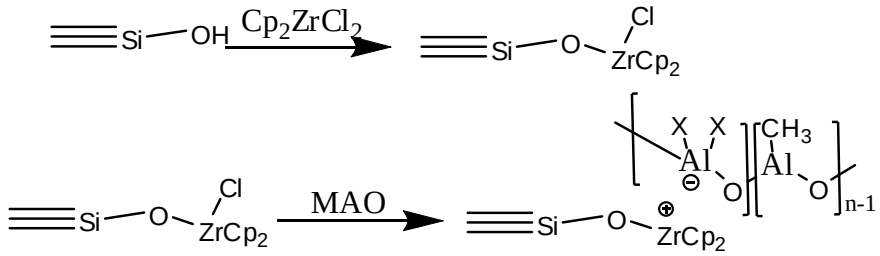

Scheme 2.8: Direct immobilization of the metallocene followed by activation with MAO.

Polymers with very high molecular weight and narrow molecular weight distribution were obtained using this method [99, 111, 112]. It was suggested that zirconocene immobilization on silica prevents deactivation by bimolecular processes and thus increases molecular weight [113]. This method yields only catalyst systems with low activities since the metallocenes are decomposed by reaction with the surface hydroxyl groups [114, 115].

2.3.1.2 Treatment of support with MAO before metallocene immobilization

The second method is the reaction of the cocatalyst MAO with the hydroxyl groups on the surface of the silica gel, followed by washing, drying, and impregnation with an appropriate zirconocene complex [105, 116-118] (Scheme 2.9). Polymerization of ethylene using these catalyst systems afforded polyethylene with high molecular weight and narrow molecular weight distribution [118].

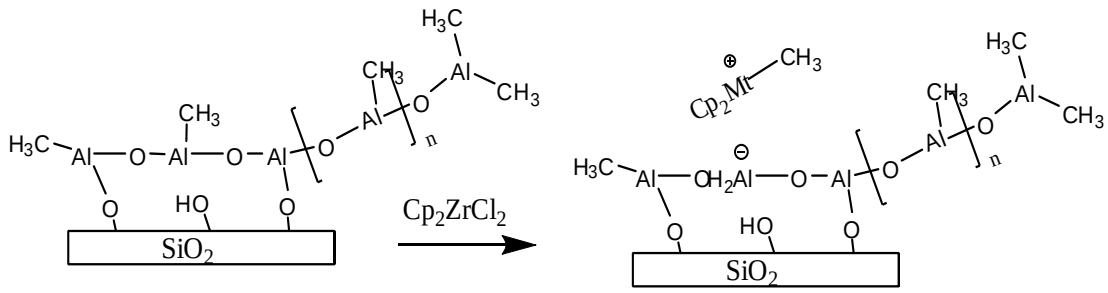

Scheme 2.9: Treatment of support with MAO followed by supporting the metallocene.

The activity of this material is often inadequate, but it can be increased with an activator such as AlR_3 or MAO, which scavenges impurities, alkylates zirconocene complexes, and separates ion pairs.

2.3.1.3 Immobilization of a preactivated MAO/metallocene

This method involves the one-step immobilization of a preactivated MAO/metallocene complex on a porous SiO_2 support [119]. The process maximizes the number of active centres by activating the metal component in solution, instead of carrying out the process with one or the other component in an immobilized state. Highly active catalysts can be produced by this method, even at low Al/Zr ratios.

2.4 Overview of PP nanocomposites

2.4.1 Potential of polymer nanocomposites

Inorganic fillers with dimensions in the micrometer range, e.g. calcium carbonate, glass beads and talc, have been used extensively to enhance the mechanical properties of polymers. Such properties can be tailored by changing the volume fraction, and shape and size of the filler particles [120-122]. Further improvements in the mechanical properties can be achieved by using filler materials with larger aspect ratios, such as short glass fibers [120, 123-127].

It is logical to anticipate that the dispersion of fillers, with dimensions in the nanometer range and having a very large aspect ratio, in a polymer matrix could lead to even higher mechanical performances. Improvement in the mechanical properties of a nanocomposite system compared with a microcomposite system can be explained on the basis of the interaction between the filler and the matrix. If a strong interaction between filler and matrix exists, then an interfacial layer will be formed around the filler particles, as shown in Figure 2.11. This interfacial layer has a higher density and subsequently higher modulus than the rest of the matrix [128-131].

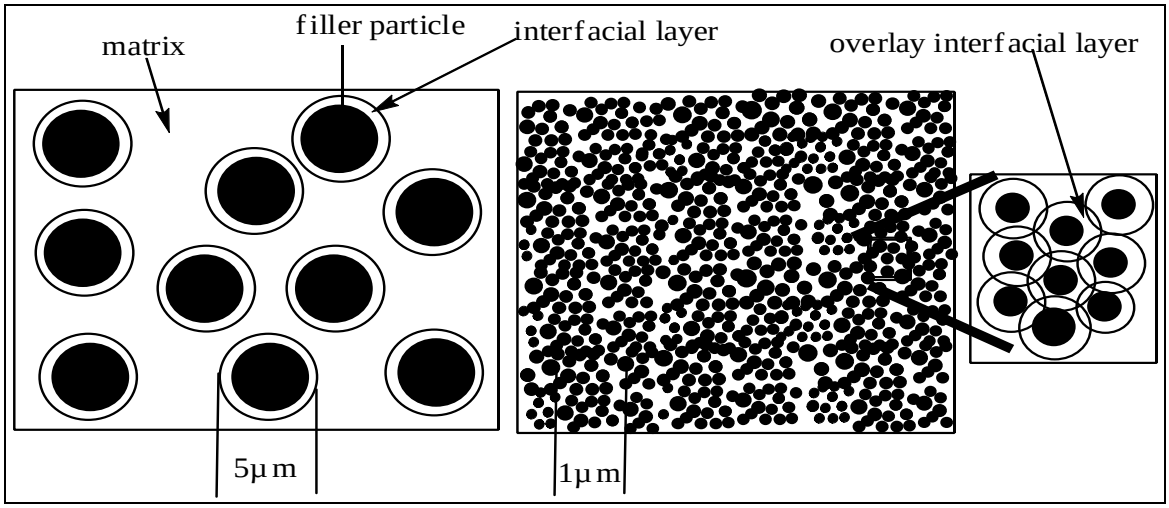

Figure 2.11: Comparison between conventional composite and nanocomposites.

The strength of the interaction plays a role in the thickness and density of the interphase, which consists of a layer of high density polymer around the particle. The effects of the interface on the behaviour of a composite depend upon the interparticle distance. For a constant filler content the number of filler particles increases with reduction in particle size, bringing the particles closer to one another. Thus, the interface layers from adjacent particles overlap, altering the bulk properties significantly.

Under the effect of an external load, fillers induce a stress concentration, which depends on the size of the filler and on interfacial adhesion. An increased number of homogeneously distributed stress concentration sites, created by well dispersed filler nanoparticles, will lead to overlapping of stress concentration fields around filler particles. The latter is responsible for shear yielding of the matrix, which is the dominant energy dissipation mechanism [3, 132, 133].

Furthermore, the advantages of polymer nanocomposites derive from the exceptionally large particle surface area that can be achieved by only a small addition of particles (e.g. 5% by weight) [134]. Thus, they offer dramatic improvements in material performance, with significant increases in mechanical properties, without sacrificing processability and density.

2.4.2 Technical problems

2.4.2.1 Nanoparticle dispersion

In polymer nanocomposites the major problem arises from the aggregation of the filler particles. The surface free energy of the filler determines the particle–particle interactions and particle–polymer interactions. The particle–particle interactions determine aggregation, and particle–polymer interactions have a pronounced effect on the mechanical properties. The aggregation tendency of the filler increases with decreasing particle size due to the increase in surface tension [135-138].

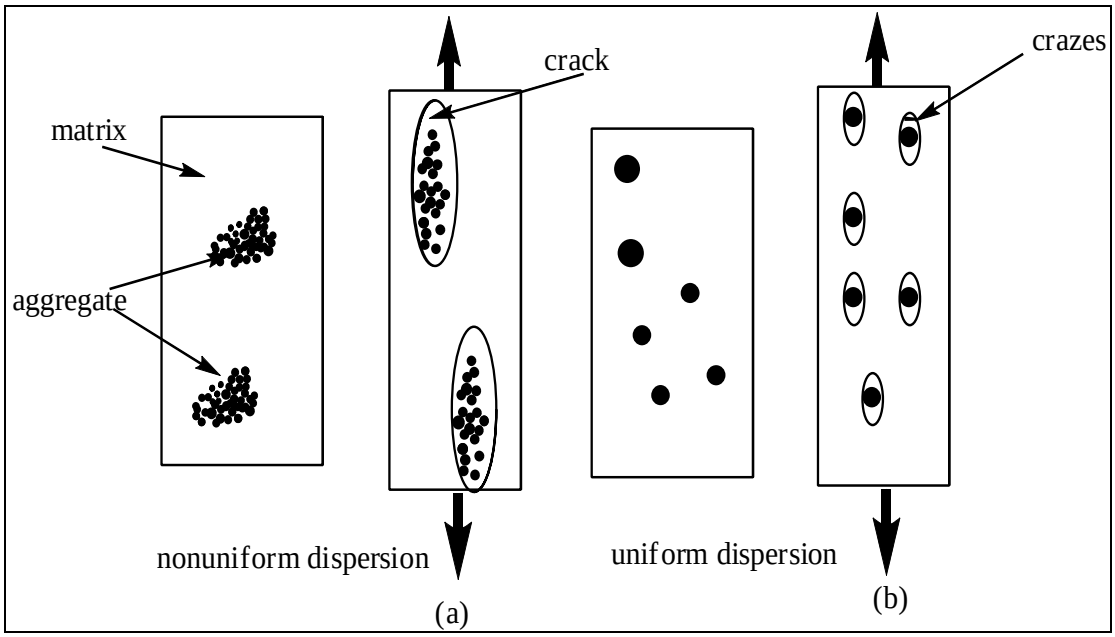

Figure 2.12: Effect the filler particle aggregation on the mechanism of deformation.

Uniform dispersion is important because if the matrix consists of aggregates of particles the stress field around the aggregate will be high (creating stress localization), resulting in easier crack initiation and propagation, and consequently premature failure [139]. In addition, under the effect of external load, the aggregate will tend to flow without inducing matrix crazing (see Figure 2.12 (a)) [128, 140, 141]. If the filler nanoparticles are homogenously dispersed, on the other hand (see Figure 2.12 b), crazes or plastic deformations will be formed uniformly throughout the polymer matrix when an external load is applied. The formation of multiple crazes during the

application of an external load will lead to more energy absorption during the fracture process.

2.4.2.2 Interfacial interaction

Filler–matrix interaction significantly influences the mechanical properties. In traditional polymer composites, when the fillers have a high surface energy the polymer chains are adsorbed onto the filler surface. Adsorption of polymer chain molecules leads to the development of a layer that has properties different from those of the polymer matrix. The formation of an interphase layer between the matrix and filler has been observed in most polymer composite systems [134, 142-144]. As seen in Figure 2.13, the structure of the interphase is different to both the filler and the matrix phases, and it varies depending on the distance from the filler surface.

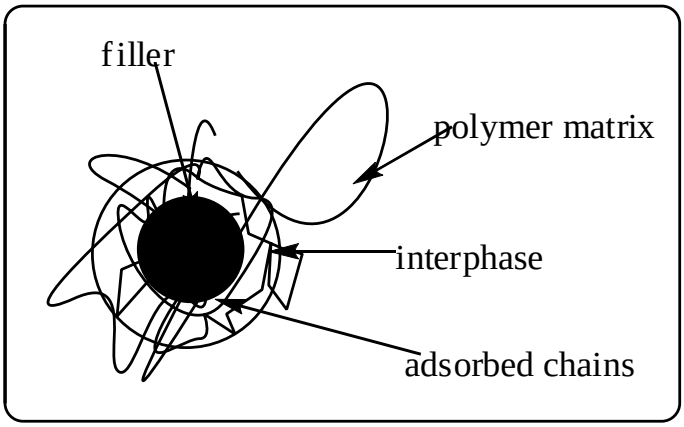

Figure 2.13: Schematic of interphase area between the filler and polymer matrix [144].

It is reported that one of the main processes that contribute to energy consumption is the debonding of the polymer matrix from the particle surface [141, 145-147]. Thus, the strength of the interphase layer plays a key role in determining the properties of nanocomposites. It is worth noting that the debonding energy is decreased with increasing particle size [141].

The interfacial interaction in polymer composites can be modified by the surface treatment of fillers [137, 148-150]. Nonreactive treatment results in a decrease in the surface tension of the filler leading to a decrease in particle–particle and particle–polymer interaction [28, 151]. As a result, aggregation of

the filler decreases but the yield stress and tensile strength of the composite decrease [28, 152, 153]. Reactive treatment assumes the presence of reactive groups both on the surface of the filler and in the polymer matrix, and results in improved strength [137].

2.4.3 Crystallization of nanocomposites

A great amount of scientific research has been devoted to the study of the effect of the filler on the crystallization behaviour of the polymer matrix [154-159]. Generally, incorporation of nanofiller has little effect on the degree of crystallinity of PP. There may be some changes in the degree of crystallinity in various nanocomposite systems, but overall no major differences in crystallinity of nanocomposites versus neat PP were observed in any of the systems examined.

On the other hand, the crystallization temperature increased upon the addition of the nanofillers. It is generally believed that the crystallization temperatures increase with nanofiller content as a result of the nucleating effect. Furthermore, the size of the crystalline domain spherulites was found to decrease significantly upon addition of nanofillers [160-162]. Many fillers act as primary nucleation agents, increasing the number of spherulites, reducing their mean diameter, and changing the crystallization kinetics.

2.4.3.1 Crystallization kinetics

The crystallization kinetics of polymer nanocomposites is essential for assessing their microstructure development in melt processing. Furthermore, a change in the crystallization rate leads to a change in the duration of the manufacturing cycle, thus affecting productivity. The trend in current processing techniques is toward shorter cycle times and high cooling rates.

The process of crystallization can be assessed through isothermal crystallization at a constant temperature or by nonisothermal crystallization at a constant cooling rate.

The most common approach used to analyze the isothermal crystallization is the Avrami method [163]. Accordingly, the relative degree of crystallinity, X(t), is related to the crystallization time, t, according to:

$$1 - X(t) = \exp(-kt^n) \qquad (2.3)$$

where *n* is the Avrami exponent, which is a function of the nucleation process and *k* is the growth function, which is dependent on nucleation and crystal growth. The values of *n* and *k* can be calculated from fitting to experimental data using the double logarithmic form of Eq. (2.3):

$$\ln[-\ln(1 - X(t)] = \ln k + n \ln t \qquad (2.4)$$

However, during processing, the crystallization of polymers is known to take place nonisothermally. Several methods for describing the nonisothermal crystallization kinetics are based on the Avrami equation [126, 158].

Ozawa [164] modified the Avrami equation by incorporating a heating/cooling factor. The following equations have been derived:

$$1 - X(t) = \exp[-K(T)/\phi^m] \quad \text{or} \quad \ln[-\ln(1 - X(t))] = \ln K(T) - m \ln \phi \qquad (2.5)$$

where *Φ* is the cooling rate, *K(T)* is a function of cooling rate, and *m* is the Ozawa exponent depending on the dimensions of crystal growth.

Qian et al. [165] and Jain et al. [166] studied the nonisothermal crystallization behaviours of PP nanocomposites. Qian et al. [165] reported that the Ozawa equation can be used to describe the nonisothermal crystallization of the nanocomposites very well.

2.4.4 Mechanical properties of nanocomposites

The mechanical properties of polymer–nanofiller composites are controlled by several microstructural parameters, such as the properties of the matrix, properties and distribution of the filler, as well as interfacial bonding, and by the synthesis or processing methods. The interfaces may affect the effectiveness of load transfer from the polymer matrix to nanofillers. Thus,

surface modification of nanofillers is needed to promote better dispersion of fillers and to enhance the interfacial adhesion between the matrix and fillers.

While there is a significant amount of data available on polymer nanocomposites, agreement has not yet been reached on how nanosized inclusions affect mechanical properties [126, 128, 167]. For example, both improvements in [168] and deterioration of [169] the mechanical performance of nanocomposites have been reported. The possible reason for such contradiction is the dispersion of the nanofillers and adhesion between the polymer and fillers due to different filler treatments and different preparation methods.

Generally, for all nanocomposite systems the elastic modulus increases with increasing volume fraction of the fillers regardless of the adhesion and particles dispersion. The increase in modulus proceeds with an increase in nanoparticle volume fraction. Furthermore, all nanocomposite systems show a decrease in the elongation at break [134, 170-172].

Enhancements in the impact strength [140, 156, 173], tensile strength [3, 173], and yield stress [3, 173] have also been observed in most PP nanocomposite systems. However, many nanocomposites exhibit toughness, tensile strength, and yield stress lower than the corresponding neat polymers [174].

2.4.5 Toughening mechanism of polymer nanocomposites

The enhancement of PP toughness has only been achieved by incorporation of rubber particles. This is, however, associated with a significant loss of both tensile strength and stiffness of PP [175, 176]. It was recently reported that semicrystalline polymers can be toughened by incorporation of a rigid filler, while retaining the high stiffness [120, 132, 133, 168]. It is believed that the rigid filler generates a process in the polymer matrix that leads to increased toughness.

Much work has been devoted to explaining this behaviour, as rigid particles do not deform to contribute to the energy absorption [120, 132]. It

has been proposed that the major toughening mechanisms are interfacial debonding and plastic deformation of interparticle ligaments and crack deflection (see Figure 2.14).

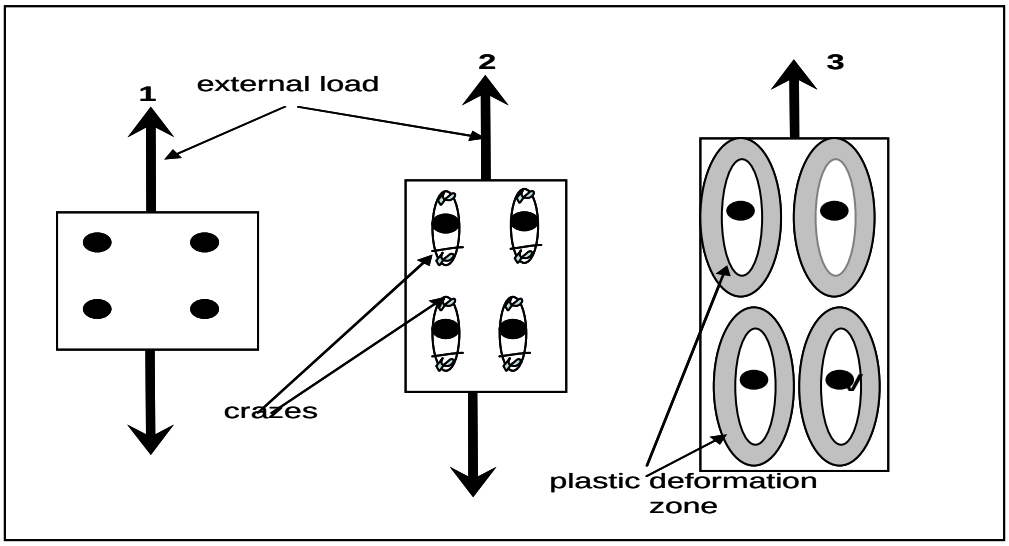

Figure 2.14: Toughing mechanism of semicrystalline polymer reinforced with rigid particle [132].

The micromechanical deformation processes in various toughened and particle filled semicrystalline polymers have been described by a three-stage mechanism [132]. In the first stage, the modifier particles act as stress concentrators, because they have different elastic properties than the matrix (Figure 2.14 (1)).

In the second stage, stress concentration gives rise to the build up of triaxial stress around the filler particles and this leads to debonding at the particle–polymer interface and the formation of crazes (Figure 2.14 (2)). In the last stage, the voids resulting from debonding alter the stress state in the matrix polymer surrounding the voids. This subsequently promotes shear yielding or plastic deformation (Figure 2.14 (3)). The shear yielding mechanism becomes functional and the material is able to absorb large quantities of energy upon fracture.

2.4.6 Methods of preparation of nanocomposites

The preparation of nanocomposites is not an easy task and needs considerable effort. The separation of agglomerates into individual

nanoparticles is a difficult task and requires the application of great forces and adequate shear in order to break their interaction force.

Researchers have tried using a variety of preparative methods to prepare polymer matrix nanocomposites. The preparative methods are divided into three main groups according to the starting materials and processing techniques [128, 177]: melt-mixing, in situ polymerization, and solution blending.

2.4.6.1 Solution blending method

In this method a solvent system is used in which the polymer is soluble and the filler is swellable. The filler is first swollen and aggregations are broken apart in the solvent. Ultrasonic vibration may also be used in this step. The polymer is then dissolved in solvent and added to the filler mixture. In the final step the solvent is removed by evaporation under reduced pressure (rotary evaporator) [178-180].

Many nanocomposites have been studied both in aqueous and nonaqueous solvents such as poly(vinyl alcohol) [181], poly(l-lactide) [182], polyimides [183], and high-density polyethylene [184].

It is believed that the distribution of the fillers in the composites by the solution method is much better than by the melt-mixing method [185, 186]. However, the main drawback of the technique is that very large volumes of solvents are required in this process.

2.4.6.2 Melt-mixing method

Mixing fillers with melten polymer in an extruder or mixer is the main process by which to obtain conventional polymer composites. A standard melt-mixing procedure involves one or two stages. In the two-stage procedure, powder filler is premixed with a polymer powder in a high-speed mixer. Different kinds of mixing devices, such as a twin-screw extruder and Haake mixer, are available for this task. It is important that the shear forces exerted by the mixer are sufficient to tear the individual particles apart.

This method is regarded as the most promising method and it has great advantages over other methods being both compatible with current industrial processes and environmentally friendly, due to the absence of solvents. However, it is less efficient when the reinforcing filler is on a nanoscale due to the agglomeration of nanoparticles and the high melt viscosity of the polymers [135, 136]. As the size of the filler particle decreases the surface tension of the particle increases and the melt-mixing does not provide sufficient shear toward the aggregated particle to break it apart [135-138, 156, 187].

It is nevertheless possible to overcome this by chemical modification of the filler surface with functional silanes and titanate esters, or by encapsulating the filler in a polymer coating [149, 150]. These methods can be used to promote the adhesion and distribution of the nanoparticles in the polymer matrix and hence enhance the mechanical properties of the nanocomposites. However, the low heat resistance of the modifiers makes them prone to degradation under the compounding conditions, and the presence of aggregates still occurs. The agglomerate structure has been observed in composites even after the use of chemical modification or coupling agents [156, 187, 188].

Highly viscous melts of polymers are also inadequate for this method, because the mixing is hindered, and the high shear forces can lead to a partial degradation of the polymer.

2.4.6.3 In situ polymerization method

In situ polymerization is another technique that has been used to make polymer matrix nanocomposites [126, 189-191]. This method involves the in situ polymerization of monomer directly in the presence of filler. The catalyst or the initiator can be supported on the filler or soluble in the polymerization medium (Figure 2.15). The nanoparticles are generally pretreated with a chemical agent to improve their compatibility with the polymer matrix.

There is evidence that the in situ synthesis of polymer (in the presence of nanofillers) is a useful approach for achieving a more homogeneous distribution of inorganic nanoparticles, due to the ability of the small molecules

(e.g. monomer, catalyst) to diffuse inside the particle aggregates. In addition, close contact of polymer and filler during synthesis improves the interactions between the filler and matrix [190, 192-197].

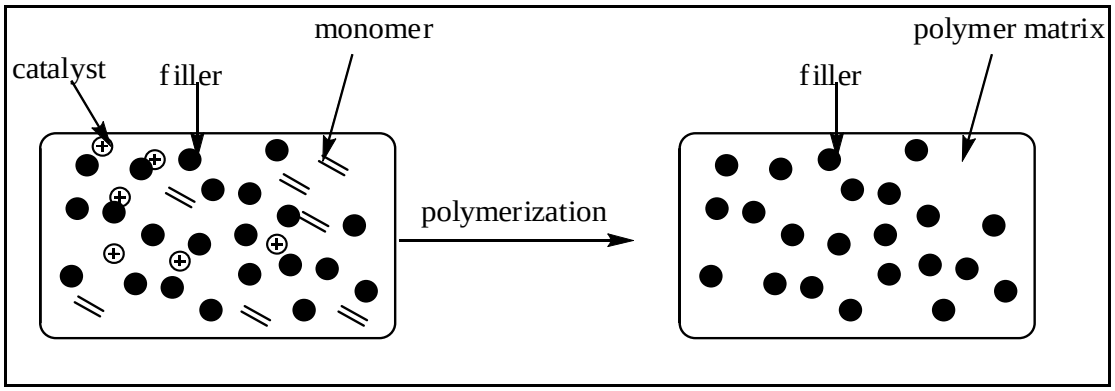

Figure 2. 15: Schematic of in situ polymerization.

In situ polymerization has been used for the preparation of polyolefin nanocomposites [193, 198-208] and has proven to be one of the most efficient and versatile methods by which to synthesize polyolefin nanocomposites with good dispersion of the fillers inside the polymer matrix.

Most of the in situ polymerization of olefins has been carried out with metallocene/MAO catalysts and only a few with heterogeneous Ziegler-Natta catalysts [205]. This was a result of the development of an effective immobilization method of the metallocene catalyst on either organic or inorganic materials for commercial applications (see Section 2.3).

The effect of the presence of nanofillers on the microstructure of the polymer matrices produced, during the in situ polymerization, is of some importance. For example, if the presence of nanofillers induces changes in the matrix microstructure, the material produced may ultimately be defined as a new material, which cannot be effectively compared to nanocomposites prepared by other methods.

Only a few scientific studies were dedicated to performing a comparative study of the different methods by which to prepare polyolefin nanocomposites [199, 206]. However, most of these studies compared the dispersed phase morphologies and crystallization behaviour of the different

nanocomposites, and detail on the matrix microstructure was not fully addressed. For instance, Trujillo et al. [199] investigated the effect of the preparation method on the behaviour of polyethylene/carbon nanotube nanocomposites. They found that lamellae produced within the in situ polymerized polyethylene nanocomposite are thicker than those produced in pure polyethylene or in physical blends prepared by the melt-mixing.

Heinemann et al. [206] prepared nanocomposites of high density polyethylene, and linear low density polyethylene, by means of both melt-compounding and by in situ ethylene homo and copolymerization, in the presence of layered silicates using MBI catalysts. They found that the addition of modified and unmodified layered silicates did not affect either the incorporation of 1-octene, or the polymer molar masses. They found that, in comparison to melt-compounding, in situ ethylene homo and copolymerization catalyzed by a MAO-activated zirconocene was more effective in nanocomposite formation.

2.5 Conclusion

From this brief historical background and literature review it is clear that much has been achieved in the field of PP nanocomposites during the last two decades. It is also clear that in situ polymerization is regarded as the most promising synthetic method for the preparation of PP nanocomposites with good dispersion of nanoparticles in the polymer matrix. However, although the synthesis of PP/filler nanocomposites via in situ polymerization with MAO-activated metallocene catalysts has been investigated in numerous scientific studies, it follows from the literature review that certain aspects concerning the effect of the filler on the polymer microstructures remain unsolved. There is also little information in the open literature concerning the comparisons of the different techniques by which to prepare PP nanocomposite.

In the following chapters the synthesis of PP/filler nanocomposites via in situ polymerization with MAO-activated metallocene catalysts will be described and the effect of filler nanoparticles on the polymerization kinetics and consequently on the matrix microstructure will be demonstrated. The

synthesis of PP/filler nanocomposites via the melt-mixing method using PP homopolymers with different microstructures will also be carried out. The dispersed phase morphologies of the different nanocomposites were investigated and compared. Finally comparison of the different properties of PP nanocomposites prepared by melt-blending and by in situ polymerization is given. Two types of fillers, silica and calcium carbonate, were chosen for use in this study because silica is regarded as the most widely used material for supporting a metallocene catalyst and calcium carbonate is the most widely used inorganic filler for PP.

2.6 References

1. Van Reenen, A.; Sultan, O., *Z. Naturforsch., B: Chem. Sci.*, 2007. **62** p. 362
2. Marques, M.; Conte, A., *J. Appl. Polym. Sci.*, 2006. **99**: p. 628.
3. Rong, M.; Zhang, M.; Zheng,Y.; Zeng, H.; Friedrich, K., *Polymer*, 2001. **42**: p. 3301.
4. Edward, P.; Moore, J, *Introduction*, in *Polypropylene Handbook*, P.M. Edward, J, Editor. 1996, Hanser: Munich. p. 10.
5. Natta, G.; Pino, P.; Corradini, P.; Danusso, P.; Mantica, E.; Mazzanti, G., *J. Am. Chem. Soc.*, 1955. **77**: p. 1708.
6. Resconi, L.; Cavallo, L.; Fait, A.; Piemontesi, F., *Chem. Rev.*, 2000. **100**: p. 1253.
7. Resconi, L.; Piemontesi, F.; Camurati, I.; Balboni, D.; Sironi, A.; Moret, M.; Rychlicki, H.; Zeigler, R., *Organometallics*, 1996. **15**: p. 5046.
8. Rieger, B.; Mu, X.; Mallin, D.; Rausch, M.; Chien, J, *Macromolecules*, 1990. **23**: p. 3559.
9. Schupfner, G.; Kaminsky, W., *J. Mol. Catal. A: Chem.*, 1995. **102**: p. 59.
10. Prosenc, M.; Brintzinger, H, *Organometallics*, 1997. **16**: p. 3889.
11. Carvill, A.; Zetta, L.; Zannoni, G.; Sacchi, M., *Macromolecules*, 1998. **31**: p. 3783.
12. Resconi, L.; Camurati, I.; Sudmeijer, O., *Top. Catal.*, 1999. **7**: p. 145.
13. Ferro, D.; Zambelli, A.; Provasoli, A.; Locatelli, P.; Rigamonti, E, *Macromolecules*, 1980. **13**: p. 179.

14. Brintzinger, H.; Fischer, D.; Muelhaupt, R.; Rieger, B.; Waymouth, R., *Angew. Chem. Int. Ed. Engl.*, 1995. **34**: p. 1143.
15. Zambelli, A.; Dorman, D.; Brewster, A.; Bovey, F, *Macromolecules*, 1973. **6**: p. 925.
16. Zambelli, A.; Locatelli, P.; Bajo, G.; Bovey, F, *Macromolecules*, 1975. **8**: p. 687.
17. Grassi, A.; Zambelli, A.; Resconi, L.; Albizatti, E.; Mazzochi, R, *Macromolecules*, 1988. **21**: p. 617.
18. Busico, V.; Cipullo, R.; Monaco, G.; Vacatello, M, *Macromolecules*, 1997. **30**: p. 6251.
19. Janimak, J.; Cheng, S.; Giusti, P., *Macromolecules*, 1991. **24**: p. 2253.
20. Arranz, J.; Pena, B.; Benavente, R.; Perez, E.; Cerrada, M., *Eur. Polym. J.*, 2007. **43**: p. 2357.
21. Yamada, K.; Matsumoto, S.; Tagashira, K.; Hikosaka, M., *Polymer*, 1998. **39**: p. 5327.
22. Vasile, C.; Seymour, R, *Handbook of Polyolefins: Synthesis and Properties*. 1993, New York: Dekker p. 155.
23. Roger, A.; Michael, D., *Structure and Morphology*, in *Polypropylene Handbook*, P.M. Edward, J, Editor. 1996, Hanser: Munich. p. 125.
24. Kroschwitz, j.; Mark, H.; Bikales, N.; Overberger, C.; Menges, G., *Propylene Polymers*, in *Encyclopedia of Polymer Science and Engineering*. 1988, John Wiley & Sons: New York. p. 477.
25. Bruckner, S.; Meille, S.; Petraccone, V.; Pirozzi, B., *Prog. Polym. Sci.*, 1991. **16**: p. 361.
26. Lotz, B., *Eur. Phys. J., E*, 2000. **3**: p. 185.
27. Tsai, F.; Chen, J.; Yeh, J., *Polymer*, 2005. **46**: p. 5680.
28. Akovali, G.; Akman, M., *Polym. Int.*, 1997. **42**: p. 195.
29. Xu, J.; Guan, F.; Yasin, T.; Fan, Z., *J. Appl. Polym. Sci.*, 2003. **90**: p. 3215.
30. Romankiewicz, A.; Sterzynski, T.; Brostow, W., *Polym. Int.*, 2004. **53**: p. 2086.
31. Mezghani, K.; Phillips, P., *Polymer*, 1995. **36**: p. 2407.
32. Edward, P.; Moore, J, *Polypropylene Handbook*. 1996: Hanser Publishers: Munich Vienna New York. p. 119.

33. Meille, S.; Bruckner, S., *Polypropylene: An A-Z Reference*. X-ray scattering, ed. J. Karger-Kocsis. 1999, Dordrecht: Kluwer. p. 908.
34. Kroschwitz, j.; Mark, H.; Bikales, N.; Overberger, C.; Menges, G., *Propylene Polymers*, in *Encyclopedia of Polymer Science and Engineering*. 1988, John Wiley & Sons. p. 485.
35. Auriemma, F.; De Rosa, C.; Boscato, T.; Corradini, P, *Macromolecules*, 2001. **34**: p. 4815.
36. De Rosa, C.; Auriemma, F.; Perretta, C. , *Macromolecules*, 2004. **37**: p. 6843.
37. De Rosa, C.; Auriemma, F.; Circelli, T.; Waymouth, R., *Macromolecules*, 2002. **35**: p. 3622.
38. Auriemma, F.; De Rosa, C., *Macromolecules*, 2002. **35**: p. 9057.
39. De Rosa, C.; Auriemma, F.; Circelli, T.; Longo, P.; Boccia, A., *Macromolecules*, 2003. **36**: p. 3465.
40. De Rosa, C.; Auriemma, F.; Spera, C.; Talarico, G.; Tarallo, O., *Macromolecules*, 2004. **37**: p. 1441.
41. De Rosa, C.; Auriemma, F.; Ruiz de Ballesteros, O.; Resconi, L.; Fait, A.; Ciaccia, E.; Camurati, I., *J. Am. Chem. Soc.*, 2003. **125**: p. 10913.
42. Katti, S.; Schultz, J., *Polym. Eng. Sci.*, 1982. **22**: p. 1001.
43. Fujiyama, M.; Wakino, T.; Kawasaki, Y., *J. Appl. Polym. Sci.*, 1988. **35**: p. 29.
44. Fujiyama, M.; Wakino, T., *J. Appl. Polym. Sci.*, 1991. **43**: p. 97.
45. Phillips, R.; Herbert, G.; News, J.; Wolkowicz, M., *Polym. Eng. Sci.*, 1994. **34**: p. 1731.
46. Isai, R.; Graham, A.; Mandelkern, L.; Alamo, G., *Polymer*, 2000. **41**: p. 8813.
47. Wal, A.; Mulder, J.; Thijs, A.; Gaymans, J. , *Polymer* 1998. **39**: p. 5467.
48. Wal, A.; Mulder, J.; Thijs, A.; Gaymans, J., *Polymer*, 1998. **39**: p. 5477.
49. Nitta, K.; Takayanagi, M., *J. Polym. Sci., Part B: Polym. Phys.*, 1999. **37**: p. 357.
50. Patel, M.; Sehanobish, K.; Knight, W., *J. Appl. Polym. Sci.*, 1996. **60**: p. 749.
51. Stern, C.; Frick, A.; Weickert, G., *J. Appl. Polym. Sci.*, 2007. **103**: p. 519.

52. Schrauwen, B.; Govaert, L.; Peters, G.; Meijer, H., *Macromol. Symp.*, 2002. **185**: p. 89.
53. Karger-Kocsis, J., *Polypropylene: structure, blends and composites*. Vol. 3. 1995, London: Chapman and Hall. p. 5.
54. Yang, R.; Liu, Y.; Yu, J.; Wang, K., *Polym. Degrad. Stab.*, 2006. **91**: p. 1651.
55. Lee, G.; Jagannathan, S.; Chae, H.; Minus, M.; Kumar, S., *Polymer*, 2008. **49**: p. 1831.
56. Dasari, A.; Rohrmann, J.; Misra, R., *Mater. Sci. Eng., A*, 2004. **364**: p. 357.
57. Al-Hosney, H.; Grassian, V., *J. Am. Chem. Soc.*, 2004. **126**: p. 8068.
58. Santschi, C.; Rossi, M., *J. Phys. Chem. A*, 2006. **110**: p. 6789.
59. Kuriyavar, S.; Vetrivel, R.; Hegde, Sooryakant., *J. Mater. Chem*, 2000. **10**: p. 1835.
60. Unger, K. K., *Porous silica : Its Properties and Use as Support in Column Liquid Chromatography*. 1979, Amsterdam: Elsevier Science p. 15.
61. Pham, K.; Fullston, D.; Crentsil, K., *J. Colloid Interface Sci.*, 2007. **315**: p. 123.
62. Bourgeat-Lami, E.; Lang, J., *J. Colloid Interface Sci.*, 1998. **197**: p. 293.
63. Kim, J.; Kim, L.; Kim, C., *Biomacromolecules*, 2007. **8**: p. 215.
64. Edward, P.; Moore, J, *Polypropylene Handbook*. 1996: Hanser Publishers: Munich Vienna New York. p. 13.
65. Ziegler, K.; Holzkamp, E.; Breil, H., *Angew. Chem.*, 1955. **67**: p. 541.
66. Welch, M.; Hsieh, H., *Olefin Polymerization Catalyst Technology*, in *Handbook of Polyolefins: Synthesis and Properties*, C.S. Vasile, R, Editor. 1993, Dekker New York. p. 21.
67. Albizzati, E.; Giannini, U.; Collina, G.; Noristi, L.; Resconi, L., *Catalysts and Polymerizations*, in *Polypropylene handbook*, J. Edward P. Moore, Editor. 1996, Hanser: Munich. p. 15.
68. Huang, J.; Rempel, G., *Prog. Polym. Sci.*, 1995. **20**: p. 459.
69. Wilkinson, G.; Birmingham, M., *J. Am. Chem. Soc.*, 1954. **76**: p. 4281.
70. Breslow, D.; Newburg, N., *J. Am. Chem. Soc.*, 1957. **79**: p. 5072.
71. Breslow, D.; Newburg, N., *J. Am. Chem. Soc.*, 1959. **81**: p. 81.

72. Reichert, K.; Meyer, R., *Makromol. Chem.*, 1973. **169**: p. 163.
73. Sinn, H.; Kaminsky, W., *Adv. Organomet. Chem.*, 1980. **18**: p. 99.
74. Wild, F.; Zsolnai, L.; Huttner, G.; Brintzinger, H., *J. Organomet. Chem.*, 1982. **232**: p. 233.
75. Ewen, J.; Jones, R.; Razavi, A.; Ferrara, J., *J. Am. Chem. Soc.*, 1988. **110**: p. 6255.
76. Yang, X.; Stern, C.; Marks, T., *J. Am. Chem. Soc.*, 1991. **113**: p. 3623.
77. Yang, X.; Stern, C.; Marks, T., *J. Am. Chem. Soc.*, 1994. **116**: p. 10015.
78. Bochmann, M.; Lancaster, S., *Organometallics*, 1993. **12**: p. 633.
79. Chien, J.; Tsai, W.; Rausch, M., *J. Am. Chem. Soc.*, 1991. **113**: p. 8570.
80. Mason, M.; Smith, J.; Bott, S.; Barron, A., *J. Am. Chem. Soc.*, 1993. **115**: p. 4971.
81. Harlon, C.; Mason, M.; Barron, A., *Organometallics*, 1994. **13**: p. 2957.
82. Sugano, T.; Matsubara, K.; Fujita, T.; Takahashi, T., *J. Mol. Catal.*, 1993. **82**: p. 93.
83. Zurek, E.; Ziegler, T., *Prog. Polym. Sci.*, 2004. **29**: p. 107.
84. Jordan, R., *Adv. Organomet. Chem.*, 1991. **32**: p. 325.
85. Arlman, E.; Cossee, P., *J. Catal.*, 1964. **33**: p. 99.
86. Green, M., *Pure Appl. Chem.*, 1972. **30**: p. 373.
87. Brookhart, M.; M, Green., *J. Organomet. Chem.*, 1983. **250**: p. 395.
88. Ewen, J., *J. Am. Chem. Soc.*, 1984. **106**: p. 6355.
89. Zakharov, V.; Bukatov, D.; Yermakov, I., *Adv. Polym. Sci.*, 1983. **51**: p. 61.
90. Mejzlik, J.; Lesna, M.; Kratochvila, J., *Adv. Polym. Sci.*, 1987. **81** p. 83.
91. Burfield, R., *Polymer*, 1984. **25**: p. 1645.
92. Coates, G., *Chem. Rev.*, 2000. **100**: p. 1223.
93. Busico, V.; Cipullo, R.; Esposito, V., *Macromol. Rapid Commun.*, 1999. **20**: p. 116.
94. Jungleing, S.; Mulhaupt, R.; Stehling, U.; Brintzinger, H., *J. Polym. Sci., Part A: Polym. Chem.*, 1995. **33**: p. 1305.

95. Stehling, U.; Diebold, J.; Kirsten, R.; Roell, W.; Brintzinger, H.; Juengling, S.; Muelhaupt, R.; Langhauser, F., *Organometallics* 1994. **13**: p. 964.
96. Resconi, L.; Fait, A.; Piemontesi, F.; Colonnesi, M.; Rychlicki, H.; Zeigler, R., *Macromolecules*, 1995. **28**: p. 6667.
97. Ochoteco, E.; Vecino, M.; Montes, M.; de la Cal, J., *Chem. Eng. Sci.*, 2001. **56**: p. 4169.
98. Huang, J.; Rempel, G., *Ind. Eng. Chem. Res.*, 1997. **36**: p. 1151.
99. Hlatky, G., *Chem. Rev.*, 2000. **100**: p. 1347.
100. Naundorf, C.; Matsui, S.; Saito, J.; Fujita, T.; Klapper, M.; Mullen, K., *J. Polym. Sci., Part A: Polym. Chem.*, 2006. **44**: p. 3103.
101. Wu, L.; Zhou, J.; Lynch, D.; Wanke, S., *Appl. Catal., A*, 2005. **293**: p. 180.
102. Fink, G.;Steinmetz, B.; Zechlin, J.; Przybyla, C.; Tesche, B., *Chem. Rev.*, 2000. **100**: p. 1377.
103. Sano, T.; Niimi, T.; Miyazaki, T.; Tsubaki, S.; Oumi, Y.; Uozumi, T., *Catal. Lett.*, 2001. **71**: p. 105.
104. Collins, S.; Kelly, W.; Holdenlc, D., *Macromolecules*, 1992. **25**: p. 1780.
105. Kaminsky, W.; Renner, F. Macromol., *Rapid Commun.*, 1993. **14**: p. 239.
106. Guimaraes, R.; Stedile, F.; dos Santos, J., *J. Mol. Catal. A: Chem.*, 2003. **206**: p. 353.
107. Kaminsky, W.; Winkelbach, H., *Top. Catal.*, 1999. **7**: p. 61.
108. Soga, K.; Kim, H. J.; Shiono, T., *Macromol. Rapid Commun.*, 1994. **15**: p. 139.
109. Jin, J.; Uozumi, T.; Soga, K., *Macromol. Rapid Commun.*, 1995. **16**: p. 317.
110. Bonds, D.; Brubaker J., H.; Chandrasekaran, S.; Gibbons, C.; Grubbs, H.; Kroll, C., *J. Am. Chem. Soc.*, 1975. **97**: p. 2128.
111. Britcher, L.; Rahiala, H.; Hakala, K.; Mikkola, P.; Rosenholm, J., *Chem. Mater.*, 2004. **16**: p. 5713.
112. Ribeiro, M.; Deffieux, A.; Portela, M., *Ind. Eng. Chem. Res.*, 1997. **36**: p. 1224.

113. dos Santos, J.; Larentis, A.; da Rosa, M.; Krug.; Baumvol, I.; Forte, M., *Macromol. Chem. Phys.*, 1999. **200**: p. 751.
114. Franceschini, F.; Tavares, T.; Santos, J.; Ferreira, M.; Soares., *J, Macromol. Mater. Eng.*, 2006. **291**: p. 279.
115. Chu, K.; Soares, J.; Penlidis, A., *J. Polym. Sci., Part A: Polym. Chem.*, 2000. **38**: p. 462.
116. Chen, X.; Rausch, D.; Chien, W., *J. Polym. Sci., Part A: Polym. Chem.*, 1995. **33**: p. 2093.
117. Chien, J.; He, D., *J. Polym. Sci., Part A: Polym. Chem.*, 1991. **29**: p. 1603.
118. Bianchini, D.; Stedile, F.; dos Santos, J., *Appl. Catal., A*, 2004. **261**: p. 57.
119. Soga, K.; Kaminaka, M., *Macromol. Rapid Commun.*, 1992. **13**: p. 221.
120. Bartczak, Z.; Argon, S.; Cohen, E.; Weinberg, M., *Polymer*, 1999. **40**: p. 2347.
121. Misra, R.; Nerikar, P.; Bertrand, K.; Murphy, D., *Mater. Sci. Eng., A*, 2004. **384**: p. 284.
122. Long, Y.; Shanks, A., *J. Appl. Polym. Sci.*, 1996. **61**: p. 1877.
123. Unal, H.; Mimaroglu, A.; Alkan, M., *Polym. Int.*, 2004. **53**: p. 56.
124. Takahara, A.; Magome, T.; Kajiyama, T., *J. Polym. Sci., Part B: Polym. Phys.*, 1994. **32**: p. 839.
125. Dibenedetto, A., *Mater. Sci. Eng., A*, 2001. **302**: p. 74.
126. Tjong, S., *Mater. Sci. Eng., R*, 2006. **53**: p. 73.
127. Lazzeri, A.; Thio, Y.; Cohen, R., *J. Appl. Polym. Sci.*, 2004. **91**: p. 925.
128. Jordan, J.; Jacob, K.; Tannenbaum, R.; Sharaf, M.; Jasiuk, I., *Mater. Sci. Eng., A*, 2005. **393**: p. 1.
129. Petrovic, Z.; Javni, I.; Waddon, I.; Banhegyi, G., *J. Appl. Polym. Sci.*, 2000. **76**: p. 133.
130. Vollenberg, P.; Heikens, D., *Polymer*, 1989. **30**: p. 1656.
131. Aso, O.; Eguiazabal, J.; Nazabal, J., *Compos. Sci. Technol.*, 2007. **67**: p. 2854.
132. Kim, G.; Michler, G., *Polymer*, 1998. **39**: p. 5689.
133. Kim, G.; Michler, G., *Polymer*, 1998. **39**: p. 5698.

134. Wu, L.; Zhang, Q.; Rong, Z.; Friedrich, K., *Compos. Sci. Technol.*, 2002. **62**: p. 1327.
135. Valentini, L.; Biagiotti, J.; Kenny, J.; Santucci, S., *Compos. Sci. Technol.*, 2003. **63**: p. 1149.
136. Assouline, E.; Lustiger, A.; Barber, A.; Cooper, C.; Wagner, H., *J. Polym. Sci., Part B: Polym. Phys.*, 2003. **41**: p. 520.
137. Demjen, Z.; Pukanszky, B.; Nagy, J., *Polymer*, 1999. **40**: p. 1763.
138. Wang, Y.; Lu, J.; Wang, G., *J. Appl. Polym. Sci.*, 1997. **64**: p. 1275.
139. Sudeep, P.; Emrick, T., *Polym. Rev.*, 2007. **74**: p. 155.
140. Yuan, Q.; Misra, R., *Polymer*, 2006. **47**: p. 4421.
141. Zebarjad, S.;Tahani, M.; Sajjadi, S., *J. Mater. Process. Technol.*, 2004. **155**: p. 1459.
142. Kovacevic, V.; Lucic, S.; Leskovac, M., *J. Adhesion Sci. Technol.*, 2002. **16**: p. 1343.
143. Karger-Kocsis, J., *Polypropylene: structure, blends and composites*. Vol. 3. 1995, London: Chapman and Hall. p. 8.
144. Aubouy, M.; Raphael, E, *Macromolecules*, 1998. **31**: p. 4357.
145. Pukanszky, B.; Fekete, E., *Adv. Polym. Sci.*, 1999. **139**: p. 109.
146. Isasi, R.; Mandelkern, L.; Galante, M.; Alamo, J., *J. Polym. Sci., Part B: Polym. Phys.*, 1999. **37**: p. 323.
147. Stricker, F.; Mulhaupt, R., *Polym. Eng. Sci.*, 1998. **38**: p. 1463.
148. Yu, Yiu-Wing Mai.; Zhong-Zhen, *Polymer nanocomposites*. 2006, Boca Raton: Woodhead Publishing Limited. p. 415.
149. Carrot, G.; Rutot-Houze, D.; Pottier, A.; Dege, P.; Hilborn, J.; Dubois. P., *Macromolecules*, 2002. **35**: p. 8400.
150. Reddy, C.; Das, C., *J. Appl. Polym. Sci.*, 2006. **102**: p. 2117.
151. Fekete, E.; Pukanszky, B.; Toth, A.; Bertoti, I., *J. Colloid Interface Sci.*, 1990. **135**: p. 200.
152. Demjen, Z.; Pukanszky, B.; Nagy, J., *Composites Part A*, 1998. **29**: p. 323.
153. Renger, C.; Burrows, J.; Shanks, A., *J. Appl. Polym. Sci.*, 2001. **82**: p. 3091.
154. Lin, D.; Huang, Z.; Zhang, Y.; Mai, C.; Zeng, M., *J. Appl. Polym. Sci.*, 2004. **91**: p. 2443

155. Zhu, P.; Zhang, P.; Yu, Y.; Dai, C., *J. Appl. Polym. Sci.*, 2004. **91**: p. 431.
156. Zhang, X.; Yu, Z.; Xie, L.; Mai,Y., *Polymer*, 2004. **45**: p. 5985.
157. Wan, W.; Chen, L.; Chua, C.; Lu, X., *J. Appl. Polym. Sci.*, 2004. **94**: p. 1381.
158. Xu, J.; Wang, Q.; Fan, Z., *Eur. Polym. J.*, 2005. **41**: p. 3011.
159. Shentu, B.; Li, J.; Gan, T.; Weng, Z., *Eur. Polym. J.*, 2007. **43**: p. 3036.
160. Nitta, K.; Asuka, K.; Liu, B.; Terano, M., *Polymer*, 2006. **47**: p. 6457.
161. Valentini, L.; Biagiotti, J.; Kenny, J.; Manchado, A., *J. Appl. Polym. Sci.*, 2003. **79**: p. 2657.
162. Zhang, G.; Yan, D., *J. Appl. Polym. Sci.*, 2002. **88**: p. 2181.
163. Gopakumar, T.; Lee, J.; Kontopoulou, M.; Parent, J., *Polymer*, 2002. **43**: p. 5483.
164. Ozawa, T, *Polymer* 1971. **12**: p. 150.
165. Qian, J.; He, P.; Nie, K., *J. Appl. Polym. Sci.*, 2004. **91**: p. 1013.
166. Jain, J.; Goossens, H.; Lemstra, P, *Polymer*, 2005. **46**: p. 8805.
167. Gersappe, D., *Phys. Rev. Lett.*, 2002. **89**: p. 1.
168. Zuiderduin, W.; Westzaan, C.; Huetink,J.; Gaymans, R., *Polymer*, 2003. **44**: p. 261.
169. Thio, Y.; Argon, A.; Cohen, R.; Weinberg, M, *Polymer*, 2002. **43**: p. 3661.
170. Chan, M.; Wu, J.; Li, X.; Cheung, K., *Polymer*, 2002. **43**: p. 2981.
171. Reynaud, E.; Jouen, T.; Gauthier, C.; Vigier, G.; Varlet, J., *Polymer*, 2001. **42**: p. 8759.
172. Lin, Y.; Chen, H.; Chan, C.; Wu, J., *Macromolecules*, 2008. **41**: p. 9204.
173. Chen, J.; Rong, M.; Ruan, W.; Zhang, M., *Compos. Sci. Technol.*, 2009. **69**: p. 252.
174. Beckera, O.; Varleyb, R.; Simon, G., *Polymer*, 2002. **43**: p. 4365.
175. Muratoglu, O.; Argon, S.; Cohen, R.; Weinberg, M., *Polymer*, 1995. **36**: p. 921.
176. Jiang, W.; Yuan, Q.; An, L.; Jiang, B., *Polymer*, 2002. **43**: p. 1555.

177. Enikolopian, N.; Volfson, S., *Filled Polyolefins*, in *Handbook of Polyolefins: Synthesis and Properties*, C.S. Vasile, R, Editor. 1993, Dekker New York. p. 767.
178. Kurokawa, Y.; Yasuda, H.; Oya, A., *J. Mater. Sci. Lett.*, 1996. **15**: p. 1481.
179. Pramanik, M.; Srivastava, S., *Macromol. Res.*, 2003. **11**: p. 260.
180. Oya, A.; Kurokawa, Y.; Yasuda, H., *J. Mater. Sci.*, 2000. **35**: p. 1045.
181. Greenland, D., *J. Colloid Sci.*, 1963. **18**: p. 647.
182. Ogata, N.; Jimenez, G.; Kawai, H.; Ogihara, T., *J. Polym. Sci., Part B: Polym. Phys.*, 1997. **35**: p. 389.
183. Agag, T.; Koga, T.; Takeichi, T., *Polymer*, 2001. **42**: p. 3399.
184. Jeon, H.; Jung, H.; Jung, S., *Polym. Bull.*, 1998. **41**: p. 107.
185. Zheng, J.; Ozisik, R.; Siegel, R., *Polymer* 2006. **47**: p. 7786.
186. Zheng, J.; Ozisik, R.; Siegel, R., *Polymer*, 2005. **46**: p. 10873.
187. Kontou, E.; Niaounakis, M., *Polymer*, 2006. **47**: p. 1267.
188. Rong, M.; Zhang, M.; Zheng,Y.; Zeng, H.; Friedrich, K., *Polymer*, 2001. **42**: p. 167.
189. Ou, Y.; Yang, F.; Yu, Z., *J. Polym. Sci., Part B: Polym. Phys.*, 1998. **36**: p. 789.
190. Ray, S.; Okamoto, M., *Prog. Polym. Sci.*, 2003. **28**: p. 1539.
191. Alexandre, M.; Dubois, P., *Mater. Sci. Eng., R*, 2000. **28**: p. 1.
192. Sun, T.; Garces, J., *Adv. Mater.*, 2002. **14**: p. 128.
193. Kaminsky, W.; Wiemann, K., *Compos. Interfaces*, 2006. **13**: p. 365.
194. Funck, A.; Kaminsky, W., *Compos. Sci. Technol.*, 2007. **67**: p. 906.
195. He, J.; Li, H.; Wang, X.; Gao, Y., *Eur. Polym. J.*, 2006. **42**: p. 1128.
196. Kaminsky, W.; Funck, a.; Klinke, C., *Top. Catal.*, 2008. **48**: p. 84.
197. Xie, X.; Liu, Q.; Li, R.; Zhou, X.; Zhang, Q., *Polymer*, 2004. **45**: p. 6665.
198. Jia, C.; Guo, H.; Hong, H., *Polym. Test.*, 2005. **2** p. 94.
199. Trujillo, M.; Arnal, M.; Muller, A., *Macromolecules*, 2007. **40**: p. 6268.
200. Zhou, X.; Xie, X.; Yu, Z.; Mai, Y., *Polymer*, 2007. **48**: p. 3555.
201. He, A.; Wang, L.; Li, J.; Dong, J.; Han, C., *Polymer*, 2006. **47**: p. 1767.
202. Shina, S.; Simona, L.; Soares, J.; Scholz. G., *Polymer*, 2003. **44**: p. 5317.

203. Jongsomjit, B.; Panpranot, J.; Praserthdam, P., *Mater. lett.*, 2006. **61**: p. 1376.
204. Scharlach, K.; Kaminsky, W., *Macromol. Symp.*, 2008. **261**: p. 10.
205. Garcıa, M.; van Zyl, W.; ten Cate, M.; Stouwdam, J.; Weickert, G., *Ind. Eng. Chem. Res.*, 2003. **42**: p. 3750.
206. Heinemann, J.; Reichert, P.; Thomann, R.; Mulhaupt, R., *Macromol. Rapid Commun.*, 1999. **20**: p. 423.
207. Alfred, C.; Jong-Young, L., *Polym. Rev.*, 2007. **47**: p. 217.
208. Pavlidoua, S.; Papaspyrides, C., *Prog. Polym. Sci.*, 2008. **33**: p. 1119.

Chapter 3: Heterogenization of metallocene catalysts: Methods and polymerization activity

.

3.1 Introduction

In situ polymerization with metallocene catalysts activated by MAO has received increasing attention in recent years. The significant growth in this field was driven by the expansion of the heterogenization processes of metallocene catalysts on supports for use in existing polymerization processes.

Many different supports have been investigated as carriers for these catalysts [1-3]. Among these, silica has emerged as a good choice. Compared with other supports, it exhibits improved catalytic activity after immobilization of the homogeneous catalysts [1, 4, 5]. The success of silica as a support is due to its surface characteristics in which the density of the OH group can be adjusted by means of thermal treatment and can easily be modified. On the other hand, $CaCO_3$ failed as a suitable carrier for metallocene catalysts due its hydrophobicity and low concentration of OH groups on the surface. Only a few papers report the use of $CaCO_3$ as support for metallocene catalysts [1].

As described in Chapter 2, there are three main methods by which to immobilize metallocene catalysts on these supports. The choice of method used in the preparation of supported catalysts has a great impact on the subsequent catalyst activity and the properties of the produced polymer.

The characteristics of these two fillers, in terms of their functional groups and their suitability as supports for the catalyst and the cocatalyst are described in this chapter. Different methods for heterogenization of metallocene catalyst were examined, and then optimized in terms of catalyst activity and polymer microstructure.

3.2 Experimental

3.1.1 Materials

All reactions were carried out under argon atmosphere. Nanosilica (15 nm) was obtained from Sigma-Aldrich. Uncoated calcium carbonate SOCAL® 31 (70 nm) was kindly donated by Solvay. The metallocene catalyst dimethylsilyl bis(2-methyl-4,5-benzo-indenyl)zirconium dichloride (rac-E$ZrCl_2$)

(MBI) was obtained from Boulder Scientific, and used as received. The cocatalyst MAO (10% solution in toluene) was purchased from Sigma-Aldrich and used as received. Toluene was dried by refluxing over sodium/benzophenone, distilled under a nitrogen atmosphere, and then stored over 4 Å molecular sieve.

3.1.2 Thermal treatment of filler

The filler particles were heated under vacuum at 100 ^{o}C and 250 ^{o}C in Schlenk tubes. The filler particles were heated until the desired temperature was reached and then held isothermally for 12 h, after which the sample was cooled to ambient temperature under a nitrogen atmosphere.

3.1.3 Preparation of supported catalysts

All air- and moisture-sensitive compounds (e.g. catalyst and cocatalyst) were handled using standard Schlenk techniques, or in a glovebox under a deoxygenated and dry argon atmosphere.

Different immobilization methods were used in this study for the preparation of the supported catalysts and different polymerization procedures were adapted accordingly. Scheme 3.1 illustrates all the different methods that were used to prepare the different supported catalysts. (*pre- means that the treated filler was used in propylene polymerization with preactivated catalyst solution).

3.1.3.1 Method 1: Direct adsorption of metallocenes on fillers (Zr-filler)

After the filler was heated to the desired temperature, a solution of 5 mg MBI (1.2 x 10^{-5} mol) in toluene was added to 1.0 g of pretreated filler in a Schlenk tube and the mixture stirred for 6 h at room temperature. The resulting solid produced was washed with toluene (5 x 10 mL). The clear supernatant was removed with a syringe and the powder was dried under vacuum. The zirconium content on the filler was measured by EDX analysis. [Note: 3 mL of external MAO was added during polymerization]

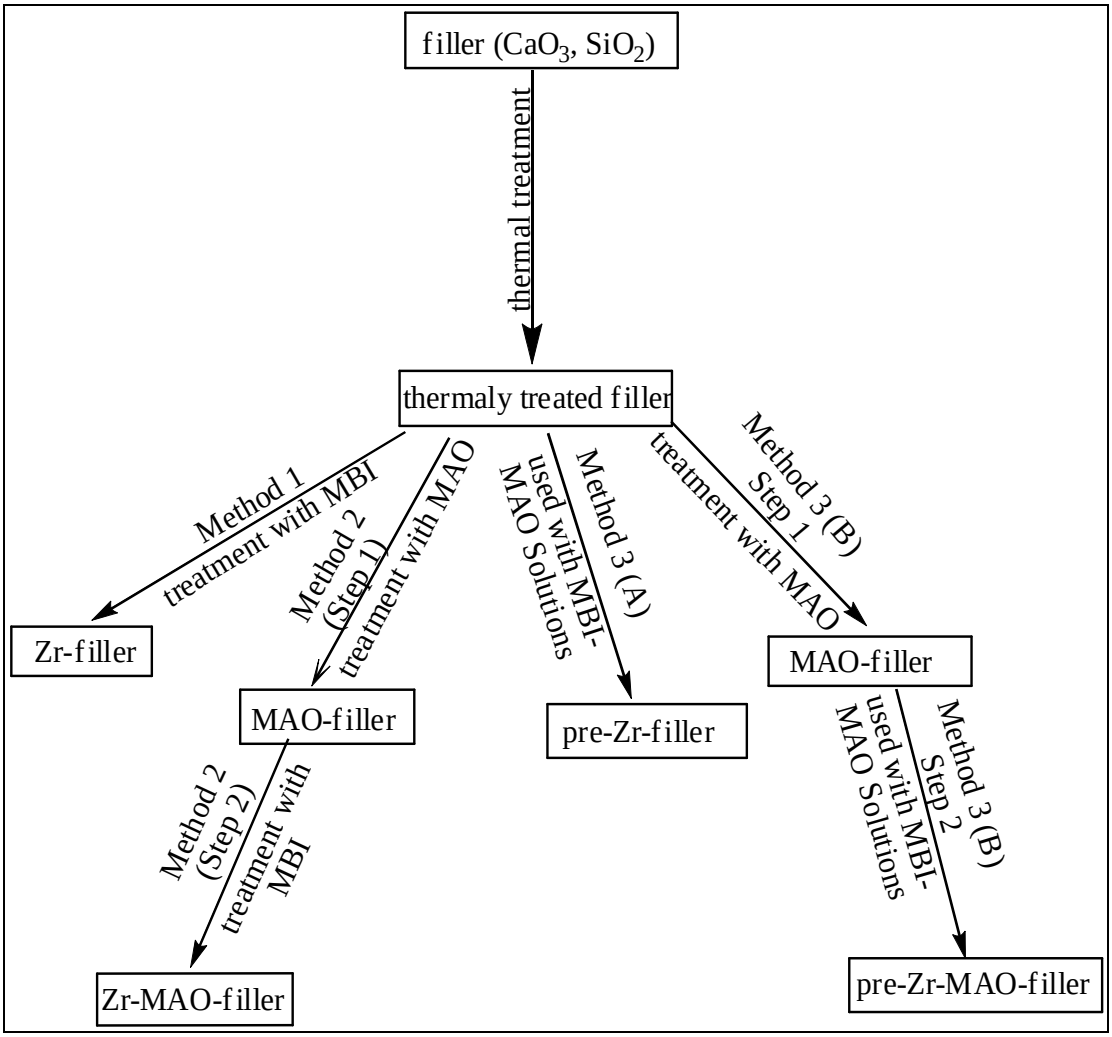

Scheme 3. 1: The different methods used for the preparation of the catalyst supports.

3.1.3.2 Method 2: Treatment of fillers with MAO followed by adsorption of metallocenes (Zr-MAO-filler)

After heating to the desired temperature, 1 g of filler was suspended in toluene (5 mL) in a Schlenk tube. A predetermined quantity of MAO (0.5, 1.5, 3.0 or 6.0 mL of a 10% solution in toluene) was added and the mixture stirred for 24 h at 60 ^{o}C. After cooling, the solid was washed with toluene (5 x 10 mL) and a white, powdery product was isolated. The products were MAO-SiO_2 or MAO-$CaCO_3$, respectively. EDX analysis was then used to determine the Al content on the filler. Typically 1 g of the product obtained in the previous step was reacted with 5 mg MBI (1.2 x 10^{-5} mol) for 6 h and then the resultant product was washed with toluene (5x10 mL). The supernatant solution was removed with a syringe and the yellow residue was dried under N_2 and

vacuum at 50 ^{o}C. The Al and Zr content on the fillers were measured by EDX analysis.

3.1.3.3 Method 3: Supporting of MAO preactivated metallocene

A) Using thermally treated fillers (pre-Zr -filler)

A toluene solution of MBI ($1.2x10^{-6}$ mol) was activated with 3 mL MAO and the mixture was allowed to react for 15 min. The mixture was then added to 1.0 g of thermally pretreated filler in a Schlenk tube and the mixture stirred for 6 h at room temperature. The catalyst mixture was used in propylene polymerization without further modification.

B) Using MAO treated fillers (pre-Zr-MAO-filler)

A toluene solution of MBI ($1.2x10^{-6}$ mol) was activated with 3 mL MAO and the mixture was allowed to react for 15 min. The mixture was then added to 1.0 g of MAO treated filler (MAO-SiO_2 or MAO-$CaCO_3$, method 2) in a Schlenk tube and the mixture stirred for 6 h at room temperature. This catalyst mixture was also used in propylene polymerization without further modification. (Note: the MAO treated fillers, MAO-SiO_2 and MAO-$CaCO_3$, are later used in different quantities with preactivated catalyst as described in the following chapter).

3.1.4 Propylene polymerization

The polymerization reactions were carried out in a 300 mL stainless steel autoclave. The empty reactor was pretreated under vacuum at high temperature to remove traces of water and oxygen. For each experiment, a certain mass of catalyst system corresponding to 1 g of the supported filler was suspended in 30 mL of toluene and transferred into the reactor via a syringe under argon. Three millilitres of MAO were added to the reactor as cocatalyst for the catalysts prepared by method 1 and method 2. No external MAO was used in the polymerization with catalysts prepared by method 3. The reactor was heated to the desired temperature and then pressurized with propylene (1.5 MPa). The reaction mixture was stirred at 60 ^{o}C for 1 h. To terminate the polymerization reaction the reactor was first vented and cooled,

and then acidic methanol (10% HCl) was added. The resulting polymer was filtered off, washed with methanol, and finally dried at 60 ^{o}C under reduced pressure.

3.1.5 Characterization techniques

3.1.5.1 EDX

Analyses of composition of the samples were accomplished using a Leo® 1430VP scanning electron microscope. Prior to imaging, the samples were sputter-coated with a thin gold layer. Phase compositions were quantified by EDX analysis using an Oxford Instruments® 133 KeV detector and Oxford INCA software.

3.1.5.2 FTIR

FTIR analyses were performed on a Perkin Elmer Paragon 1000 FTIR instrument at 32 scans, using a photo-acoustic (PAS) cell, eliminating the need for sample preparation. FTIR spectra were recorded in the range 4000-500 cm^{-1}, with a resolution of 4 cm^{-1}.

3.1.5.3 UV/Vis

The UV/Vis spectrometer operates on the double-beam principle, with one beam passing though the sample and the other passing though a reference cell. A Perkin Elmer UV/visible Lambda 20 spectrometer was used to identify the UV absorption band of the sample. The data were analyzed with UV Winlab v.4.2 software. Quartz cuvettes (supplied by CND Scientific) with a 10 mm path length were used.

3.1.5.4 HT-GPC

Mw and MWD of the polymers were determined by using HT-GPC. A PL-GPC 220 high temperature chromatograph was used at a solvent flow rate of 1 mL/min at 160 ^{o}C with a differential refractive index detector. Columns packed with a polystyrene/divinylbenzene copolymer (PL gel MIXED-B) from Polymer Laboratories were used. The length and diameter of these columns were 300 mm and 7.5 mm, respectively. Particle size was 10 µm. The concentration of the samples was 0.75 mg/mL. 1,2,4-trichlorobenzene (TCB),

stabilized with 0.0125 wt% 2,6-di-tert-butyl-4-methylphenol (BHT), was used as solvent. The calibration was done with monodisperse polystyrene standards. The PP samples were extracted from the nanocomposites using boiling xylene.

3.1.5.5 ^{13}C NMR

The isotactic pentad content (*mmmm%*) of PP was determined by ^{13}C NMR. ^{13}C NMR spectra of the samples were recorded at 120 ^{o}C on a Varian VXR 600 MHz spectrometer, with a repetition time of 0.82 seconds and a pulse angle of 45^{o}. The samples were dissolved in a 9:1 mixture of 1,2,4-trichlorobenzene:C_6D_6 by using the C_6D_6 at δ=128.02 ppm as internal secondary reference. Before recording the spectra the samples were placed in an oil bath at 120 ^{o}C for 2 h to homogenize the polymer solution in the NMR tube.

3.3 Results and discussion

3.3.1 Functional groups on the filler surface: Effect of the thermal treatment

Prior to treatment, the surface of the filler contains OH groups and adsorbed water molecules. When the filler is subjected to thermal treatment, water is removed at about 100 ^{o}C and with increasing temperature, the density of OH groups decreases by intermolecular reactions.

The FTIR spectrum of the silica particles before and after thermal treatment is shown in Figure 3.1. The bands at 3410 and 3650 cm^{-1}, for silica without any treatment, are attributed to physically adsorbed water. Thermal treatment of the silica particles under vacuum leads to a reduction in those bands.

The two bands at 1860 and 1625 cm^{-1} are due to Si–O stretching and should be of equal intensity in the absence of water.

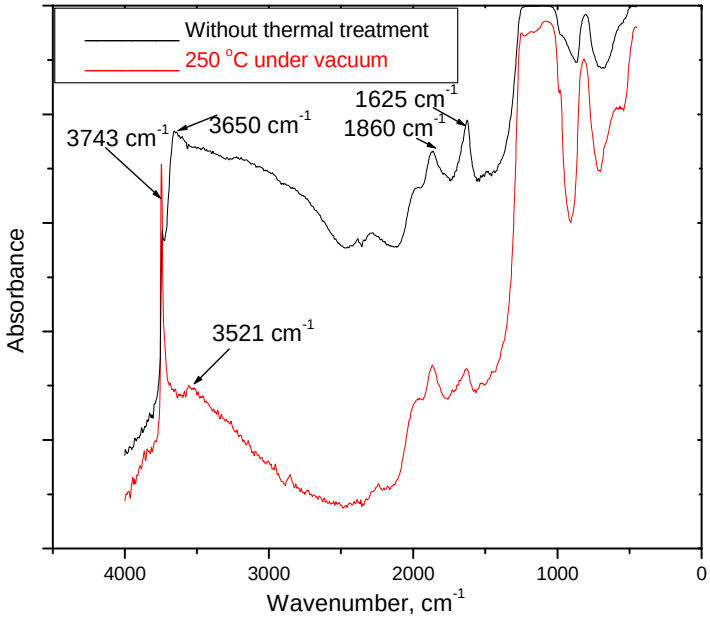

Figure 3.1: FTIR spectra of the silica particles before and after thermal treatment at 250 °C.

The silica surface after thermal treatment at 250 °C is characterized by a strong band at 3743 cm^{-1} attributed to Si-OH of isolated silanol groups (Figure 3.1). The absorption band at 3521 cm^{-1} may be due to vicinal silanol groups. All the vicinal silanol groups should convert to isolated silanol at 200 °C [6]. Thus the existence of the absorption band at 3521 cm^{-1} may have occurred as a result of handling the sample during FTIR analyses, or otherwise the thermal treatment is not as effective as reported [6].

The FTIR spectra of the $CaCO_3$ particles before and after thermal treatment are shown in Figure 3.2. FTIR spectra display characteristic absorption bands in the region 1850–650 cm^{-1}, corresponding to the four types of C–O bond vibrations.

The spectra exhibit a well defined sharp band at 3644 cm^{-1}, attributed to OH stretching. The intensity of this band did not change with thermal treatment under vacuum. It is reported that under ambient conditions of pressure, temperature and relative humidity, the surface chemistry of calcium carbonate will terminate with OH groups that persist even under ultrahigh vacuum conditions [7].

The broad band centred at 3400 cm^{-1} in the spectra is due to adsorbed water and to OH species having hydrogen bonding. With increasing temperature, the broad band was found to decrease in intensity due to water desorption (Figure 3.2). The band centred at 3000 cm^{-1} in the spectra is due to the stretching of the C=O and the C–H, which is attributed to the hydrocarbon groups and carbonic acid. The presence of hydrocarbon groups on the surface of $CaCO_3$ enhances its hydrophobicity.

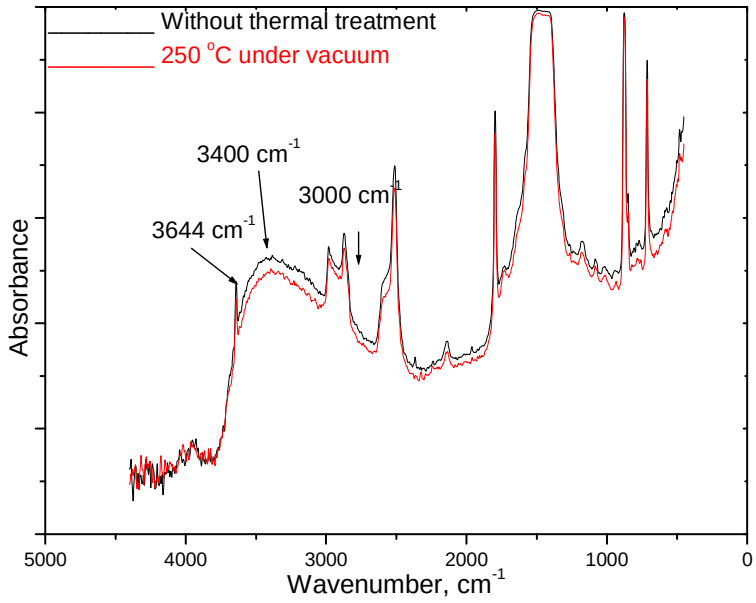

Figure 3.2: FTIR spectra of the $CaCO_3$ nanoparticles before and after thermal treatment at 250 °C.

3.3.2 Characterization of the supported catalysts

3.3.2.1 Direct reaction of metallocene on fillers

The reaction between the filler surface and a metallocene takes place by elimination of one or more of the original organometallic ligands (such as a halide) with the OH group (filler–OH) of the filler [8]. The OH groups of the filler play two conflicting roles in supporting the catalyst. On one hand the filler must have a number of OH groups in order for the catalyst to absorb on the support. On the other hand a large number of OH groups will deactivate the catalyst and result in low polymerization activity.

Figure 3.3 shows the surface catalyst loading as a function of thermal treatment temperature of the filler. It must be mentioned here that EDX analysis does not provide the exact Zr content on the support but rather it gives the relative percentage of Zr on the filler and provides a relative value of Zr loading for different supported catalysts. Figure 3.3 clearly shows that the Zr loading on the SiO_2 filler is much higher than that on the $CaCO_3$ filler. This can be explained by the higher intensity of the OH group on the SiO_2 than on the $CaCO_3$, as is evident from the FTIR spectra of the two fillers. The presence of hydrophobic hydrocarbon groups on the $CaCO_3$ surface, as indicated by the band at 3000 cm^{-1}, also has an impact in terms of reducing the reactivity of the $CaCO_3$ surface towards the metallocene catalyst.

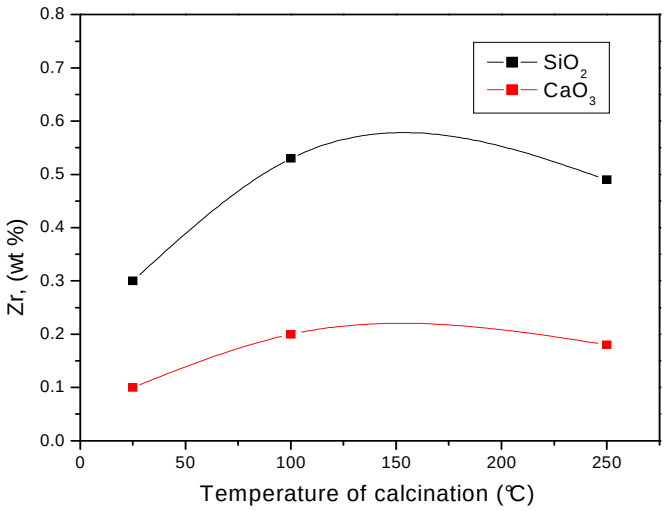

Figure 3.3: Zirconium content versus calcination temperature for SiO_2 and $CaCO_3$ fillers.

The effect of thermal treatment temperature on the Zr loading was similar for both fillers. The Zr loading increased as the thermal treatment temperature was increased from 25 to 100 ^oC. This might be due to the presence of the adsorbed water molecules on the filler surface. When the catalyst reacts with the filler, water molecules can act as an obstruction, preventing the catalyst from reacting with the OH groups on the filler surface. These water molecules and the excess catalyst can be easily removed during the washing step, resulting in a low Zr load in the final product. Unlike in the case of $CaCO_3$, where no change in the Zr content was observed as the treatment temperature of the fillers increased from 100 to 250 ^oC, a slight

decrease in the Zr loading in the case of SiO_2 was observed. This might be caused by a decrease in the density of OH groups at the higher calcination temperature.

3.3.2.2 Metallocene supported on MAO treated fillers

a) Optimization of initial MAO used for treatment

The effect of using various MAO concentrations on the final MAO loading in the filler was evaluated by EDX analysis. Figure 3.4 shows the effect of the initial MAO quantity per 1 g filler on the final MAO load on the filler surface (filler thermally treated at 250 ^{o}C). The MAO loading on both filler surfaces initially increases with an increase in the initial MAO quantity and tends to level off at MAO loadings higher than 1.5 mL (1.2 mmol) per g filler.

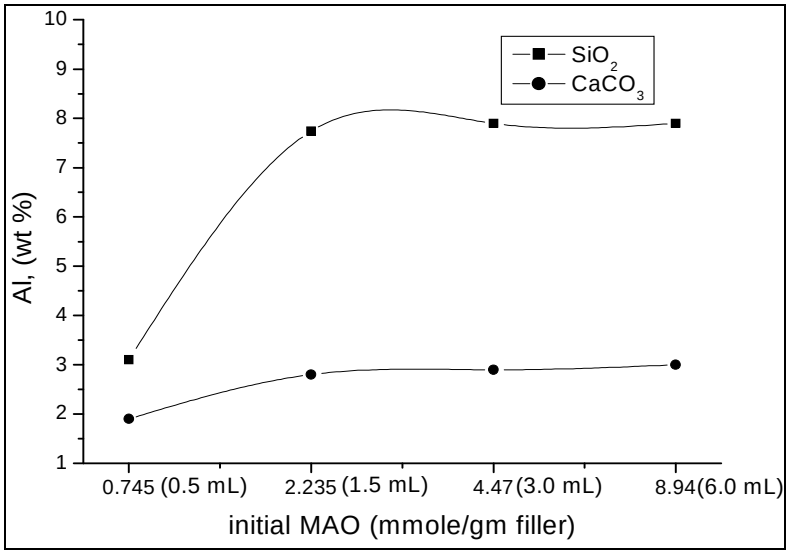

Figure 3.4: Effect of the initial MAO quantity on the final MAO loading in the filler (filler thermally treated at 100 ^{o}C and 250 ^{o}C for $CaCO_3$ and SiO_2, respectively).

These results suggest that the filler surface is saturated as the concentration of MAO reaches 2.2 mmol.g^{-1} filler. The concentration of the OH groups is the crucial factor that determines the reactivity of the filler surface toward the cocatalyst. For the silica, the initial amount of Al (MAO) is estimated according to the concentration of silanol groups per unit grams of silica at room temperature. The concentration of silanol groups of silica particles with a specific surface area identical to the silica used in this study is 1.9 mmol.g^{-1} [9].

b) Effect of filler thermal treatment temperature on MAO and metallocene loading for Zr-MAO-filler supported catalyst

The change in the OH group concentration as a result of thermal treatment will influence the MAO and metallocene loads on the support, and subsequently the microstructure of the polymer formed and the final nanocomposite properties.

Figure 3.5 shows the amount of MAO and Zr immobilized on the different filler surfaces versus the pretreatment temperature. Generally the loading of MAO and Zr on SiO_2 are higher than on $CaCO_3$, proving that silica is a better carrier than $CaCO_3$. Comparing Figure 3.5 with Figure 3.3 one can see that the impregnation of MAO on fillers prior to catalyst immobilization leads to a higher final catalyst content in both fillers.

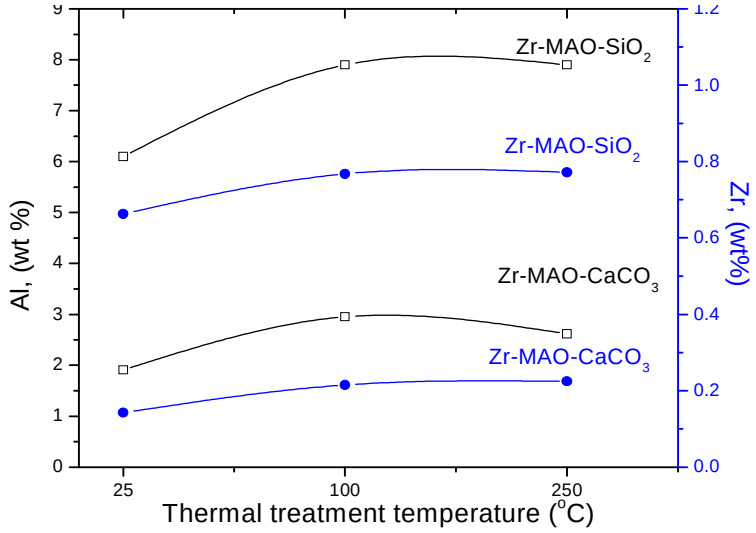

Figure 3.5: Effect of thermal treatment temperature of the filler on the final MAO and Zr loading for Zr-MAO-filler supported catalyst system (filler treated with 1.5 mL MAO).

Figure 3.5 shows that, for $CaCO_3$, the Al and Zr loading increased as the treatment temperature increased from 25 to 100 ^oC, and then decreased after this point. The low Al loading at low temperature is explained by the presence of water molecules at the filler surface. These water molecules act as a hindrance to MAO in reaching the surface, resulting in a physically absorbed MAO compound, which can be easily removed by the washing step after the immobilization step. In the case of $CaCO_3$, the decrease in the Al

loading above 100 ^{o}C is due to the decrease in the concentration of OH groups. For SiO_2 nanoparticles, on the other hand, Figure 3.5 shows that the MAO and Zr loading increase as the temperature increases until 100 ^{o}C, after which it levels out. This result indicates that the optimum calcination temperatures were 250 ^{o}C and 100 ^{o}C for silica nanoparticles and calcium carbonate, respectively.

3.3.2.3 Determination of the catalyst content in the filler

The Zr contents presented in the previous sections were relative percentage contents as determined by EDX. However, EDX analysis only gives the percentage of Zr on the support and not the quantity of Zr on the support. In order to compare the activity of the different polymerizations, as polymerization activity is determined per mol catalyst, the exact amount of the catalyst on the filler has to be obtained. In this study UV/Vis analysis was used to determine the Zr loading on the fillers according to the following procedure [10].

A standard curve was created, depicting the UV absorbance (A) of different concentrations of MBI catalyst solutions in toluene at 432 nm (see Figure 3.6).

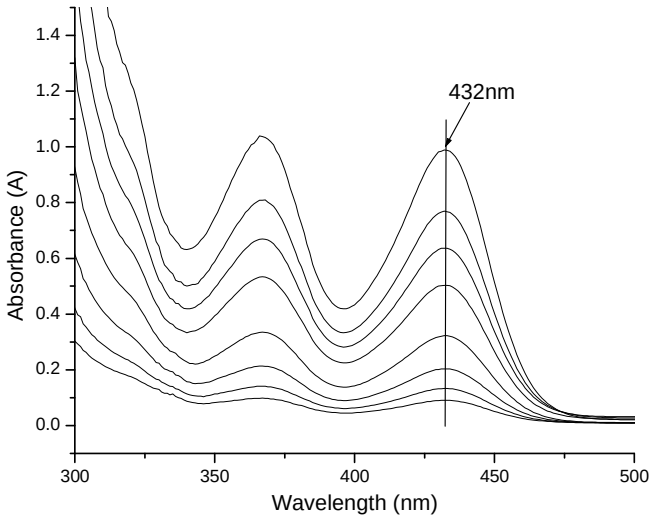

Figure 3.6: UV spectra of MBI catalyst solutions of various concentrations in toluene.

The metallocene content of the Zr-SiO_2 supported systems was calculated by determining the amount of unreacted metallocene present in the toluene solution used in preparation and subtracting this value from the total amount of metallocene compound originally present. Using the relative Zr percentage on the filler obtained from EDX, the Zr loadings of Zr-$CaCO_3$, Zr-MAO-SiO_2 and Zr-MAO-$CaCO_3$ supported systems were calculated. Table 3.1 shows the results of the Zr content for the different preparation procedures.

Table 3.1: Zr content on the filler [a]

Catalyst system	Zr (wt%) [b]	Zr (mol) [c]
Zr-SiO_2	0.49	$6.0x10^{-7}$
Zr-CaO_3	0.18	$2.3x10^{-7}$
Zr-MAO-SiO_2 [d]	0.772	$9.4x10^{-7}$
Zr-MAO-$CaCO_3$ [d]	0.225	$2.7x10^{-7}$

[a] calcination temperatures are 100 ^oC and 250 ^oC for $CaCO_3$ and SiO_2, respectively

[b] expressed in terms of wt% Zr/filler, determined by EDX

[c] expressed in terms of mol Zr g^{-1} catalyst

[d] initial MAO concentration was 2.2 mmol.g^{-1}.

3.3.3 Polymerization activity

All the results that are reported in this section were obtained from experiments in which the optimum conditions determined in the previous section. Table 3.2 presents data concerning the concentration of the catalyst species in the polymerizations, catalyst activity, and Mw of the polymers obtained with the homogeneous catalyst system, as well as for the supported catalysts.

The catalytic activity can be related to both the nature and the concentration of the species formed on the filler surface during immobilization. The concentration of the catalyst species per gram supported catalyst in the polymerization reaction is very low (see Table 3.2), despite the large amount of catalyst that was used in the supporting process ($1.2x10^{-5}$ mol). This is

more evident in the case of $CaCO_3$ filler due to its low OH group concentration as explained earlier.

The low zirconium concentration in the supported catalyst is, however, not the main reason for the low yield as the activity is measured as a function of catalyst concentration. For instance, the zirconium concentration of the Zr-$CaCO_3$ catalyst is approximately equivalent to that of the Zr-MAO-$CaCO_3$ catalyst. However, the latter was more active, indicating that there was inactive catalyst species within the Zr-$CaCO_3$ catalyst. This indicates that the OH groups have a negative effect on the catalyst activity when the catalyst is directly supported on the fillers.

Normally activities found for catalysts prepared by direct immobilization are much lower compared to soluble systems [1]. It is believed that only 1% of zirconocene-grafted species are active in polymerization [1, 11]. By supporting the metallocene catalysts, the bond energies in the transition state of the active site are increased, resulting in low activity [12]. Moreover, the steric role played by the filler surface itself may render difficult the access of the monomer to the active centres. These two factors may cause, in part, the reduction in activity.

The results also show that treatment of the filler surface before metallocene immobilization results in an improvement in activity compared to the direct immobilization, although activity is still lower compared to homogeneous systems. The activity of the Zr-MAO-$CaCO_3$ catalyst, which was slightly higher than that of Zr-MAO-SiO_2, indicates that deactivation of the catalyst by the filler remains one of the main factors responsible for reduced activity. Among the other possible reasons for this poor catalytic activity of the supported systems is the significant steric hindrance around the active site caused by the support surface, and the inefficient production of active sites during the immobilization process [13, 14].

Supported catalysts prepared using method 3, on the other hand, show a drastic increase in the polymerization activity. Given that no washing steps were performed during the preparation of these catalysts systems, the

presence of soluble metallocene (pre-Zr-filler and pre-Zr-MAO-filler) in the polymerizations probably has the major effect on improving the catalyst activity. As illustrated in Table 3.2, the activity of the pre-Zr-SiO_2 catalyst is high compared to the other systems in which the washing step was performed. It is, however, still lower than that of the homogenous system, illustrating the deactivation of the catalyst species that are adjacent to the filler surface. These results are consistent with those reported in literature [1, 5], where a one-step immobilization of a preactivated MAO/metallocene complex on a porous SiO_2 support is regarded as the best method and produces highly active polymerization catalysts.

Table 3.2: Experimental details and polymerization results of propylene polymerizations using different catalyst systems [a]

Catalyst	Zr (mol)	yield [b] (g)	activity [c]	Mw (Kg/mol)	*mmmm* (%)
homogenous [d]	$1.2x10^{-6}$	8.6	7125	123	94
Zr-SiO_2	$6.0x10^{-7}$	traces	-	-	-
Zr-CaO_3	$2.3x10^{-7}$	traces	-	-	-
Zr-MAO-SiO_2	$9.4x10^{-7}$	1.2	1280	162	90
Zr-MAO-$CaCO_3$	$2.7x10^{-7}$	0.7	2600	179	90
pre-Zr-SiO_2 [d]	$1.2x10^{-6}$	5.4	4500	116	89
pre-Zr-$CaCO_3$ [d]	$1.2x10^{-6}$	6.1	5080	112	84
pre-Zr-MAO-SiO_2 [d]	$1.2x10^{-6}$	7.5	6250	99	82
pre-Zr-MAO-$CaCO_3$ [d]	$1.2x10^{-6}$	7.9	6581	103	89

[a] polymerization conditions: filler 1 g; MAO 3mL; Tp 60 ^oC; polymerization time 1 h.

[b] weight of the filler was subtracted from the yield.

[c] activity (kg PP/molZr.h).

[d] Al/Zr 3700.

The results also indicate that the pre-Zr-$CaCO_3$ catalyst has higher activity than that of the pre-Zr-SiO_2 catalyst due to the differences in the concentration of OH groups and reactivity of the fillers.

The pre-Zr-MAO-filler catalyst, on the other hand, exhibits activity comparable to that of the homogenous catalyst. Theoretically, there are two types of catalyst species present in the polymerization reaction: supported catalyst, which would be an insignificant proportion of the total catalyst and would have lower activity, and the other homogenous catalyst species making up a high percentage and having higher activity.

The author elected to use the pre-Zr-MAO-filler catalyst system in the synthesis of PP nanocomposites, because it has the advantage of both the supported and the homogeneous catalyst species. The supported catalyst species produces PP chains on the surface of the filler to assure a good interaction between the filler and the matrix and the homogeneous catalyst provides reasonable productivity. More detail on this catalyst system will be provided in the following chapter.

3.3.4 PP microstructure

Table 3.2 also shows that the polymer Mw obtained with the Zr-MAO-filler system is higher than that obtained with the homogenous system. It is reported that the molecular weights of PP obtained with the supported systems are higher than those obtained with the homogeneous ones [15, 16]. However, it is also reported that catalyst systems analogous to Zr-MAO-filler catalyst systems afford PP having a Mw identical to PP produced by homogeneous metallocenes [17].The increase in the Mw of the PP obtained by Zr-MAO-filler catalyst compared to that of PP obtained the by homogenous system could be attributed to the blocking of one of the two active sides by the support, hindering the deactivation step. In other words, the β-elimination transfer between two metallocene centres is hindered, resulting in a larger growth of the polymer chain, and thus in a higher molecular weight [18]. Another possible explanation for the increase in the Mw of PP produced using Zr-MAO-filler catalyst is the reduction in the concentration the active species in the polymerization reaction [19, 20].

Use of pre-Zr-filler catalyst resulted in PP that had a Mw slightly lower than that produced by the homogenous catalyst. These results might be due

to the steric role played by the filler surface, which may retard the monomer's access to the active centres, reducing the propagation rate, and creating opportunity for chain termination to take place.

Use of pre-Zr-MAO-filler catalyst systems, on the other hand, resulted in PP that had a Mw lower than that resulting from the use of both the pre-Zr-filler catalyst system and the homogenous catalyst. Besides the steric role played by the filler surface in similar way to the pre-Zr-filler catalyst, the decrease in the Mw was also aided by the increase in the concentration of the active sites after MAO treatment.

Concerning the tacticity of polymer, the isotacticity of the obtained PP is lower compared with that obtained when using the homogeneous catalyst. This result was in agreement with what has been reported in the literature [12, 21]. The steric hindrance around the active sites caused by the filler surface decreases the $\Delta\Delta E^{\ddagger}$ between the insertion of the two enantiofaces. Thus, stereoerrors are more likely to occur, and polymer with a lower tacticity is produced.

3.4 Conclusions

Results reported in this chapter show that a metallocenes catalyst can be successfully supported on both silica and calcium carbonate nanoparticles and the catalyst produced can be used for the synthesis of nanocomposites via in situ polymerization. The influence of selected parameters in the development of a procedure for metallocene immobilization was studied. In general, the impregnation of MAO on filler prior to metallocene immobilization (Zr-MAO-filler) led to higher catalyst content on the filler and higher activity than the direct grafting of the metallocene on the fillers (Zr-filler). Generally, all Zr-filler and Zr-MAO-filler supported catalysts showed low activity compared with a homogenous catalyst. On the other hand, the supported catalyst prepared with preactivated catalyst (pre-Zr-filler and pre-Zr-MAO-filler (method 3)) showed a huge improvement in polymerization activity. Furthermore there is a strong indication that in order to make in situ nanocomposites comparable

to melt-mixed nanocomposites, supported catalyst systems prepared via method 3 should be used.

3.5 References

1. Hlatky, G., *Chem. Rev.*, 2000. **100**: p. 1347.
2. Naundorf, C.; Matsui, S.; Saito, J.; Fujita, T.; Klapper, M.; Mullen, K., *J. Polym. Sci., Part A: Polym. Chem.*, 2006. **44**: p. 3103.
3. Wu, L.; Zhou, J.; Lynch, D.; Wanke, S., *Appl. Catal., A*, 2005. **293**: p. 180.
4. Sano, T.; Niimi, T.; Miyazaki, T.; Tsubaki, S.; Oumi, Y.; Uozumi, T., *Catal. Lett.*, 2001. **71**: p. 105.
5. Fink, G.;Steinmetz, B.; Zechlin, J.; Przybyla, C.; Tesche, B., *Chem. Rev.*, 2000. **100**: p. 1377.
6. Unger, K. K., *Porous silica : Its Properties and Use as Support in Column Liquid Chromatography*. 1979, Amsterdam: Elsevier Science p. 15.
7. Al-Hosney, H.; Grassian, V., *J. Am. Chem. Soc.*, 2004. **126**: p. 8068.
8. dos Santos, J.; Krug, C.; da Rosa.; M.; Stedile, F.; Dupont, J.; Forte, M., *J. Mol. Catal. A: Chem.*, 1999. **139**: p. 199.
9. Rahman, I.; Vejayakumaran, C.; Sipaut, S.; Ismail, J.; Chee, C., *Mater. Chem. Phys.*, 2009. **114**: p. 328.
10. Collins, S.; Kelly, W.; Holdenlc, D, *Macromolecules*, 1992. **25**: p. 1780.
11. Guimaraes, R.; Stedile, F.; dos Santos, J., *J. Mol. Catal. A: Chem.*, 2003. **206**: p. 353.
12. Kaminsky, W.; Winkelbach, H., *Top. Catal.*, 1999. **7**: p. 61.
13. Franceschini, F.; Tavares, T.; Santos, J.; Ferreira, M.; Soares., *J, Macromol. Mater. Eng.*, 2006. **291**: p. 279.
14. Chu, K.; Soares, J.; Penlidis, A., *J. Polym. Sci., Part A: Polym. Chem.*, 2000. **38**: p. 462.
15. Britcher, L.; Rahiala, H.; Hakala, K.; Mikkola, P.; Rosenholm, J., *Chem. Mater.*, 2004. **16**: p. 5713.
16. Bianchini, D.; Stedile, F.; dos Santos, J, *Appl. Catal., A*, 2004. **261**: p. 57.

17. Ribeiro, M.; Deffieux, A.; Portela, M., *Ind. Eng. Chem. Res.*, 1997. **36**: p. 1224.
18. dos Santos, J.; Larentis, A.; da Rosa, M.; Krug.; Baumvol, I.; Forte, M., *Macromol. Chem. Phys.*, 1999. **200**: p. 751.
19. Palza, H.; Velilla, T.; Quijada, R., *Polym. Plast. Technol. Eng.*, 2006. **45**: p. 85.
20. Huang, J.; Rempel, G., *Prog. Polym. Sci.*, 1995. **20**: p. 459.
21. Kaminsky, W.; Funck, A.; Klinke, C., *Kinet. Catal.*, 2006. **24**: p. 221.

Chapter 4: Synthesis and characterization of PP nanocomposites via in situ polymerization and melt-mixing

4.1 Introduction

The properties of PP nanocomposites are largely determined by the microstructure of the polymer matrices, the nature of nanofillers, and the way in which the nanocomposites are prepared.

Furthermore, the way in which the nanofillers are incorporated into the polymer matrix has a huge influence on the performance of the final product as it determines the dispersion of nanofillers in a polymer matrix and interactions with the matrix. The uniform dispersion of nanofillers in a polymer matrix is a general prerequisite for achieving the desired mechanical and physical characteristics.

In situ polymerization of monomers in the presence of nanofillers is a useful method for achieving a more homogeneous distribution of inorganic nanoparticles, due to the close contact of polymer and filler during synthesis [1-5]. However, the in situ preparation of the polymer matrix in the presence of the nanofillers will add new parameters to the polymerization reaction and control over the polymer microstructure becomes more complicated.

One of the drawbacks of the in situ polymerization is the uncontrolled and drastic decrease in the catalyst activity, which makes determining the final filler loading more complicated. In addition, the changes that occur in the polymer microstructure during polymerization due to the presence of the fillers could have a significant effect on the properties of the nanocomposites.

Although some authors have reported that there is no correlation between the presence of the nanofillers and the chemical properties of the polymer matrix [4, 6], others have found that the polymer matrix microstructure depends on the filler content [7, 8].

Investigating the effect of the presence of the fillers with different filler loadings on the catalyst activity and on the matrix microstructure obtained is essential. This then enables the preparation of in situ prepared nanocomposites with controlled final filler loads and polymer matrix microstructures.

This chapter deals with the effect of the filler on the polymerization kinetics and also the effect of different filler loadings on the catalyst activity and on the produced polymers' microstructure. Comparison of the morphological characteristics of various PP nanocomposites prepared via in situ polymerization and melt-mixing methods is also addressed.

4.2 Experimental

4.2.1 Materials

See Section 3.1.1

4.2.2 Polymerization kinetics

For the polymerization kinetics study, the stainless steel autoclave reactor was divided into four different minireactors of 30 mL each. Four reactions could therefore be performed simultaneously namely a homogeneous polymerization, an in situ polymerization using MAO-SiO_2, and using MAO-$CaCO_3$, and to eliminate experimental error, a homogenous reaction was performed in the fourth reactor as a reference. The empty reactor was pretreated under vacuum at high temperature to remove water and oxygen traces. In a typical polymerization reaction, 100 mg of MAO-filler (see Section 3.1.3.3) was reacted with 5.5 x 10^{-7} mol preactivated catalyst solution with MAO (reacted for 15 min) equivalent to Al/Zr 2000. This mixture was introduced into the minireactor. A continuous monomer pressure of 1.5 MPa was maintained throughout the duration of the polymerization. The reaction was stirred at room temperature to the designated period of time, after which the reactor was vented and then acidic methanol (10% HCl) was added.

4.2.3 Synthesis of the nanocomposites

4.2.3.1 In situ polymerized nanocomposites

The polymerization reactions were carried out in a 300 mL stainless steel autoclave. The empty reactor was pretreated under vacuum at high temperature to remove water and oxygen traces. The desired amount of MAO

treated filler was reacted with activated catalyst (MBI 2.2 x 10^{-6} mol; Al/Zr 2000) in a Schlenk tube for 6 h. Toluene (30 mL) was then added to the mixture, which was then transferred into the reactor via a syringe, under an argon atmosphere. The reactor was heated to the desired temperature then pressurized with propylene (1.5 MPa). The reaction mixture was stirred at the desired temperature for 1 h. In order to terminate the polymerization reaction the reactor was first vented and cooled, and then acidic methanol (10% HCl) was added. The resulting polymer was filtered off, washed with methanol, and finally dried at 60 ^{o}C under reduced pressure.

4.2.3.2 Melt-mixed nanocomposites

A) The preparation of PP homopolymer

The method used here was similar to that described in Section 4.2.3.1 except that no MAO treated filler was added.

B) Compounding procedure

The filler particles were dried by heating to 100 ^{o}C under vacuum for 6 h before melt-compounding. In a typical experiment, 1.0 g of PP homopolymer and the predetermined filler quantity were compounded in a Schlenk tube under nitrogen with mechanical stirring at 200 ^{o}C. A rotation speed of 60 rpm was used for 10 min. Due to the low Mw of the PP, and the small quantity of the PP homopolymer used, it was possible to use a Schlenk tube with mechanical stirring for the melt-compounding.

4.2.4 Characterization techniques

4.2.4.1 HT-GPC

High-temperature GPC analyses of the samples were performed according to the procedure described in Chapter 3 (Section 3.2.5.4).

4.2.4.2 CRYSTAF

Crystallization analysis fractionation was carried out using a CRYSTAF commercial apparatus model 200 manufactured by Polymer Char S.A. The

crystallization from solution was carried out in 5 stainless steel reactors of 60 ml capacity each where dissolution and filtration takes place automatically. A sample of 20 mg was used in each reactor. TCB was used as the solvent. The temperature was decreased from 100 to 30 ^{o}C at a cooling rate of 0.25 ^{o}C/min.

4.2.4.3 DSC

The Tc, Tm, and Xt were determined by DSC. DSC analyses on the different polymers were carried out with a TA Instruments Q100 DSC system. The DSC was calibrated by measuring the melting temperature of indium metal according to a standard procedure. All measurements were conducted under a nitrogen atmosphere flow rate of 50 mL/min. The samples (1.0 to 3.0 mg) were heated in aluminum pans from 25 to 220 ^{o}C at 10 ^{o}C/min, held isothermally at 220 ^{o}C for 5 minutes, and cooled to –30 ^{o}C at a rate of 10 ^{o}C/min while recording the crystallization curve. At –30 ^{o}C the temperature was kept constant for 5 min after which the melting curve was recorded between –30 and 190 ^{o}C at a heating rate of 10 ^{o}C/min.

4.2.4.4 ^{13}C NMR

The ^{13}C NMR data of the samples were obtained according to the procedure described in Chapter 3 (Section 3.2.5.5)

4.2.4.5 TEM

TEM experiments were performed using a JEOL 200 CX instrument. Prior to analysis, samples of the nanocomposites were stained with OsO_4, then embedded in epoxy resin and cured for 24 h at 60 ºC. The embedded samples were then cut into slices of a nominal thickness of 100 nm using an ultra-microtome with a diamond knife on a Reichert Ultracut S ultra microtome at room temperature.

4.2.4.6 SEM

SEM images were obtained using a Leo® 1430VP scanning electron microscope. Prior to imaging the samples were sputter-coated with a thin gold layer.

4.2.4.7 OM

A Zeiss Axiolab polarized optical microscope with a high resolution digital camera was used to examine the effect of the nanofiller on the crystal structure of the composites.

4.2.4.8 TGA

Thermogravimetric analyses were carried out using a TGA-50 SHIMADZU thermogravimetric instrument, with a TA-50 WSI thermal analyzer connected to a computer. Samples (10–15 mg) were degraded in a nitrogen atmosphere. The gas flow rate was 50 mL/min, and the heating rate was 20 ℃/min.

4.3 Results and discussion

A challenging aspect related to the in situ polymerization of olefins is the decline in the catalyst activity due to the deactivation of the active sites by the filler surface. Therefore, considerable effort has been made in this study to obtain catalyst activity comparable to that of a homogenous catalyst.

4.3.1 Effect of the filler particles on the polymerization kinetics

Before addressing the effect of the filler on the catalyst performance in terms of its activity and the microstructure of the formed polymer matrix, it is important to discuss the polymerization kinetics and how the filler influences the rate of polymerization.

There are two different active sites present in the polymerization media: one is supported on the filler (to facilitate good interaction between the filler and the matrix), and the other is a soluble active site, necessary to maintain the high activity of the metallocene catalyst.

Olefin polymerization catalyzed by a metallocene catalyst involves several steps: catalyst activation, propagation, and catalyst deactivation. The effect of the filler will only be on the propagation and the deactivation reactions. The effect of the filler on the activation step is, however, insignificant as the metallocene catalyst was allowed to react with the MAO for 15 min before the polymerization was carried out.

As mentioned earlier (Section 3.3.3) the percentage and reactivity of the soluble active species are much higher than of the supported active species. Therefore, the latter should have little effect on the polymerization rate.

The polymerization rate (R_p) curve for each of the experiments was generated from the productivity of the catalyst at different polymerization times with continuous monomer pressure. The monomer pressure, amount of MAO-filler, Tp, and catalyst and cocatalyst concentrations were kept constant for all runs. Table 4.1 summarizes the polymerization conditions, the experimental details, and polymer yields of each run.

Table 4.1: Polymerization conditions, experimental details and polymer yields of each polymerization run [a]

Polymerization time (min)	No Filler		SiO_2 fillers		$CaCO_3$ fillers	
	Yield (g)	Activity [b]	Yield [c] (g)	Activity [b]	Yield [c] (g)	Activity [b]
3	0.17	6036	0.097	3527	0.060	2181
7	0.47	7371	0.286	4457	0.339	5282
10	0.71	7789	0.480	5236	0.514	5607
20	0.94	5664	0.552	3556	0.760	4145
40	1.18	3218	0.900	2454	1.270	3463
60	1.43	2600	1.450	2636	1.800	3272

[a] 100 mg MAO-filler; Tp 25 ^{o}C; [M] 1.5 MPa; [Zr] 5.5 X 10^{-7} mol; Al/Zr 2700.

[b] activity (kg PP/molZr.h). [c] weight of the filler was substrated from the yield.

The R_p curves for the homogenous polymerization and in situ polymerization in the presence of different fillers are shown in Figure 4.1. All the curves show a similar trend. The polymerization activities reach a maximum at the beginning of the reaction and then decreases over time. The induction period in the polymerization rate is due to the propylene monomer saturation and should not be considered as a catalytic decay period or catalyst activation period. It has been explained as a slow rate of insertion of the first monomer unit in the Zr–methyl bond of the alkylated metallocene [9].

The reduction of the R_p after the maximum is reached is attributed to the formation of both reversibly and permanently deactivated sites. Deactivation is known to occur via a bimolecular mechanism [10, 11]. Busico et al. [12] suggest that diffusion limitations might occur at longer times.

Figure 4.1 shows that at low polymerization times the R_p of the homogenous polymerization is higher than that of the in situ polymerizations and decreases more rapidly with polymerization time.

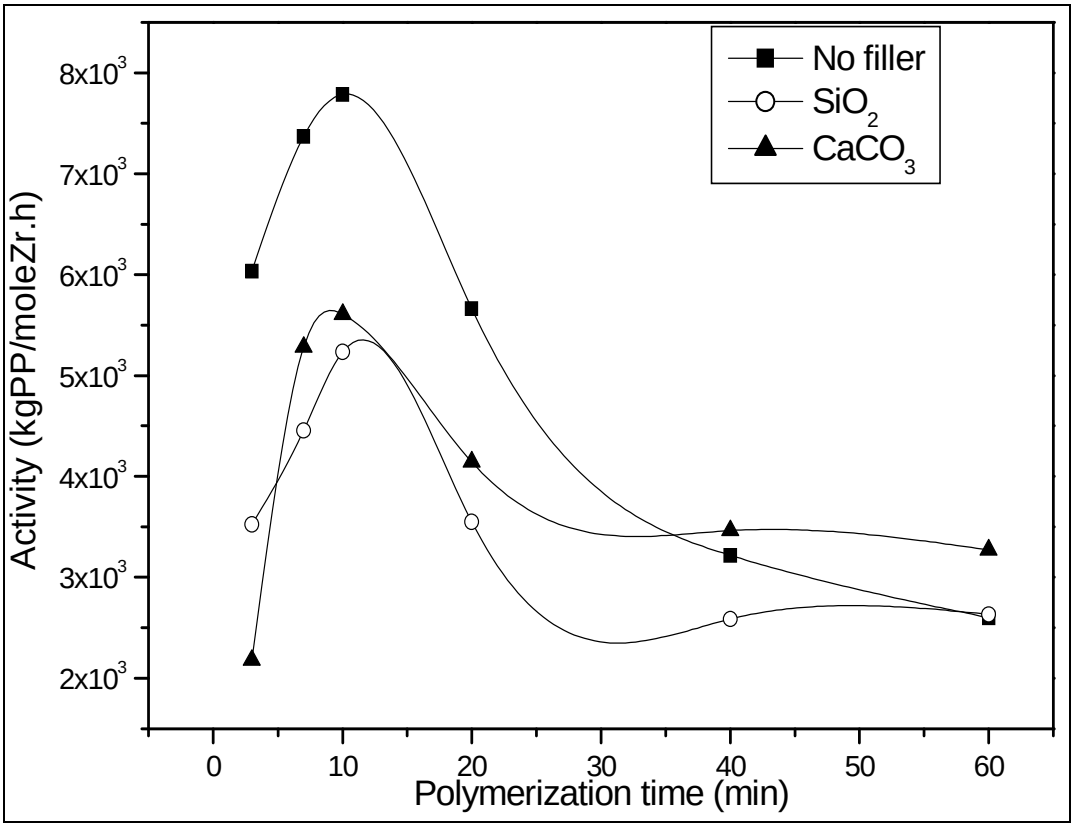

Figure 4.1: Polymerization rate versus time profiles for propylene polymerizations with homogenous and in situ polymerization.

The pathway of a polymerization reaction in which a metallocene catalyst is used is complicated, and several different reactions can occur at the active centre. The relative values of the rate constants of these different possible reactions determine the activity of the catalyst and the microstructure of the polymer subsequently obtained under certain polymerization conditions. To understand the effect of the different fillers on the rate constants of these possible reactions it is essential to identify the parameters that control these rate constants and examine how the filler possibly influences these parameters.

The R_p depends on the concentration of viable active sites [C*], the monomer concentration [M], and the average propagation rate constant (k_p), and can be expressed as:

$$R_p = k_p [C^*] [M]$$

If one assumes that no monomer diffusion limitations arise and that the monomer concentration is similar at all active sites and under similar polymerization conditions, the concentration of active sites determines the polymerization rate.

The deactivated sites and the dormant sites (D) influence the concentration of the active sites. The rate of deactivation depends on the concentration of active sites, thus it is not possible to estimate [C*] because it will be a function of polymerization time.

$$[C^*] = [Zr] - [C\ dormant] - [C\ dead]$$

The lower R_p of the in situ polymerization compared to that of the homogenous polymerization might be due to deactivation of the catalyst by the filler or the presence of dormant sites at low polymerization time, which will later become active. The slow decay of R_p of the in situ polymerization compared with the fast decay of the R_p of the homogenous polymerization at high polymerization time confirms that the low R_p value for the in situ polymerizations is caused by dormant sites which will be active later.

^{13}C NMR spectra of different PPs prepared via homogenous polymerization and in situ polymerization in the presence of the filler are shown in Figure 4.2.

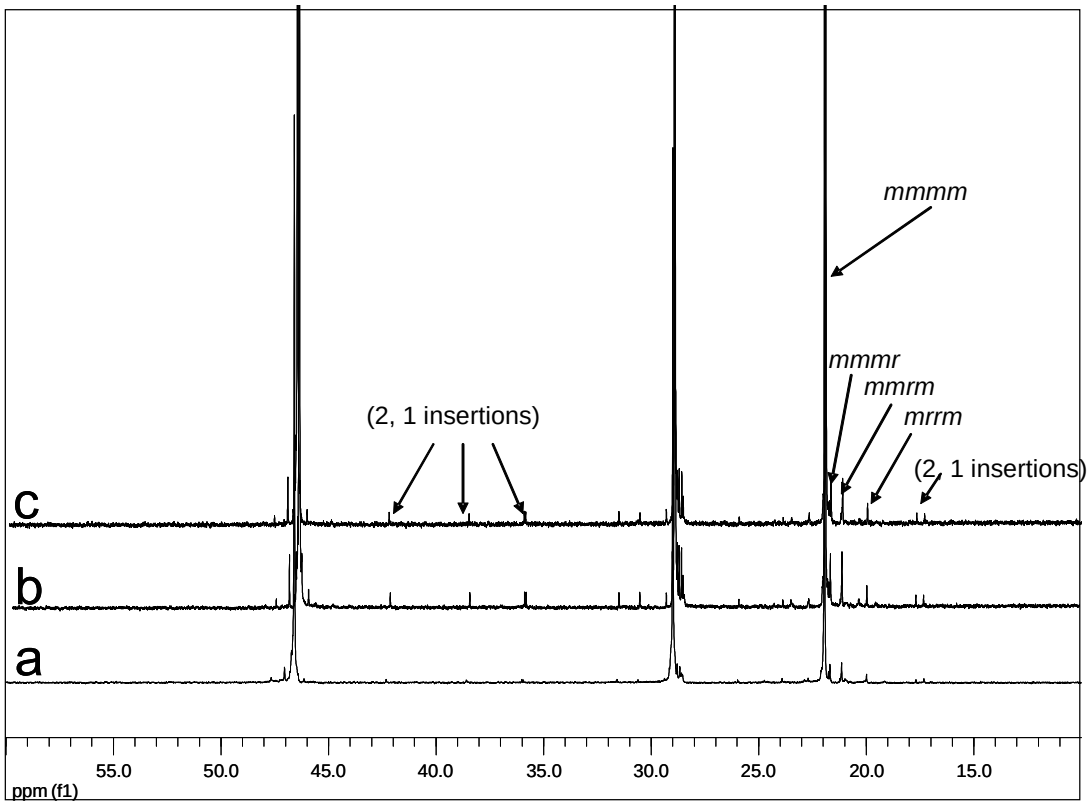

Figure 4.2: ^{13}C NMR spectra of PP prepared with MBI catalyst: a) homogenous polymerization; b) in situ polymerization using MAO-SiO_2; c) in situ polymerization using MAO-$CaCO_3$.

A higher percentage of isolated secondary propylene units (2, 1 insertions) is evident in the in situ polymerized PPs compared with the homogenous polymerized PP. These regiodefects have a strong effect in terms of reducing the propagation rate due to the lower monomer insertion rate at a secondary growing chain end [9]. This result supports the suggestion that the lower R_p of the in situ polymerization at low polymerization times is due to the reversible switching of the soluble active site to a dormant site. Due to the nanoscale size of the filler particles, steric effects are most probably the cause of the regiodefects because the monomer concentration and the Tp have been reported to have no effect on the formation of regiodefects [9] and it is only the metallocene structure that determines their formation.

The slow decay of R_p of the in situ polymerization compared with the fast decay of the R_p of the homogenous polymerization at high polymerization time could also be explained by monomer diffusion limitations. The regiodefects have a strong effect on reducing the crystallinity percentage of the formed PP and facilitates the monomer to reach the active site and hence a high polymerization rate over time is maintained for the in situ polymerization. On the other hand, the high crystallinity of the formed polymer in the homogenous polymerization will restrict the monomer diffusion and consequently a decrease in R_p was obtained at high polymerization time. The effect of the presence of the nanofiller on the PP microstructure will be discussed in Section 4.3.3.2 and Section 4.3.3.3.

4.3.2 Effect of Tp on the catalyst activity

Because temperature plays a vital role in polymerization a series of polymerizations was performed, each reaction at different temperature, in order to determine the temperature at which the best activity is obtained. Figure 4.3 shows that increasing the Tp resulted in an increase in the catalyst activity until a maximum was reached at 60 ^{o}C, after which the activity decreased slightly.

In general, higher Tp results in an increased chain propagation rate, thus higher catalytic activity. However, the accelerated deactivation rate of the catalyst and the reduction of monomer solubility in toluene at higher temperatures might decrease the catalytic activity [13, 14].

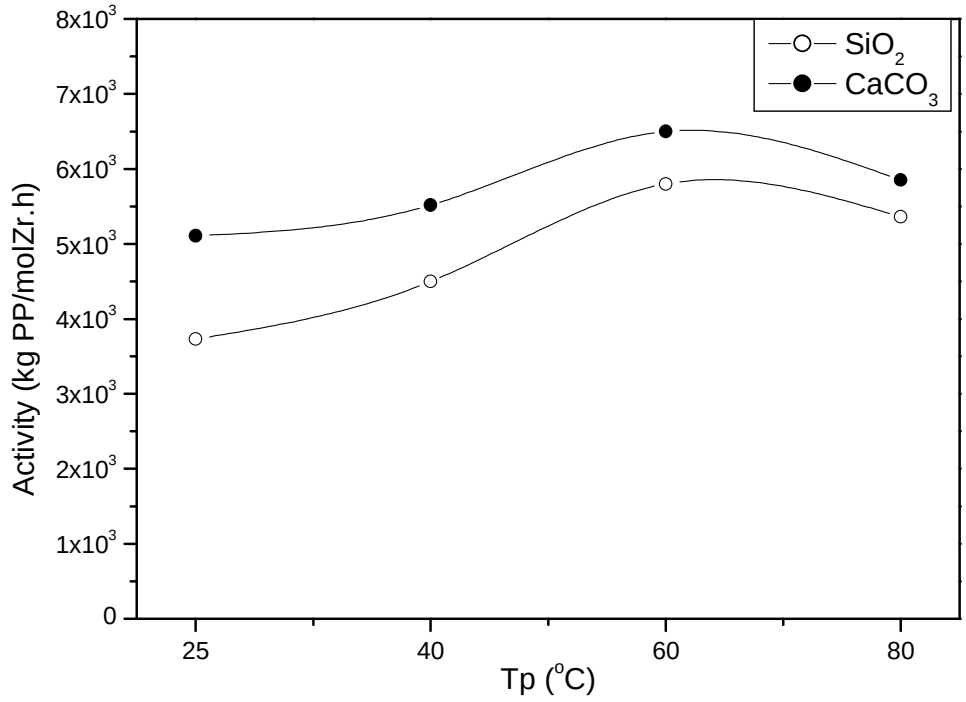

Figure 4.3: Effect of Tp on the activity of the in situ polymerizations with MAO-SiO_2 and MAO-$CaCO_3$. (Reaction conditions: MAO-filler 300 mg; MBI 2.2x10^{-6} mol; Al/Zr 2000; time 1 h)

Regarding the effect of the Tp on the microstructure of the formed polymer, results show that both the Mw and the tacticity of the polymer decrease with increasing Tp. A detailed discussion of the effect of the Tp on the polymer microstructure is presented in Section 4.3.4.

4.3.3 Influence of the initial filler load on polymerization activity and polymer microstructure

4.3.3.1 Effect of MAO-filler on catalyst activity and filler load

Tables 4.2 and 4.3 give the polymerization conditions used and the effects of the initial quantity of MAO-filler on the nanofiller load in the obtained nanocomposites and on the subsequent thermal properties of the nanocomposites prepared by in situ polymerization using MAO-SiO_2 and MAO-$CaCO_3$, respectively.

Table 4.2: Effect of the MAO treated nanosilica loading on the activity of the catalyst and on the properties of the resulting nanocomposites [a]

Run	SiO_2 (mg) [b]	Activity [c]	SiO_2 % [d]	Mw	Tc (^oC)	Tm (^oC)	PD	*mmmm* (%)
1	0	7125	0	123	110	149	2.2	94
2	100	7625	1.3	101	114	149	2.3	91
3	200	7800	2.7	116	114	149	2.3	90
4	500	7390	6.8	96	116	149	2.7	87
6	1000	7060	14.0	99	115	148	2.8	82
7[e]	1000	7950	11.1	225	115.5	151	3.7	90

[a] polymerization conditions: MBI $1.2x10^{-6}$; Al/Zr 3700; Tp 60 ^oC; [M] 6 g (1.5 MPa)

[b] 1.5 mmol MAO per gram silica after treatment at 250 ^oC (7.9% Al by EDX).

[c] activity (kg PP/molZr.h)

[d] determined by TGA

[e] [M] = 9 g (2.25 MPa).

Table 4.3: Effect of the MAO treated $CaCO_3$ nanoparticle loading on the activity of the catalyst and on the properties of the resulting nanocomposites [a]

Run	$CaCO_3$ (mg) [b]	Activity [c]	$CaCO_3$ % [d]	Mw	Tc (^oC)	Tm (^oC)	PD	*mmmm* (%)
1	0	7125	0	123	110	149	2.2	94
2	100	7750	1.3	91	114	147	3.2	93
3	200	8100	2.5	98	116.5	147.8	3.0	92
4	500	7950	6.5	96	116	150	2.9	92
6	1000	7790	13.8	103	115.5	148	3.7	89
7[e]	1000	8150	10.2	190	115	151	2.9	91

[a] polymerization conditions: MBI $1.2x10^{-6}$; Al/Zr 3700; Tp 60 ^oC; [M] 6 g (1.5 MPa).

[b] 1.5 mmol MAO per gram $CaCO_3$ after treatment at 100 ^oC (3.0% Al by EDX).

[c] Activity (kg PP/mol Zr.h)

[d] determined by TGA

[e] [M] = 9 g (2.25 MPa).

The effect of the initial amount of MAO-filler on the catalyst activity, and subsequently on the filler loading in the final nanocomposites for both fillers, is shown in Figure 4.4.

Figure 4.4 shows that at low filler feed there is an increase in the activity of the in situ polymerization compared to the homogeneous polymerization. This is explained by differences in monomer diffusion. Due to the presence of the filler, a PP with low tacticity and thus low crystallinity was obtained by the in situ polymerization. This allows the monomer to reach the active site, resulting in high activity. On the other hand, the restriction of the monomer diffusion, due to the high crystallinity of the high tacticity PP, results in low polymerization activity.

Figure 4.4 also shows a decrease in catalyst activity at high filler feed. This might be due to the deactivation of the catalyst by the filler. The in situ polymerization with MAO-$CaCO_3$ results in higher productivity than that with MAO-SiO_2.

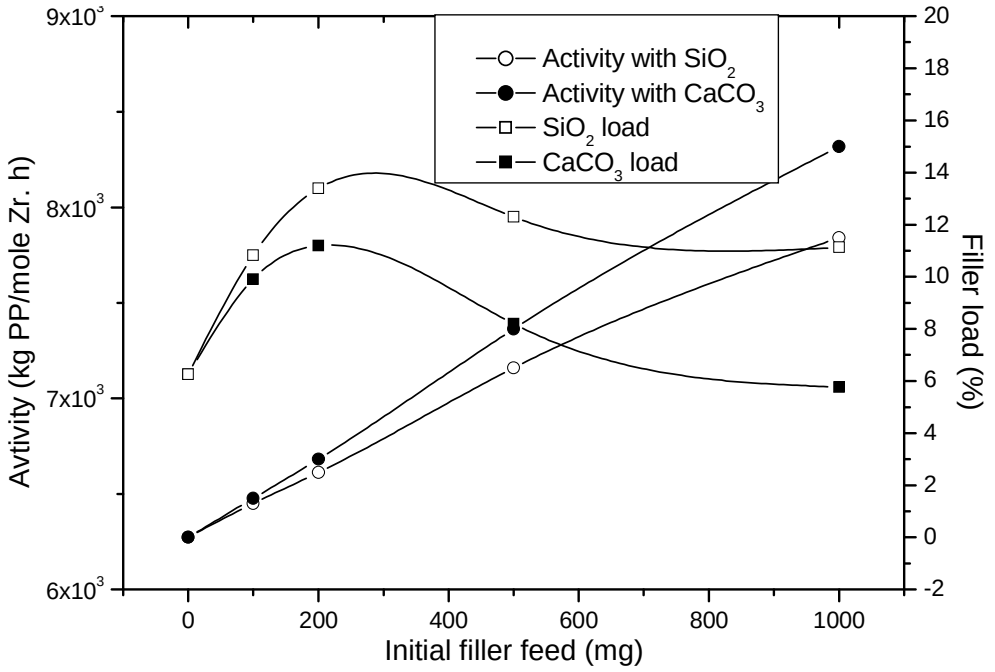

Figure 4.4: Effect of supported filler feed on the catalyst activity and the final filler load of the composites.

The low tacticity of PP produced by in situ polymerization with MAO-SiO_2 eliminates the effect of different monomer diffusion rates. Thus the

concentration of active sites plays an important role at high filler feeds. The rate of the deactivation of the catalyst is much higher in the in situ polymerization with MAO-SiO_2 than with MAO-$CaCO_3$. This is attributed to the higher concentration of OH groups on the SiO_2 surface. Figure 4.4 also shows a linear dependence of the filler load, as determined by TGA, on the initial MAO-filler in the range 0 to 13%.

4.3.3.2 Effect of filler feed on PP tacticity

Figure 4.5 shows the ^{13}C NMR spectrum of the methyl region of in situ prepared PP (run 6, Table 4.3). It illustrates the different types of stereosequences that can be formed in a single polymer chain. The same stereosequences were found in all the other samples, but the peak intensities differed.

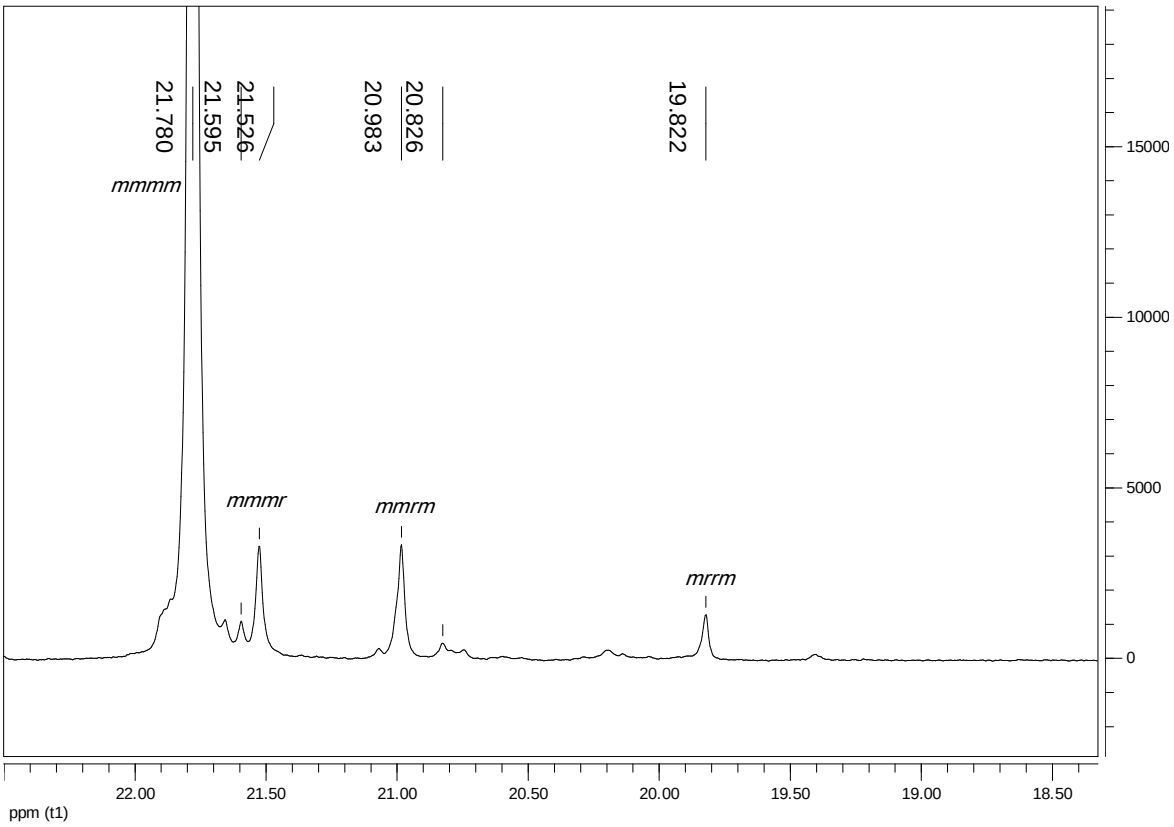

Figure 4.5: The methyl region of the ^{13}C NMR spectrum of run 6 in Table 4.3.

Table 4.4 shows the experimental ^{13}C NMR chemical shift values for the methyl pentads of the same sample compared with calculated values, which were calculated using a method proposed in literature [15].

Table 4.4: Experimental ^{13}C NMR chemical shift values for the methyl pentads of PP produced using MBI catalyst compared with calculated values

Pentad	δ (exp.)	Δ (δ)	δ (calc.)
mmmm	21.780	0.025	21.805
mmmr	21.526	0.013	21.539
mmrm	20.983	-0.087	20.896
mrrm	19.822	-0.045	19.773

Figure 4.5 also shows that, besides the intense [*mmmm*] signal, all samples exhibit stereoerrors signals arising from the [*mmmr*], [*mmrm*], and [*mrrm*] pentads. The relative intensities of the intense [*mmmm*] signal to those of the other pentads are indicative of the total tacticity of the samples.

Figure 4.6 illustrates the effect of MAO-filler feed on the tacticity of the PP.

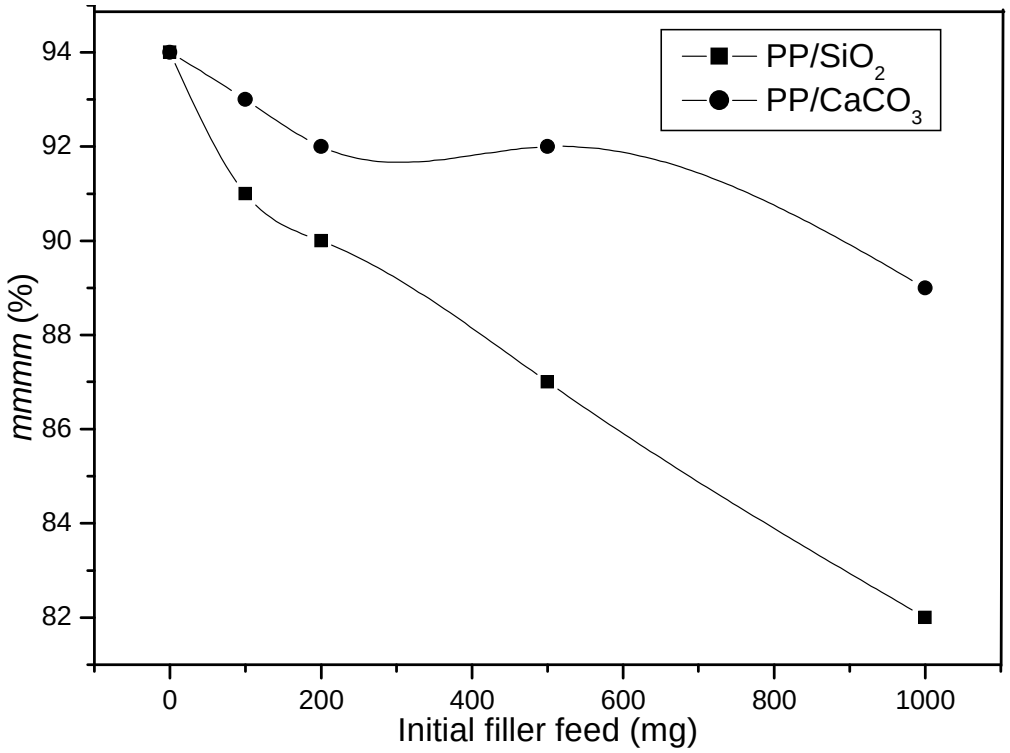

Figure 4.6: Effect of supported filler feed on the microstructure of PP of in situ polymerized PP nanocomposites.

It is observed that the *mmmm* content decreased when the MAO-filler was increased. Possible reasons for this are a steric hindrance effect caused by the filler, which might change the characteristics of the available coordination site, or a low monomer concentration at the active site. It is also observed that PPs produced via in situ polymerization with MAO-SiO_2 show lower tacticity than PPs produced with MAO-$CaCO_3$. The low average particle size of the nanosilica (15 nm) compared with the $CaCO_3$ nanoparticle (70 nm) might be the reason for this effect.

CRYSTAF was used to investigate the tacticity distribution of the samples. By combining the information obtained from CRYSTAF and ^{13}C NMR, a complete picture of the polymer microstructure, and thus the characteristics of the available active site, can be obtained.

The first derivative of the CRYSTAF analysis curves of run 1 and run 6 (see Table 4.2) are shown in Figure 4.7. Run 1 shows the typically narrow crystallization derivative curve of i-PP [16].

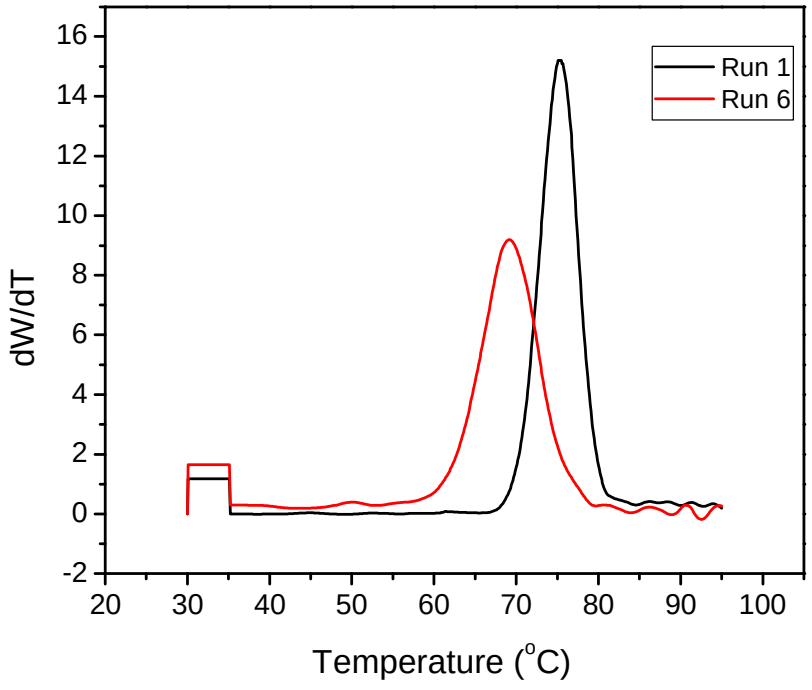

Figure 4.7: The first derivative of the CRYSTAF analysis curves of run 1 and run 6 (data in Table 4.2).

A comparison of the crystallization curve of run 1 with that of run 6 reveals that run 6 crystallizes at a lower crystallization temperature and its crystallization curve is broader than that of run 1. The soluble fraction is slightly higher for run 6. From these results together with the results obtained with ^{13}C NMR spectroscopy, it is clear that the decrease in the tacticity of PP prepared in the presence of filler was not due to the presence of different active species (supported and soluble active species) but that it was due to stereoerrors along the PP chain backbone. The decrease in the tacticity in the presence of filler could be due to the presence of soluble active species in different environments.

The presence of soluble active species inside and outside the filler particle aggregate generates active species with different characteristics. Furthermore, the differences in the polymerization conditions (different monomer concentration) around the various active sites have an effect on the microstructures of the PP produced.

4.3.3.3 Effect of filler on the Mw and the MWD

The Mw and MWD of the various PP nanocomposites that were prepared are given in Tables 4.2 and 4.3. It was found that the Mw of PP homopolymer (124 kg/mol) was slightly higher than the Mw of all the PP nanocomposites (approximately 100 kg/mol) produced under similar experimental conditions. The decrease in the Mw of PP nanocomposites can be explained by the high percentage of secondary insertions. Due to the lower monomer insertion rate at a chain end after secondary insertion, the probability for hydrogen transfer to the monomer is high, thus polymer with lower Mw and higher MWD is formed [9].

Furthermore, Tables 4.2 and 4.3 show that increasing the filler content had no effect on the Mw as the Mw of the PP nanocomposites were in the range of 100 Kg/mol. These results indicate that the ratio between the average propagation rate and the average termination rate is similar for all the in situ polymerization reaction when similar experimental conditions were used.

Figure 4.8 shows the effect of the initial filler feed on the MWD. Increasing the filler load leads to a broader MWD. This could be attributed to the random occurrence of the secondary insertion, which reduces the propagation rate and increases the probability of chain termination occurring.

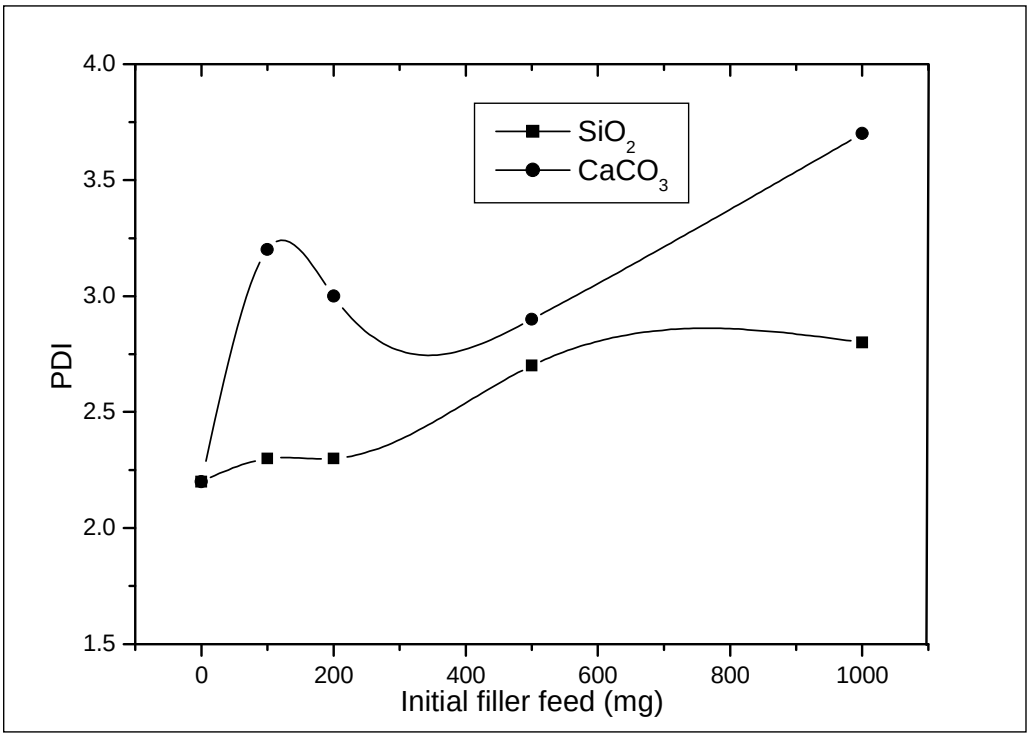

Figure 4.8: Effect of the initial filler feed on the MWD of PP prepared by in situ polymerization.

4.3.4 Effect of polymerization conditions (monomer concentration) on the in situ polymerized PP nanocomposite

In order to study the effect of the in situ polymerization conditions on the microstructure and subsequently the properties of the final product two experimental polymerizations (run 7 in Tables 4.2 and 4.3) were performed at higher propylene pressure. The experimental details and the microstructure of the PP obtained from these two runs are also given in the same tables. The results show that increasing the monomer concentration results in a slight increase in the polymerization activity and thus a small change in the filler loading. However, it seems that the monomer concentration has a pronounced effect on the microstructure of the formed PP.

Figure 4.9 demonstrates the effect of the propylene pressure (propylene concentration) on the microstructure of the PP/SiO_2 nanocomposite. The monomer concentration has a significant effect on the PP microstructure. Increasing the monomer concentration leads to an increase in the Mw and the tacticity of the polymer produced. Several metallocene catalysts have been studied to determine the extent of the influence of the monomer concentration on the microstructure of the produced PP [17-19]. All these results are in agreement with the results obtained in this study, indicating that the in situ polymerization follows a similar trend in terms of the effect of the monomer concentration on the microstructure of the produced PP.

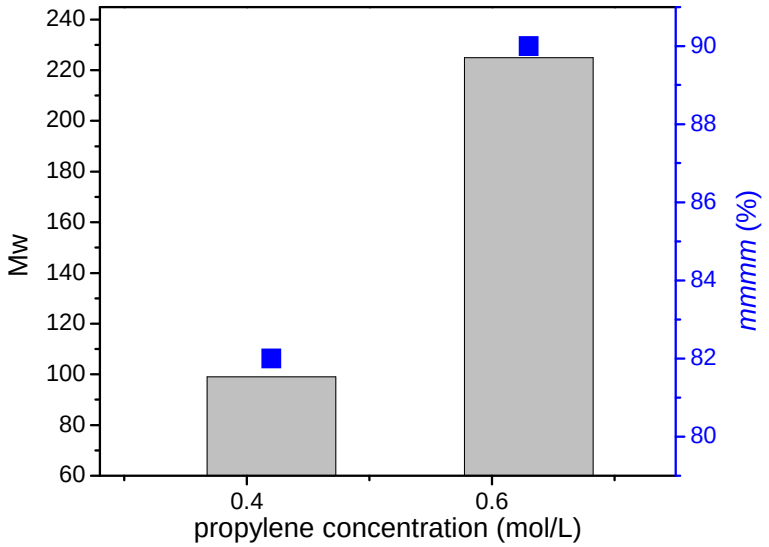

Figure 4.9: Effect of propylene concentration on the PP microstructure of in situ polymerizations with MAO-SiO_2. (Polymerization conditions are shown in Table 4.2).

4.3.5 PP/filler nanocomposites via melt-mixing

In situ polymerization produces nanocomposites with different matrix tacticities. In order to perform a comparative study between nanocomposites prepared using different methods, various PP homopolymers with different tacticities were prepared using MAO activated MBI metallocene catalyst. These homopolymers were prepared using polymerization conditions similar to those used for the in situ polymerization but using various Tp. Table 4.5

summarizes the polymerization conditions and the experimental details of each run.

Table 4.5: Propylene polymerization using various Tp [a]

Tp (^oC)	Activity [b]	Mw	Tc (^oC)	Tm (^oC)	MWD	*mmmm* (%)
25	7125	135	113	150	2.5	97
60	7540	123	114	149	2.3	94
80	7330	110	108	147	3.0	90

[a] polymerization conditions: MBI $1.2x10^{-6}$; Al/Zr 3700; [M] 6g (1.5 MPa)

[b] Activity (kg PP/mol Zr.h).

Table 4.5 shows that the Mw decreases with increasing the Tp. As the Tp increases, the rate of the chain transfer reaction (R_{tr}) becomes higher than R_p, reducing the ratio of R_p/R_{tr} which determines the molecular weight of the resultant polymer. Table 4.5 also shows that the tacticity of the polymers show a strong dependence on the Tp. The polymer tacticity decreases with increasing Tp. This can be explained by the reduction in the difference in activation energy as Tp increases. These results are consistent with those reported in literature, where studies of temperature effects, using a number of metallocene catalyst systems, show that both the tacticity and molecular weight of PP decrease with increasing Tp [20-22].

4.3.6 Morphology of nanocomposites

Optical microscopy (OM) was used to study the effect of the nanoparticles on the crystal structure of the polymer, and for comparison with the pure polymer. The crystal morphologies of pure PP and PP/SiO_2 nanocomposites are shown in Figure 4.10.

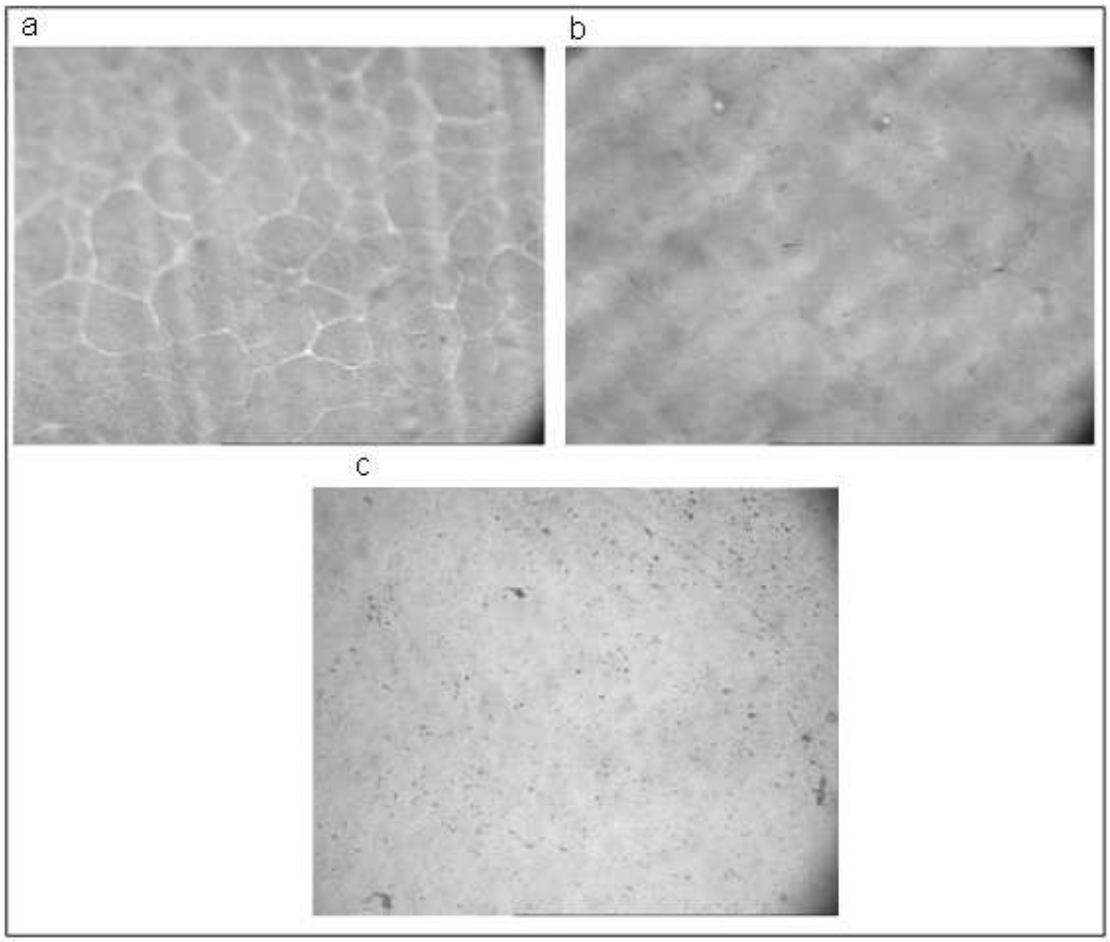

Figure 4.10: Polarized optical micrographs of samples: a) high tacticity pure PP, b) PP/SiO_2 nanocomposite film, and c) low tacticity pure PP, pressed at 210 ℃ (magnification: 5 x 10^2).

Under similar crystallization conditions, pure PP displayed larger and fewer spherulites (Figure 4.10 a) while the PP/SiO_2 nanocomposite (Figure 4.10 b) displayed many small spherulites. The PP/$CaCO_3$ nanocomposites also consist of smaller spherulites than pure PP. This effect can be explained by the restriction of movement of polymer chains during the crystallization process, resulting in slower crystallization and hence the formation of larger spherulites. In spite of the restriction of movement of polymer chains the crystallization rate of the nanocomposites was higher than that of pure PP (as will be discussed in the following chapter). From these results, one can deduce that the nanoparticles in the nanocomposite have a nucleating effect, which leads to an increase in the number of spherulites. Furthermore, the OM results show that when low tacticity pure PP crystallizes under similar

conditions, it does not display large spherulites. The spherulitic structure of low tacticity pure PP was destroyed by chain defects (Figure 4.10 c).

4.3.6.1 Filler dispersion and adhesion in the polymer matrix

Fillers are added to PP to achieve some functional properties not possessed by the PP itself. To ensure that the nanocomposite exploits the full potential of the individual components it is necessary to ensure a uniform distribution of the nanofillers in the polymer matrix as well as good adhesion between the polymer matrix and the nanofillers.

In this study various analytical techniques were used to determine the distribution and dispersion of the nanoparticles in the composites. High-resolution TEM images are useful for the characterization of nanocomposites, in particular to study the dispersion of nanoparticles in the PP matrix.

Figures 4.11 and 4.12 show TEM micrographs of various PP/SiO_2 nanocomposites prepared by in situ polymerization and melt-mixing, respectively. The low resolution images of in situ polymerized nanocomposites (Figure 4.11 (a)) and melt-mixed nanocomposite (Figure 4.12) show that the SiO_2 nanoparticles appear as a bunch of spherical-like particles, indicating the agglomeration of the primary particles. The reason for this is the strong interaction between nanoparticles [11]. However, the agglomerated silica nanoparticles in the in situ prepared nanocomposite are smaller than those in the melt-mixed nanocomposite.

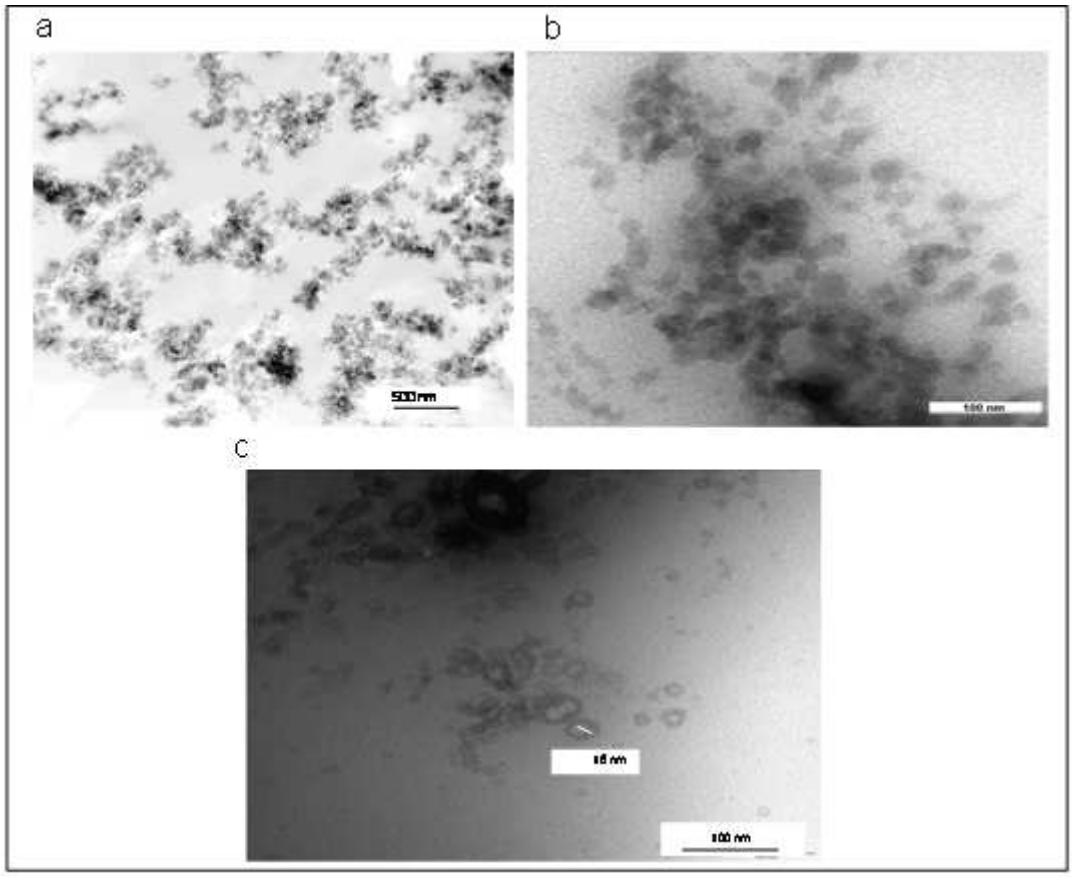

Figure 4.11: TEM micrographs of PP/silica nanocomposites prepared via in situ polymerization. (At different magnifications)

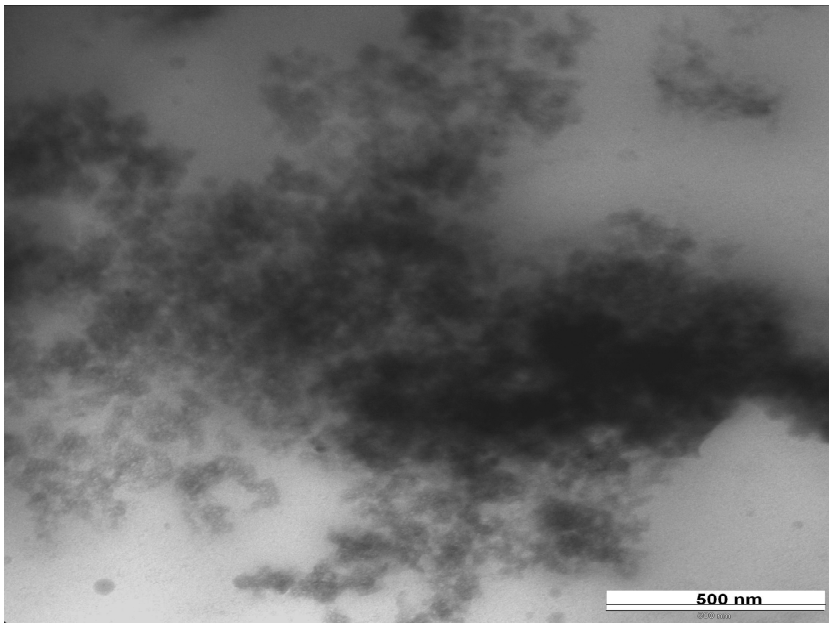

Figure 4.12: TEM micrographs of PP/silica nanocomposites prepared via melt-mixing.

High resolution images of both types of nanocomposites reveal that it was possible to separate the individual nanoparticles via in situ polymerization (Figure 4.11 (b)). This could not be seen in the melt-mixed nanocomposite. The high resolution image (Figure 4.11 (c)) also shows that the silica particle is covered by a thin PP interfacial layer of 10 nm, indicating good interactions between the polymer matrix and the silica. It is unclear whether this layer is formed from the supported active site or from the adsorption of the polymer chains onto the silica surface.

Figures 4.13 and 4.14 show TEM micrographs of PP/$CaCO_3$ nanocomposites prepared by in situ polymerization and melt-mixing, respectively.

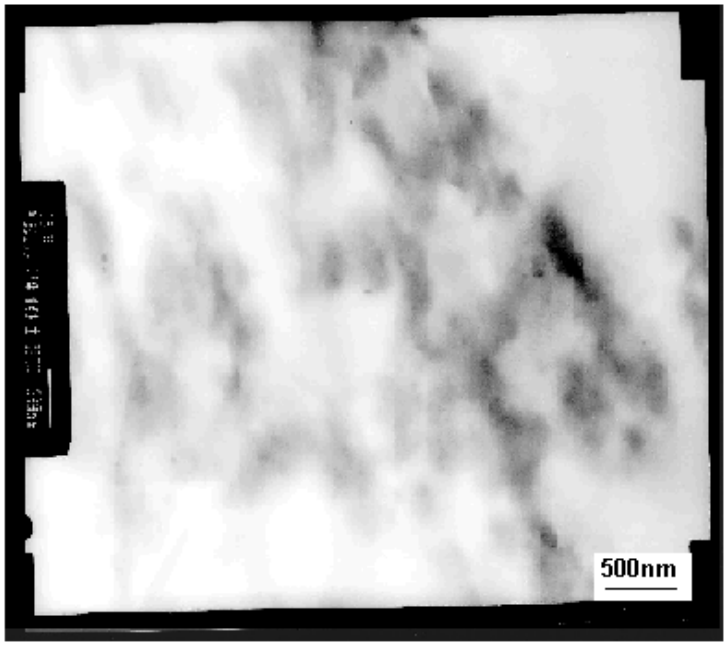

Figure 4.13: TEM micrographs of PP/$CaCO_3$ nanocomposites prepared via in situ polymerization.

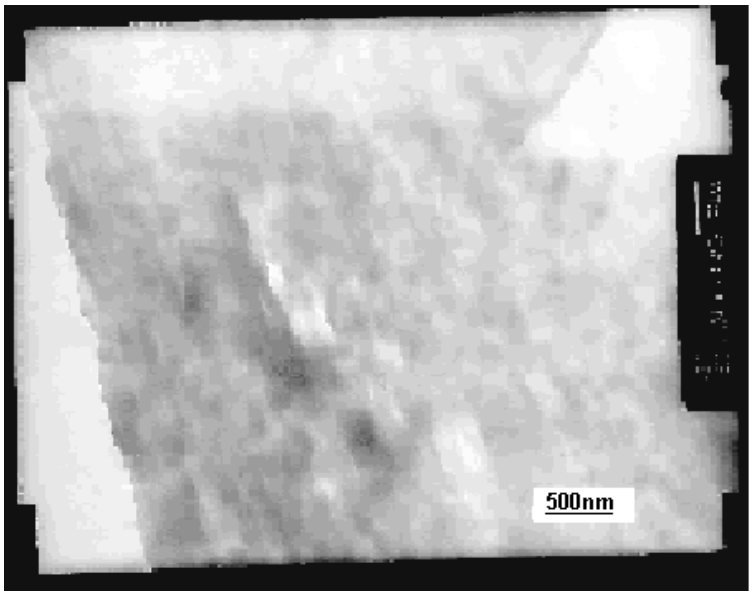

Figure 4.14: TEM micrographs of PP/$CaCO_3$ nanocomposites prepared via melt-mixing.

In the case of the PP/$CaCO_3$ nanocomposites, particle agglomeration was also observed in both types of nanocomposites. Particle agglomeration was in the micro size range for the melt-mixed PP/$CaCO_3$ nanocomposites (Figure 4.14) and in the nano size range (Figure 4.13) for the in situ polymerized PP/$CaCO_3$ nanocomposites.

For the melt-mixed PP/filler nanocomposites, the high polymer shear is the driving force to split the particle agglomeration. Due to the nanosize range of the filler particles, the shear provided by the polymer chains is not sufficient to break up the agglomerated particles. However, when propylene monomer is polymerized in the presence of filler particles the small size of the catalyst as well as the monomer allows the break up of these agglomerated particles.

SEM was used to investigate the interfacial adhesion between the polymer matrix and the filler. Figure 4.15 and 4.16 show SEM images of a fracture surface of an in situ polymerized PP/SiO_2 nanocomposite and a melt-mixed nanocomposite.

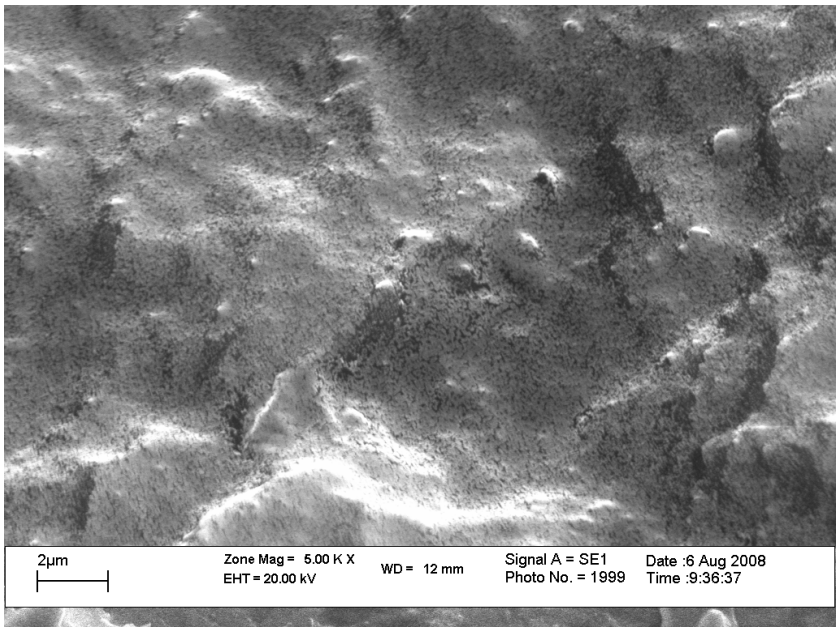

Figure 4.15: SEM image of fractured surface of in situ polymerized PP/SiO_2 nanocomposite.

Figure 4.16: SEM image of fractured surface of melt-mixed PP/SiO_2 nanocomposite.

The SEM images reveal that all the samples contain agglomerates, the size of which varied with the preparation method. SEM micrograph of the in situ polymerized PP nanocomposite reveals agglomerates with a particle size of less than 500 nm, while the SEM micrograph of the melt-mixed

nanocomposite reveals agglomerates with a particle size in the range 0.5–2.0 µm.

The SEM micrograph of the melt-mixed nanocomposite illustrates the debonding at the particle-matrix interface. This might be due to poor interfacial adhesion between the silica and the polymer matrix or due to the presence of agglomeration, which reduces the wettability of the polymer and also results in stress concentration.

Figure 4.15 shows that, for the in situ polymerized nanocomposites, the SiO_2 nanoparticles are embedded inside the polymer matrix. The reason for this is that as some of the catalyst was supported on the silica surface some of the chains will be formed on and adhere to the silica surface, which will increase the interfacial adhesion between the silica and the polymer matrix.

Figures 6.17 and 6.18 show SEM micrographs of fractured surfaces of in situ polymerized and melt-mixed PP/$CaCO_3$ nanocomposites, respectively.

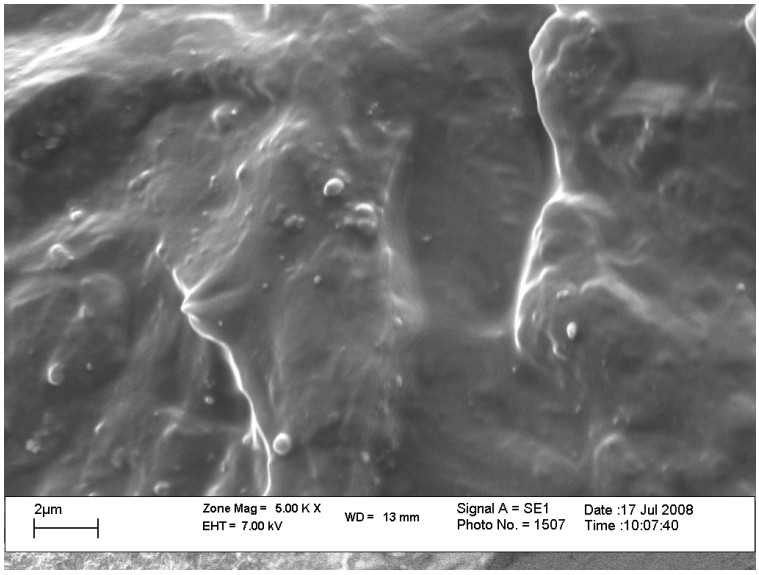

Figure 4.17: SEM image of fractured surface of in situ polymerized PP/$CaCO_3$ nanocomposite.

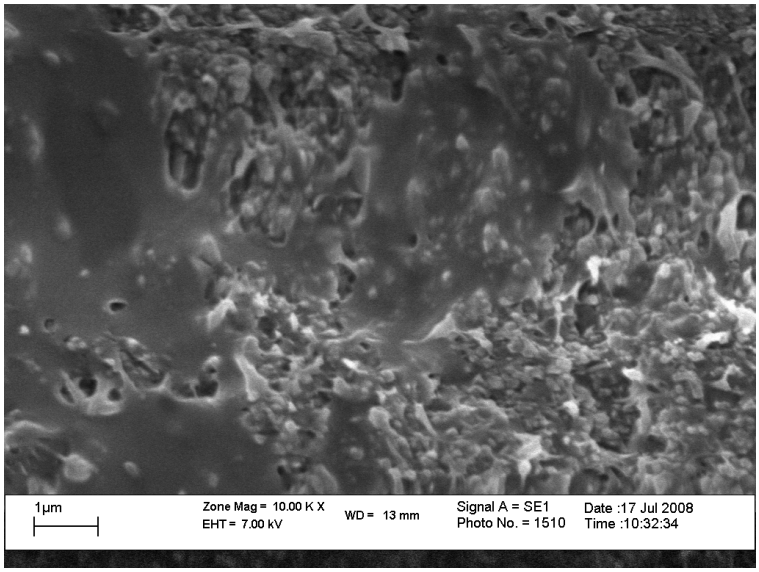

Figure 4.18: SEM image of fractured surface of melt-mixed PP/$CaCO_3$ nanocomposite.

SEM images of both melt-mixed PP/$CaCO_3$ and in situ polymerized PP/$CaCO_3$ show a good interaction between the polymer matrix and the filler. Even though there appears to be some debonding occurring in the melt-mixed PP/$CaCO_3$ between the filler and PP matrix, as can be seen in Figure 4.18, but this is basically due to the agglomeration of the $CaCO_3$ particles.

4.4 Conclusions

It was found that at low polymerization times the in situ polymerization had lower R_p than that of the homogenous polymerization. However, as the polymerization time proceeds, the decay in the R_p of the homogenous polymerization was faster than that of the in situ polymerization. It was also found that, due to the steric hindrance that arises from the presence of the filler nanoparticles and the change in the polymerization kinetics, the in situ polymerization produced PP matrices with microstructures different from that of the homogenous polymerization. The *mmmm* content decreased with increasing MAO-filler content, for both fillers. These results also showed that in situ polymerization performed with SiO_2 nanoparticles yielded an activity and PP microstructure that was slightly different from that of the in situ polymerization performed with $CaCO_3$ nanoparticles. Comparing the dispersion phase morphology of the nanocomposites synthesized via different

techniques, TEM and SEM results indicated that the filler dispersion in the PP matrix was improved in the in situ polymerized nanocomposites compared to the melt-mixed nanocomposites.

4.5 References

1. Ray, S.; Okamoto, M., *Prog. Polym. Sci.*, 2003. **28**: p. 1539.
2. Sun, T.; Garces, J., *Adv. Mater.*, 2002. **14**: p. 128.
3. Kaminsky, W.; Wiemann, K., *Compos. Interfaces*, 2006. **13**: p. 365.
4. Funck, A.; Kaminsky, W., *Compos. Sci. Technol.*, 2007. **67**: p. 906.
5. He, J.; Li, H.; Wang, X.; Gao, Y., *Eur. Polym. J.*, 2006. **42**: p. 1128.
6. Scharlach, K.; Kaminsky, W., *Macromol. Symp.*, 2008. **261**: p. 10.
7. Pavlidoua, S.; Papaspyrides, C., *Prog. Polym. Sci.*, 2008. **33**: p. 1119.
8. Alfred, C.; Jong-Young, L., *Polym. Rev.*, 2007. **47**: p. 217.
9. Resconi, L.; Cavallo, L.; Fait, A.; Piemontesi, F., *Chem. Rev.*, 2000. **100**: p. 1253.
10. Ochoteco, E.; Vecino, M.; Montes, M.; de la Cal, J., *Chem. Eng. Sci.*, 2001. **56**: p. 4169.
11. Fischer, D.; Mulhaupt, R., *J. Organomet. Chem.* , 1991. **417**: p. C7.
12. Busico, V.; Cipullo, R.; Esposito, V., *Macromol. Rapid Commun.*, 1999. **20**: p. 116.
13. Huang, J.; Rempel, G., *Ind. Eng. Chem. Res.*, 1997. **36**: p. 1151.
14. Rieger, B.; Mu, X.; Mallin, D.; Rausch, M.; Chien, J., *Macromolecules*, 1990. **23**: p. 3559.
15. Busico, V.; Cipullo, R.; Monaco, G.; Vacatello, M., *Macromolecules*, 1997. **30**: p. 6251.
16. Soares, J.; Anantawaraskul, S., *J. Polym. Sci., Part B: Polym. Phys.*, 2005. **43**: p. 1557.
17. Resconi, L.; Fait, A.; Piemontesi, F.; Colonnesi, M.; Rychlicki, H.; Zeigler, R., *Macromolecules*, 1995. **28**: p. 6667.
18. Stehling, U.; Diebold, J.; Kirsten, R.; Roell, W.; Brintzinger, H.; Juengling, S.; Muelhaupt, R.; Langhauser, F., *Organometallics* 1994. **13**: p. 964.

19. Jungleing, S.; Mulhaupt, R.; Stehling, U.; Brintzinger, H., *J. Polym. Sci., Part A: Polym. Chem.*, 1995. **33**: p. 1305.
20. Resconi, L.; Piemontesi, F.; Camurati, I.; Balboni, D.; Sironi, A.; Moret, M.; Rychlicki, H.; Zeigler, R., *J. Am. Chem. Soc.*, 1998. **120**: p. 2308.
21. Busico, V.; Cipullo, R.; Chadwick, J.; Modder, J.; Sudmeijer, O., *Macromolecules*, 1994. **27**: p. 7538.
22. Rieger, B.; Jany, G.; Fawzi, R.; Steimann, M., *Organometallics*, 1994. **13**: p. 647.

Chapter 5: The effect of the different nanofillers on the crystallization and thermal stability of the nanocomposites

.

5.1 Introduction

The crystalline morphology plays a key role in determining the properties of semi-crystalline polymers such as polyolefins. Introducing fillers increases the interfacial area and consequently alters the kinetics of nucleation and growth, and thus the crystallite fraction and morphological structure.

Different methods are used for the preparation of the nanocomposites which leads to nanocomposites with different properties and crystallization kinetics. The in situ polymerization of monomer in the presence of nanofillers shows potential as an approach for achieving a more homogeneous distribution of inorganic nanoparticles.

Several studies have shown that the addition of small quantities of a filler cause substantial changes in crystallinity of the polymer (either a large increase or decrease) [1-6], and subsequently substantial changes in the performance of the system due to alteration of the crystal form or the degree of crystallinity.

This chapter investigates the influences that nanofillers have on PP/filler nanocomposites prepared via two methods, namely melt-mixing and in situ polymerization. This chapter also compares the isothermal crystallization of these PP/filler nanocomposites.

5.2 Experimental

5.2.1 Materials

5.2.1.1 In situ polymerized PP nanocomposites

Table 5.1 comprises of a data summary for all the in situ polymerized samples used in this section of the work.

5.2.1.2 Melt-mixed PP/filler nanocomposites

PP homopolymer with Mw 123 kg/mol (MWD 2.2) and a 94% *mmmm* content was used as a matrix polymer. PP homopolymers with different tacticities were also used to investigate the effect of PP tacticity on the change

in the crystal structure of the polymer matrix due to the presence of nanofillers. The preparation of melt-mixed PP nanocomposites was described in Section 4.3.4.

5.2.2 Characterization techniques

5.2.2.1 DSC

As described in section 4.2.4.3.

The crystallinity was calculated from the melting peak of the second heating scan relative to the enthalpy of melting (ΔH_{fc}) of 209 J/g for 100% crystalline i-PP [7].

The rate constant of crystallization (K) and the Avrami exponent (n) were determined by Avrami analysis of isothermal DSC experiments. Isothermal crystallization of PP and the PP/filler nanocomposites were performed at various temperatures from 110 to 124 ^{o}C. The samples were quenched to the desired isothermal crystallization temperature after they were entirely molten at 200 ^{o}C for 5 min.

5.2.2.2 WAXD

WAXD analyses were performed on a Bruker AXS D8 ADVANCE diffractometer at room temperature with filtered Cu-Kα radiation. The scans were performed within the range 2θ = 9 - 36°, with a sampling width of 0.05° and a scanning rate of 28°/mm. The samples for WAXD were melt-pressed at 180 ^{o}C into 1 mm thick disc using a mould.

5.2.2.3 TGA

Thermal stabilities of the various nanocomposites were analyzed by TGA. TGA analysis was carried out using a TGA-50 thermogravimetric instrument, with a TA-50 WSI thermal analyzer connected to a computer. Samples (10-15 mg) were degraded in a nitrogen atmosphere. The nitrogen flow rate was 50 mL/min, and the heating rate was 20 ^{o}C/min.

5.3 Results and discussion

Table 5.1: The details of microstructures and thermal properties of all in situ nanocomposites used in this section of the study

sample code	Filler load (%)	Mw (kg/mol)	*mmmm* (%)	MWD	Tc (^oC)	Tm (^oC)
Pure PP	0	123	94	2.2	110.0	150
PP/SiO_2 (1.3%)	1.3	101	91	2.3	114.0	149
PP/SiO_2 (2.7%)	2.7	116	90	2.3	114.0	149
PP/SiO_2 (6.8%)	6.8	96	87	2.7	116.0	149
PP/SiO_2 (14.0%)	14.0	99	82	2.8	115.0	147
PP/SiO_2 (11.1%)	11.1	225	90	3.7	115.5	150
PP/$CaCO_3$ (1.3%)	1.3	91	93	3.2	114.0	147
PP/$CaCO_3$ (2.5%)	2.5	98	92	3.0	116.5	149
PP/$CaCO_3$ (6.5%)	6.5	96	92	2.9	116.0	148
PP/$CaCO_3$ (13.8%)	13.8	103	89	3.7	115.5	147
PP/$CaCO_3$ (10.2%)	10.2	190	91	2.9	115.0	151

5.3.1 Crystallization and melting behaviour of the nanocomposites

Representative crystallization exotherm and melting endothem curves for in situ polymerized PP/filler nanocomposites and melt-mixed nanocomposites are presented in Figure 5.1 and 5.2, respectively.

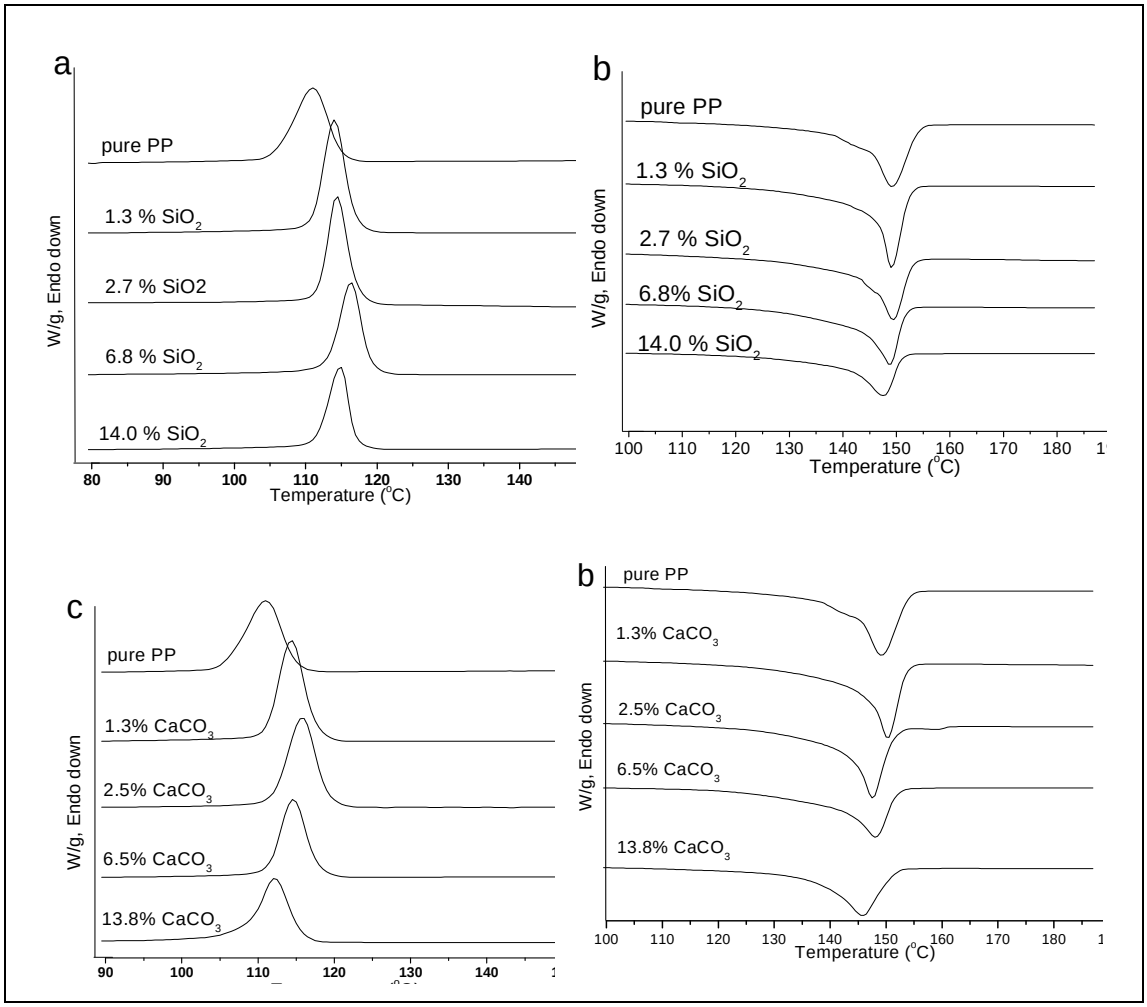

Figure 5.1: DSC crystallization (a and c) and melting (b and d) curves of various in situ polymerized PP nanocomposites at 10 ^{o}C/min.

DSC scans in Figure 5.1 (a) and (c) show that the PP nanocomposite generally crystallized at higher Tc than neat PP. The increase of the Tc upon increasing filler content shows the nucleating effects of those fillers on PP crystallization. The nucleating ability of SiO_2 and CaO_3 has been observed in PP as well as other polyolefins [8, 9]. Figure 5.1 (a) and (c) also show that the crystallization peaks in PP nanocomposites are narrower than those of pure PP. Higher crystallization temperatures and narrow crystallization peaks indicate that the nucleation rates and the overall crystallization rates are fast.

Similar results were also found for the crystallization behaviour of melt-mixed PP/filler nanocomposites, as can be seen in Figure 5.2. This implies that both fillers, regardless of the preparation method, are effective nucleating agents to increase the rate of crystallization of PP and smaller spherulites are

formed via a heterogeneous nucleation process as confirmed by polarized light microscopy in the preceding chapter.

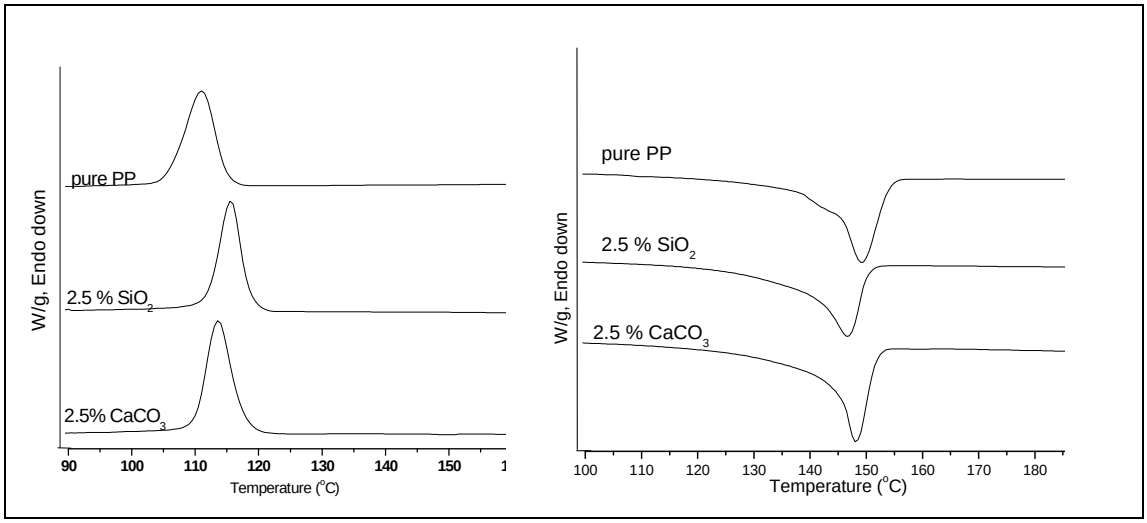

Figure 5.2: DSC of melt-mixed PP nanocomposites at 10 °C/min.

The melting behaviour of PP, which is a direct result of the lamellar thickness, indicates that the different nanocomposites behave differently. For example, a narrow melting peak with the same Tm as for pure PP was obtained for the in situ polymerized nanocomposite using silica nanoparticles with a filler load of 1.3% SiO_2. The narrow melting peak suggests that more lamellae are formed with a narrow size distribution but that the average lamellar thickness is identical to that of the pure PP.

The decrease in Tm for some of the in situ prepared PP/$CaCO_3$ and PP/SiO_2 nanocomposites is due to a tacticity effect because those samples have a lower isotacticity. The lower tacticity for the in situ polymerized nanocomposite, especially at high filler content, also leads to a reduction in the Tc (Figure 5.1 (a, c)). This indicates that, in the case of the in situ prepared composites, the filler content and the tacticity of the polymer matrix control the melt and crystallization behaviour of the nanocomposite. However, the Mw may also play a significant role in determining the melting behaviour of PP. For example, the higher Mw of sample PP/$CaCO_3$ (10.2%, Table 5.1) results in the formation of crystals which melt at a higher temperature than that of sample PP/$CaCO_3$ (1.3%, Table 5.1) despite its lower tacticity.

For the melt-mixed nanocomposite, Figure 5.2 shows a slight reduction in the Tm indicating the presence of slightly thinner lamellar. The decrease in the Tm was more evident for the PP/SiO_2 nanocomposite which might be due to the smaller size of the SiO_2 nanoparticles compared to the $CaCO_3$ particles.

Figures 5.3 and 5.4 show the Tc value of the nanocomposites prepared by in situ polymerization and melt-mixing, using SiO_2 and $CaCO_3$ respectively, as a function of the filler loading. The isotactic pentad contents of the polymer matrix of the in situ prepared nanocomposites are also shown. There is a slight increase in the Tc of the in situ prepared polymers compared to the melt-mixed polymers with the same silica load, despite the lower tacticity of the in situ nanocomposites. It is well documented that polymers with lower tacticity have lower Tc values [10, 11].

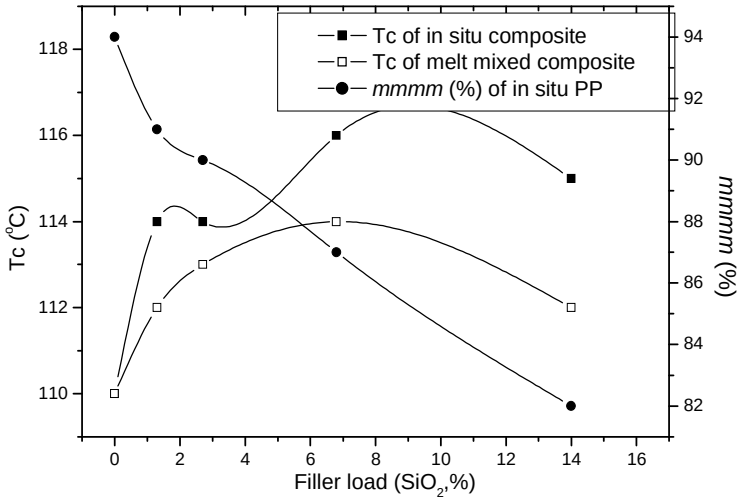

Figure 5.3: Effect of the filler loading on the Tc values of the PP/SiO_2 nanocomposites.

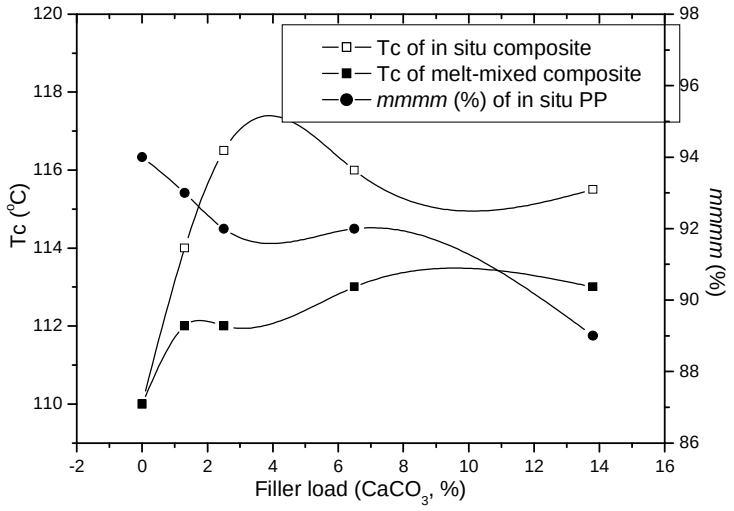

Figure 5.4: Effect of the filler loading on the Tc of the PP/$CaCO_3$ nanocomposites.

These results illustrate that the preparation method affects the thermal properties of the nanocomposites. This difference is ascribed to two factors. The first is the improved distribution of the filler in the in situ prepared nanocomposites, where the filler acts as nucleating agent, resulting in many small spherulites. The second is that, for the in situ prepared nanocomposites, the chains produced by the supported catalyst are in direct contact with the filler surface, resulting in an increased nucleating ability for the filler surface.

5.3.2 Degree of crystallinity

The effect of the filler load on the Xt for in situ polymerized PP/SiO_2 and PP/$CaCO_3$ nanocomposites is given in Figures 5.5 and 5.6, respectively. The tacticity of the PP matrix is also given for comparison. The degree of crystallinity deceases as the filler loading increases. The data also reveal that, for the in situ prepared nanocomposite, the tacticity plays the major role in determining the degree of crystallinity. This can clearly be seen from the profiles of the crystallinity curves, which follow the same trend as the tacticity curves.

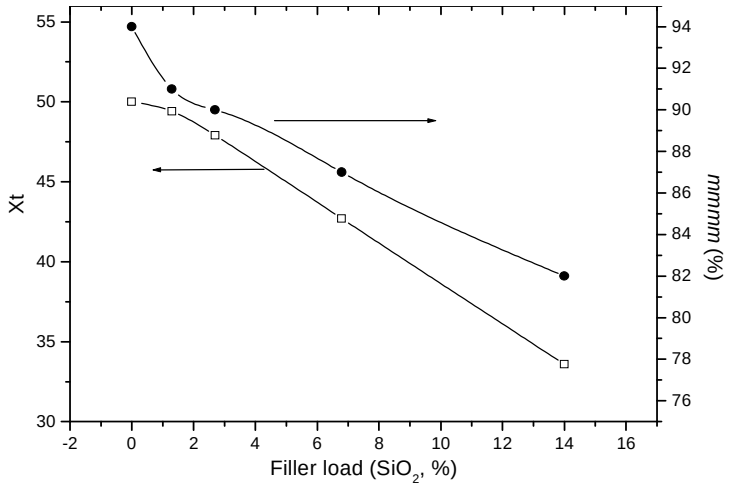

Figure 5.5: Influence of filler load on the Xt for the in situ polymerized PP/SiO_2 nanocomposites.

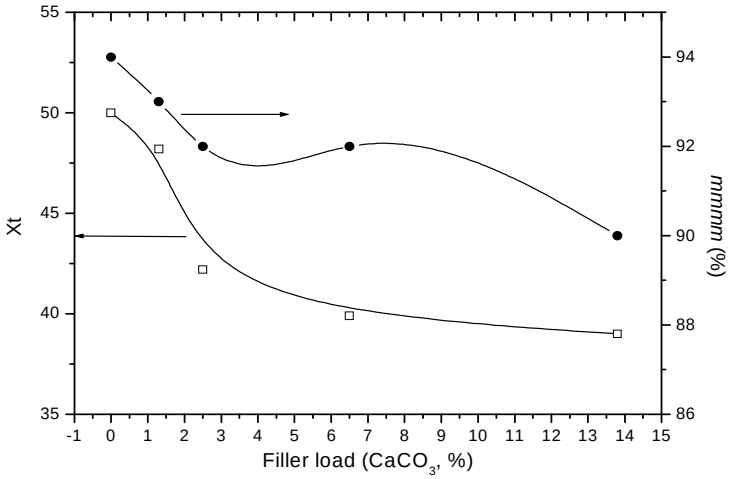

Figure 5.6: Influence of filler loading on the Xt for the in situ polymerized PP/$CaCO_3$ nanocomposites.

It is well reported that the degree of crystallinity of PP homopolymer is governed primarily by the tacticity of the chain [12]. Another reason which could play a role is the hindrance of the polymer chains' motion due to the small filler particles which results in large number of small spherulites as shown in Chapter 4. For example, when samples with similar tacticities and different filler loading (Figure 5.6) are compared, it is evident that the higher the filler loading, the lower the Xt. These results indicate that fillers also play a role in determining the degree of crystallinity.

Figure 5.7 shows the effect of the filler load on the Xt for melt-mixed PP/SiO_2 and PP/$CaCO_3$ nanocomposites. The tacticity of the PP matrix of the melt-mixed nanocomposites is 94%.

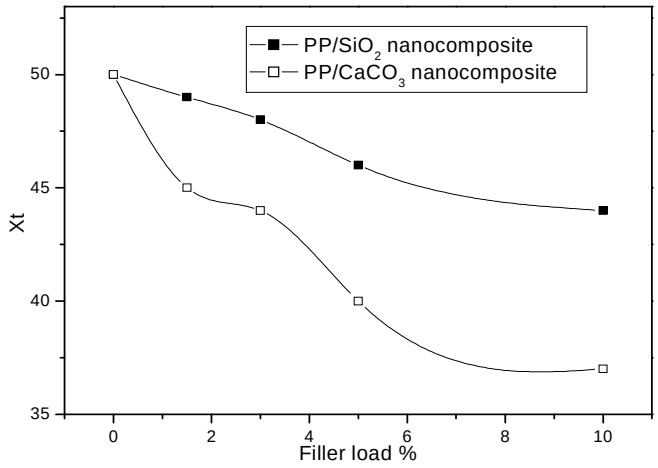

Figure 5.7: Effect of filler load on the Xt for melt-mixed PP/filler nanocomposites.

Figure 5.7 shows a decrease in the Xt with increasing filler load. This was more pronounced for the PP/$CaCO_3$ nanocomposites. The decrease in the Xt for the PP/SiO_2 nanocomposite is attributed to the weight percentage of the filler. If the filler weight is subtracted from the polymer weight no change in the Xt will be observed. The decrease in the Xt, in the case of the PP/$CaCO_3$, can be explained by the presence of an excessive number of filler particles that can hinder the motion of the polymer chain segments and thus retard crystal growth.

Figures 5.5 and 5.7 indicate that both the tacticity and the filler loading play a role in the Xt of the in situ nanocomposites, but tacticity plays the major role, while filler loading dominates the melt-mixed nanocomposites. One can also conclude that the Xt is more dependent on the tacticity than the presence of the fillers.

5.3.3 Crystallization kinetics

The crystallization kinetics of PP/filler nanocomposites is important for assessing their microstructure development during melt-processing. The process of crystallization can be studied at a constant temperature, i.e. isothermal crystallization, or at a constant cooling rate, i.e. nonisothermal crystallization.

5.3.3.1 Isothermal crystallization

Figure 5.8 shows the DSC traces for the isothermal crystallization of an in situ polymerized nanocomposite (2.7 wt% SiO_2) at different temperatures.

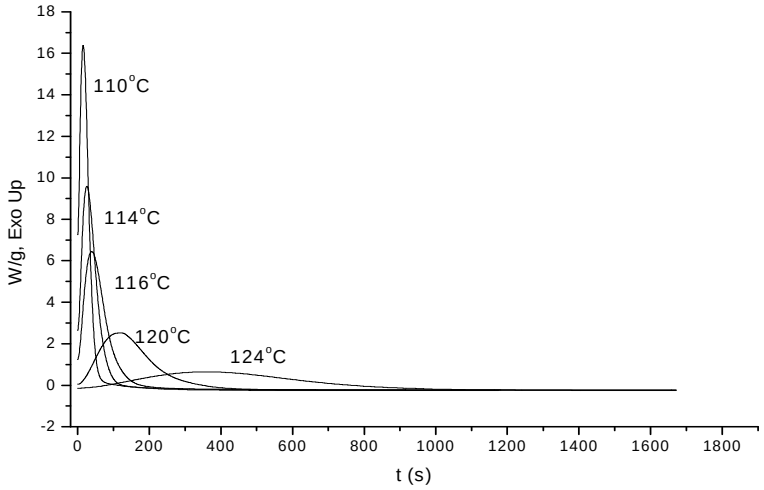

Figure 5.8: Isothermal crystallization curves of in situ polymerized PP/SiO_2 nanocomposite (2.7%, Table 5.1) at different temperatures.

As the crystallization temperature increases the crystallization rate becomes slower and the crystallization exothermic peak is shifted to longer times. Figure 5.9 shows the change in the relative crystallinity (Xc) of the same sample with time (t). The crystallinity increases with time. For the higher crystallization temperature it took a long time for sample to reach the final degree of crystallinity.

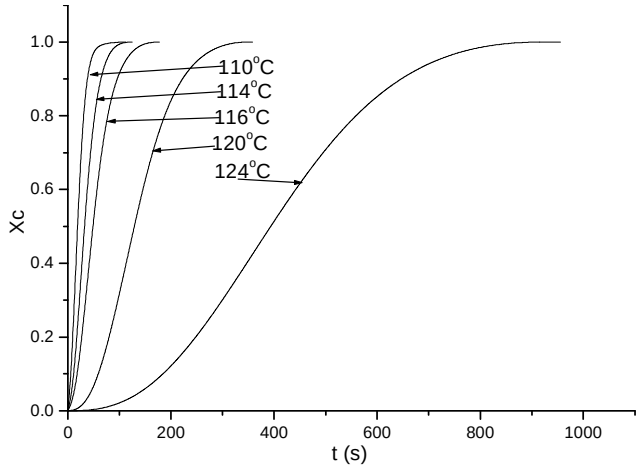

Figure 5.9: The relative crystallinity versus t (s) for PP/SiO_2 nanocomposites at different crystallization temperatures.

For the purpose of comparison, the curves at crystallization temperature of 120 ^{o}C for neat PP and in situ prepared PP/filler nanocomposites were plotted together, as shown in Figure 5.10. At the same crystallization temperature, the crystallization rate of the pure PP is slower than that of the PP/filler nanocomposite. Moreover, it is observed that crystallization commences immediately in the nanocomposite when the crystallization temperature is reached, while there is an induction period for the neat PP.

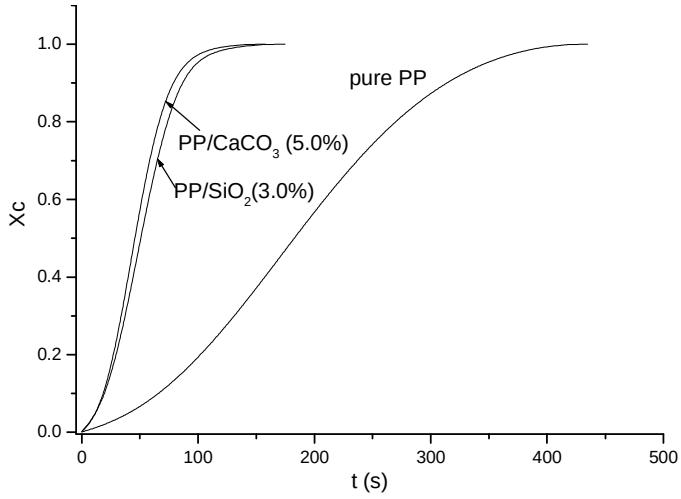

Figure 5.10: The relative crystallinity versus t (s) for pure PP and PP/filler nanocomposites at a crystallization temperature of 120 ^{o}C.

The most common approach to use for the analysis of isothermal crystallization kinetics is the Avrami method [13], based on the Avrami Equation (5.1).

$$1-(Xc)=\exp(-kt^{n}) \qquad (5.1)$$

Where Xc is the fraction of material crystallized after time t, K is a temperature dependent constant that depends on nucleation rate and growth velocity, and n is an exponent describing the dimensionality of crystal growth.

From eq. (5.1) and by taking the double logarithm, Eq. (5.2) is obtained

$$\log[-\ln(1-Xc)]=\log k+n\log(t) \qquad (5.2)$$

Plots of log (−ln(1−Xc)) versus log t at various isothermal crystallization temperatures for pure PP and various in situ prepared PP/filler nanocomposites are shown in Figure 5.11. The values of n and k were calculated from the slope and the intersection of the Avrami plots respectively, and the results summarized in Table 5.2.

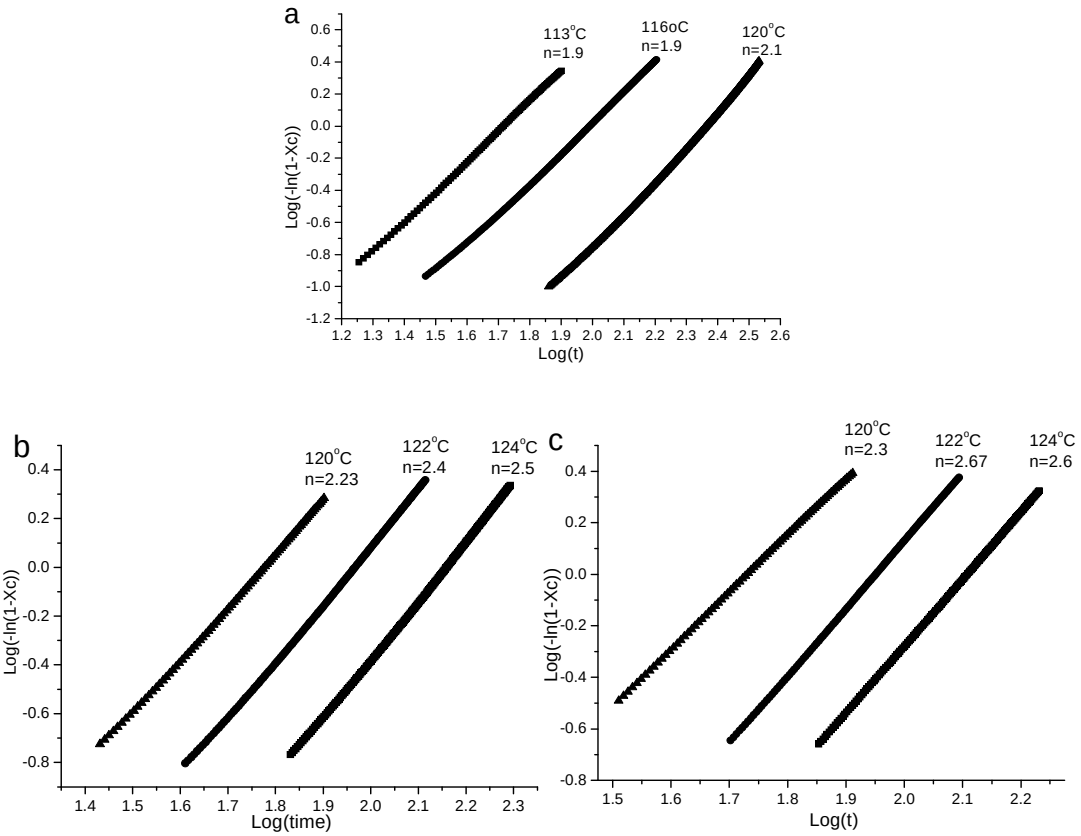

Figure 5.11: Plots of log (-ln(1-Xc)) versus log(t) for: a) pure PP, b) and in situ prepared PP nanocomposites (2.7% SiO_2), and c) in situ prepared PP nanocomposites (2.5% $CaCO_3$) at various crystallization temperatures.

Table 5.2 shows that at the crystallization temperature of 120 ^oC the value of n for pure PP is smaller than for both in situ polymerized and melt-mixed prepared PP/filler nanocomposites. The n values of PP nanocomposites were in the range of 2.5, for the crystallization temperatures from 120 to 124 ^oC, which is related to three-dimensional growth.

The crystallization half-time ($t_{1/2}$) is defined as the time at which the crystallinity reaches 50%. Thus, it can be determined from the Avrami Equation,

$$t_{1/2} = (\ln 2 / K)^{1/n} \text{ ..... (5.3)}$$

Generally the rate of crystallization (G) can be defined as the reciprocal of $t_{1/2}$.

$$G=1/t_{1/2} \text{.....(5.4)}$$

The values of both $t_{1/2}$ and G are also listed in Table 5.2.

Table 5.2: Isothermal crystallization kinetic parameters of pure PP and different PP/filler nanocomposites at different crystallization temperatures

Sample	Tc (^oC)	n	K(s^n)	$T_{1/2}$(s)	Gx10^{-3}(s^{-1})
pure PP	113	1.9	6.3x10^{-4}	33.16	30.16
	116	1.9	2.5x10^{-4}	52.65	18.99
	120	2.1	1.8x10^{-5}	152.6	6.55
In situ PP/SiO_2 (2.7%)	120	2.4	1.7x10^{-4}	31.93	31.32
	122	2.4	3.0x10^{-5}	65.79	15.2
	124	2.5	6.3x10^{-6}	103.89	9.63
In situ PP/$CaCO_3$ (2.5%)	120	2.4	1.8x10^{-4}	31.18	32.07
	122	2.67	1.4x10^{-5}	57.32	17.45
	124	2.6	4.0x10^{-6}	103.49	9.66
Melt-mixed PP/SiO_2 (2.5%)	120	2.3	2.0x10^{-4}	34.59	28.9
	122	2.3	5.6x10^{-5}	60.17	16.62
	124	2.7	1.58x10^{-6}	122.94	8.13
Melt-mixed PP/$CaCO_3$ (2.5%)	120	2.3	1.78x10^{-4}	36.39	27.48
	122	2.4	3.16x10^{-5}	64.39	15.53
	124	2.5	7.94x10^{-7}	118.90	8.41

Table 5.2 shows that, at the same crystallization temperature, the G of PP/filler nanocomposites is higher than that of neat PP and melt-mixed PP nanocomposites with the same filler load. For example, the G value of in situ

polymerized PP/$CaCO_3$ nanocomposite (5% $CaCO_3$) at a crystallization temperature of 120 ^oC is $32.07x10^{-3}$ s^{-1}, while at the same crystallization temperature neat PP has a G value of $6.55x10^{-3}$ s^{-1}, and the melt-mixed PP has a value of $27.48x10^{-3}$ s^1. This means that at comparable filler loadings and tacticities, the in situ polymerized PP sample has an enhanced crystallization rate compared to the melt-mixed PP sample. The improved dispersion of nanofiller in the in situ sample is the main reason for the enhanced crystallization rate.

5.3.4 Effect of the filler on the polymorphism of PP (crystal morphology)

WAXD patterns for pure PP and in situ prepared PP/filler nanocomposites are shown in Figure 5.12. The peaks at angles of 2θ = 18.4 and 20 are due to the α-phase and γ-phase, respectively. WAXD analysis shows that there is a difference in the PP matrix crystal structure between the two nanocomposites. The in situ polymerized nanocomposites exhibit a higher percentage of the γ-phase. No γ-phase was detected in the neat PP. It has been reported that the γ-phase can be promoted by low isotacticity and the presence of defects, such as 2,1 insertion, in the PP chains [14].

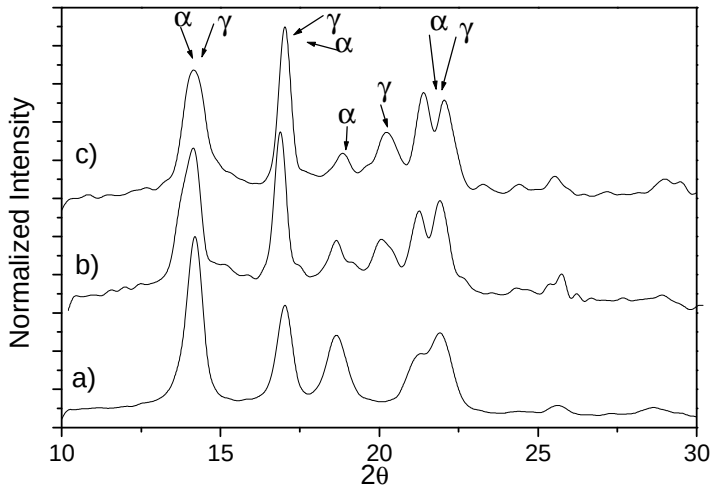

Figure 5.12: WAXD pattern of: a) pure PP, b) in situ polymerized PP/$CaCO_3$ nanocomposites, and c) in situ prepared PP/SiO_2 nanocomposites.

Thus, the high percentage of the γ-phase in the in situ polymerized nanocomposites might be due to the presence of chain defects as those

samples have low tacticities. However, when WAXD was performed on pure PP with different tacticity, there was no γ-phase crystal form detected, which is contradictory to the results reported in the literature [14]. Differences in the sample preparation procedure might explain this contradiction as isothermal crystallization is used to promote the formation of γ-phase in their samples.

However, when WAXD analysis was performed on the PP nanocomposites that were prepared with the low tacticity PPs, different results regarding the effect of the nanofillers on their crystal forms were obtained. WAXD patterns of these melt-mixed nanocomposites are shown in Figure 5.13.

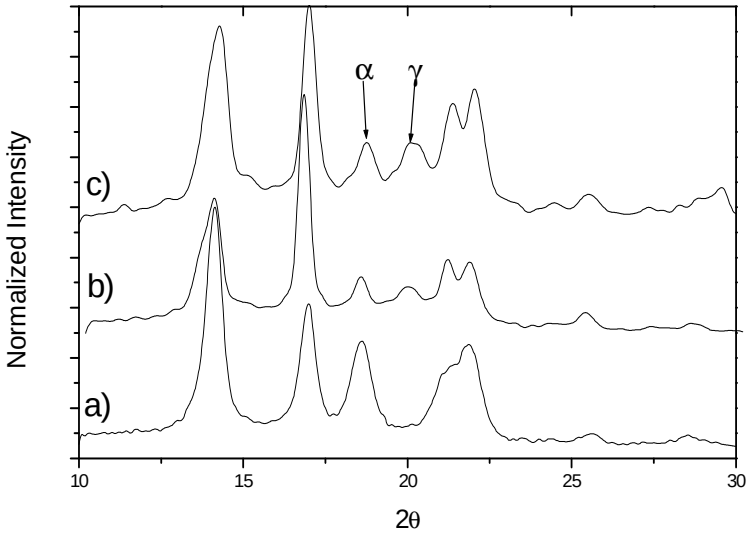

Figure 5.13: WAXD pattern of a melt-mixed PP/SiO_2 nanocomposite (5.0% SiO_2) prepared from PP with different tacticities: a) 97%, b) 94%, and c) 90%.

Melt-mixed PP/filler nanocomposites made with high tacticity PP show a WAXD pattern similar to that of the pure high tacticity PP, indicating that no change in the crystalline structure has occurred (Figure 5.13 a). The PP/filler nanocomposites made with PP of lower tacticity, on the other hand, show a small increase in the peak due to γ-phase, demonstrating the transformation of some of the α-phase to the γ-phase (Figure 5.13 b). The change of α-phase to the γ-phase by the addition of the nanofillers was more distinct in the nanocomposite made with the lowest tacticity PP (Figure 5.13 c). This result indicates that the nanofillers promote the γ-phase only when using PP of low tacticity.

5.3.5 Thermal stability of the nanocomposites

Figure 5.14 shows the TGA curves of pure PP and two different PP nanocomposites prepared by different methods: one prepared by melt-mixing and one prepared by in situ polymerization.

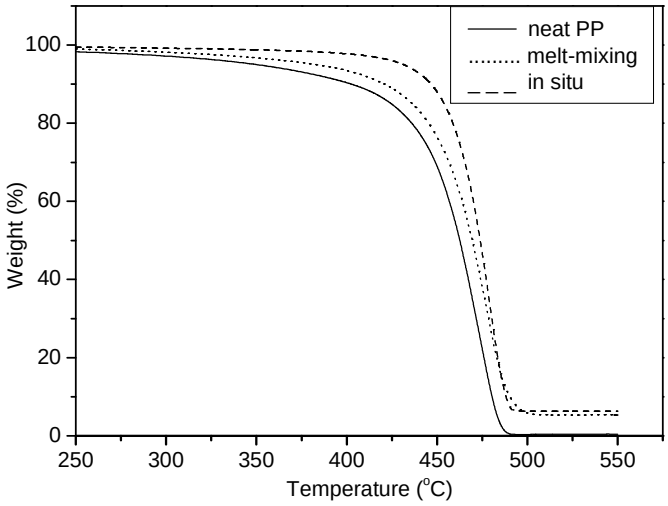

Figure 5.14: TGA curves for neat PP, and nanocomposites prepared by melt-mixing and in situ polymerization.

Both types of nanocomposite shows higher thermal stability than the pure PP, and the in situ prepared PP/silica nanocomposites have better thermal stability than the nanocomposites prepared via melt-mixing. Incorporation of filler nanoparticles into a polymer matrix generally increases the thermal stability of the nanocomposites [15, 16] This is because the presence of the nanofiller in the polymer restricts the polymer chain mobility [16, 17].

The reason for the higher thermal stability of the in situ sample over the melt-mixed sample might be due to the better dispersion of the nanofiller particles in the polymer matrix. Furthermore, in the in situ prepared nanocomposites some of the polymer chains are in direct contact with the silica surface, which contributes to enhancing the thermal stability.

5.4 Conclusions

In this part of the study, the effect of the synthesis method and filler content on the crystallization behaviour and morphology of PP/SiO_2 and PP/$CaCO_3$ nanocomposites were investigated. Results revealed that both

fillers had a nucleating effect on the crystallization of PP, leading to higher Tc of PP matrix and smaller spherulites. It was also found that, for the in situ prepared nanocomposite, the tacticity of the PP matrix played the major role in determining the Xt, while the Tc was more affected by the filler content. The results of isothermal crystallization showed that at all crystallization temperatures the crystallization rates of all PP nanocomposites were higher than that of pure PP. Furthermore, the crystallization rates of in situ prepared PP nanocomposites were higher than that of the melt-mixed PP nanocomposite at the same filler load. WAXD results showed that the incorporation of nanofiller into low tacticity PP resulted in the enhancement of the formation of the γ-phase.

5.5 References

1. Shentu, B.; Li, J.; Gan, T.; Weng, Z., *Eur. Polym. J.*, 2007. **43**: p. 3036.
2. Lin, D.; Huang, Z.; Zhang, Y.; Mai, C.; Zeng, M., *J. Appl. Polym. Sci.*, 2004. **91**: p. 2443
3. Zhu, P.; Zhang, P.; Yu, Y.; Dai, C., *J. Appl. Polym. Sci.*, 2004. **91**: p. 431.
4. Zhang, X.; Yu, Z.; Xie, L.; Mai,Y., *Polymer*, 2004. **45**: p. 5985.
5. Wan, W.; Chen, L.; Chua, C.; Lu, X., *J. Appl. Polym. Sci.*, 2004. **94**: p. 1381.
6. Xu, J.; Wang, Q.; Fan, Z., *Eur. Polym. J.*, 2005. **41**: p. 3011.
7. Edward, P.; Moore, J, *Polypropylene Handbook*. 1996: Hanser Publishers: Munich Vienna New York. p. 125.
8. Karger-Kocsis, J, *Polypropylene: structure, blends and composites*. Vol. 3. 1995. p. 8.
9. Jain, J.; Goossens, H.; Lemstra, P., *Polymer*, 2005. **46**: p. 8805.
10. Arranz, J.; Pena, B.; Benavente, R.; Perez, E.; Cerrada, M., *Eur. Polym. J.*, 2007. **43**: p. 2357.
11. Busico, V.; Cipullo, R.; Monaco, G.; Vacatello, M., *Macromolecules*, 1997. **30**: p. 6251.
12. Edward, P.; Moore, J, *Polypropylene Handbook*. 1996: Hanser Publishers: Munich Vienna New York. p. 114.

13. Gopakumar, T.; Lee, J.; Kontopoulou, M.; Parent, J., *Polymer*, 2002. **43**: p. 5483.
14. Xu, J.; Guan, F.; Yasin, T.; Fan, Z., *J. Appl. Polym. Sci.*, 2003. **90**: p. 3215.
15. Yang, R.; Liu, Y.; Yu, J.; Wang, K., *Polym. Degrad. Stab.*, 2006. **91**: p. 1651.
16. Tjong, S., *Mater. Sci. Eng., R*, 2006. **53**: p. 73.
17. Nitta, K.; Asuka, K.; Liu, B.; Terano, M., *Polymer*, 2006. **47**: p. 6457.

Chapter 6: Physical and mechanical properties of PP/filler nanocomposites prepared via melt-mixing and in situ polymerization

6.1 Introduction

It is well known that the physical and mechanical properties of a polymeric material are strongly dependent upon its structure and morphology [1]. Moreover, the properties of composite materials are determined by the characteristics of the polymer matrices themselves, together with the fillers, the adhesion fiber/matrix interface, and the preparation process [2]. Parameters such as the crystallite size and the tendency toward crystallization also play important roles.

The effects of aggregation of filler particles on the properties of composites are detrimental. Many authors emphasize this fact, together with the importance of best possible homogeneity [3, 4]. In this regard, the in situ polymerization of monomers in the presence of nanofillers offers a potential approach for achieving a more homogeneous distribution of inorganic nanoparticles. Unlike the melt-compounding method, where the addition of filler may change only the kinetics of nucleation, the crystalline fraction, and morphological organization, the in situ polymerization method may change the polymerization kinetics, resulting in a new material with completely different microstructures.

The mechanical properties of melt-mixed and in situ polymerized PP nanocomposites prepared using different natural fillers have been widely studied over the past few years [3, 4]. However, there is no information in the open literature on a comparison between these two different types of nanocomposites.

The main goal of this part of the study is to investigate and compare the mechanical behaviour of PP/filler nanocomposites prepared by melt-mixing and by in situ polymerization.

6.2 Experimental

6.2.1 Materials

6.2.1.1 In situ polymerized PP nanocomposites

A summary of the experimental details pertaining to the in situ polymerized nanocomposites samples used in this section of the work is given in Table 5.1.

6.2.1.2 Melt-mixed PP/filler nanocomposites

PP homopolymer with Mw 123 Kg/mol (MWD 2.2) and 94% mmmm pentad content was used as a matrix polymer. The syntheses of the melt-mixed PP nanocomposites were described in Section 4.2.3.2.

6.2.2 Sample preparation for mechanical tests

Test specimens were injection-moulded into standard bars for mechanical tests with a HAAKE MiniJet II injection moulder. The injection moulding temperature was 190 ℃ and the injection p ressure was 200 bars. The dimensions of the standard bar for tensile and impact tests are shown in Figure 6.1.

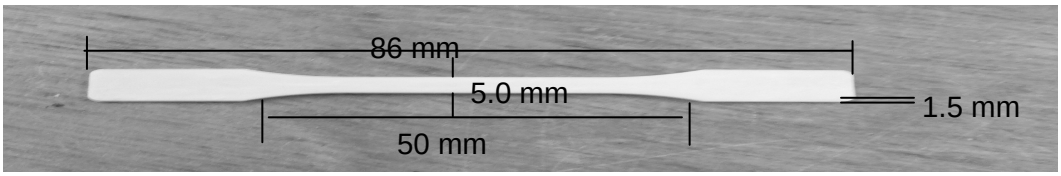

Figure 6.1: Photograph of the mechanical test bar.

6.2.3 Characterization techniques

6.2.3.1 DMA

Samples for compressive DMA analysis were examined on a Perkin Elmer DMA 7e calibrated according to standard procedures. The samples were melt-pressed at 180 ^{o}C. The samples were analyzed at a frequency of 1 Hz and the static force was kept constant at 110% of the dynamic force. The sample was heated to 130 ^{o}C to remove the thermal history and then the measurement was performed by cooling the sample to -60 ^{o}C at cooling rate of 5 ^{o}C/min.

6.2.3.2 Microhardness

MH measurements were conducted on a UHL microhardness tester equipped with a Vickers indenter. Measurements were obtained using 25 µm/s as the indentation speed and a dwell time of 15 s. Samples were analyzed at indentation loads of 10 gf.

6.2.3.3 Tensile test

Uniaxial tensile testing was performed using an Instron 4411 testing machine at room temperature. A crosshead speed of 10 mm/min was used. The yield stress, elastic modulus and elongation at break were obtained from these experiments. The size of the injected moulded specimens was 5 mm × 50 mm × 1.5 mm

6.2.3.4 Impact strength

Tensile impact testing was performed using a Ceast impact pendulum tester. The specimens were tested using a 15 J pendulum and a 60° release angle. At least three samples were tested for each sample and the average values reported.

6.2.3.5 Fracture mechanism

Samples were fractured at room temperature using very low fracture rate. The fracture surfaces were analyzed by SEM.

6.3 Results and discussion

6.3.1 Thermomechanical properties of PP nanocomposites

The storage modulus (G') is equivalent to elastic modulus in reflecting the material stiffness. The ratio of loss modulus (G'') to G' (tan δ) is related to the degree of damping of the material and is an indicator of how efficiently a material dissipates energy due to molecular rearrangements and internal friction (i.e. how well a material will stand up to impact).

The DMA results of the various samples are reported in terms of G' and tan δ. Figure 6.2 (a, b) presents the data of G' of pure PP and in situ prepared PP/filler nanocomposites as a function of temperature.

Since PP is a mixture of amorphous and crystalline regions it exhibits both a melting point and a glass transition. When PP is heated (or cooled) through the transition temperature (Tg) the storage modulus declines (or increases) rapidly, as can be seen in Figure 6.2. The value of the G', at temperatures lower than the Tg (< -18 ^{o}C), depends on the tacticity of the PP matrix, as the tacticity increases the value of the G' increases.

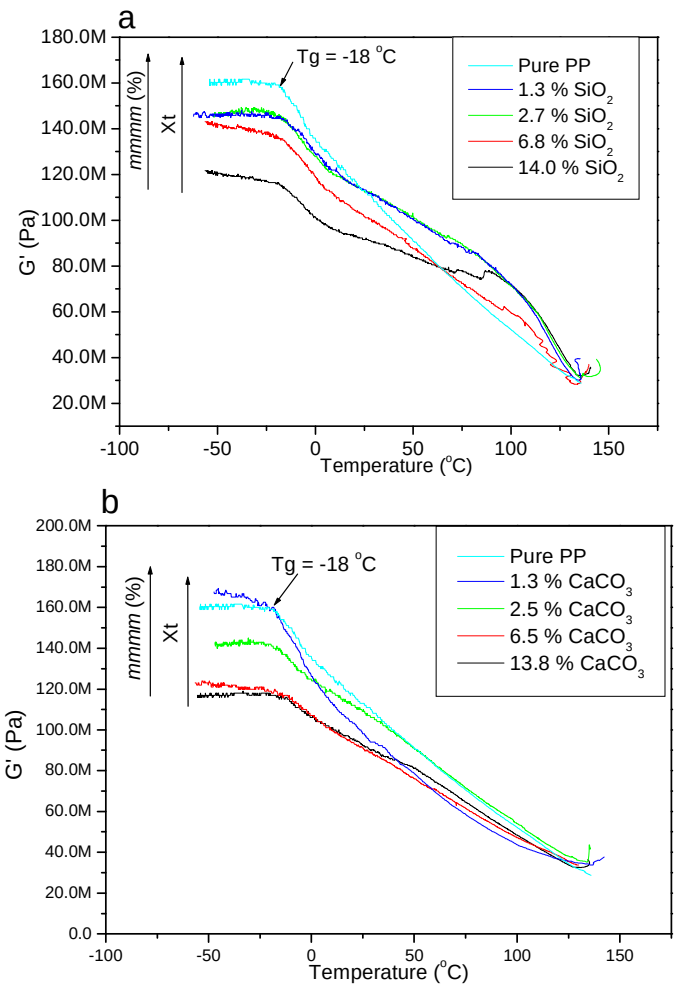

Figure 6.2: Storage modulus of pure PP and in situ prepared PP/filler nanocomposites with different filler loads at 1 Hz.

However, it seems that the presence of filler also has an effect on the value of the G'. When comparing the value of the G' of pure PP with that of the PP/$CaCO_3$ (1.3%) sample (Figure 6.2 b), it is clear that the higher the filler content the higher the value of the G' when polymers with similar tacticities are compared. It is well reported that for semicrystalline polymers (i.e. PP) the value of the storage modulus is determined by the tacticity [5], the degree of crystallinity [5], and the addition of filler [6].

Figure 6.3 shows the storage modulus of pure PP and melt-mixing prepared PP/filler nanocomposites. An increase in the storage modulus of the nanocomposites is observed despite the decrease in the degree of crystallinity (as shown in Section 5.3.2). These results, along with those obtained for the in situ prepared nanocomposites, indicate that although fillers can enhance the storage modulus, tacticity plays the key role in determining the value of the storage modulus. The DMA results of nanocomposites with different Mw values show that the storage modulus was not affected by the molecular weight of the PP matrix.

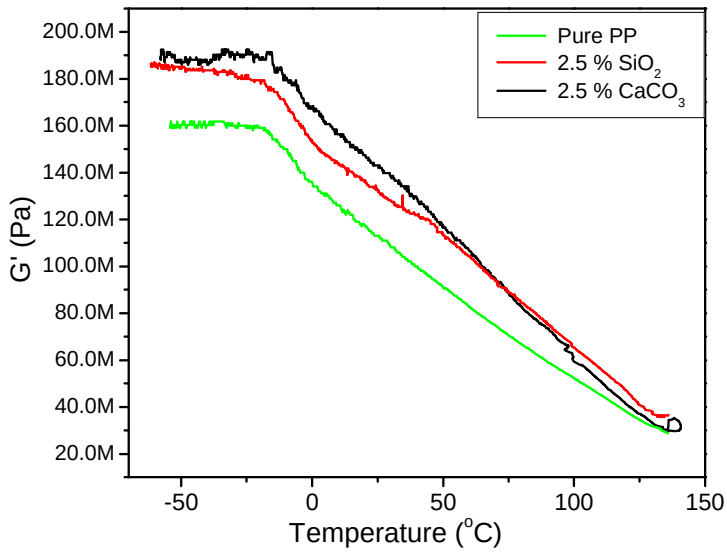

Figure 6.3: Storage modulus of pure PP and melt-mixed PP/filler nanocomposites at 1 Hz.

Figures 6.4 and 6.5 show the tan δ curves of the in situ prepared and melt-mixed PP/filler nanocomposites with different filler loads. The peak that appears over a temperature range, in the region of 0 ^{o}C, corresponds to the β-transition or glass transition temperature of isotactic PP.

Both figures clearly show that the intensity of the β-transition peaks of all PP/filler nanocomposites are higher than that of pure PP. PP samples that have a high intensity of the β-transition are expected to show high impact strengths above their glass transitions temperature because the intensity of the tan δ is related to the damping of the material and chain mobility.

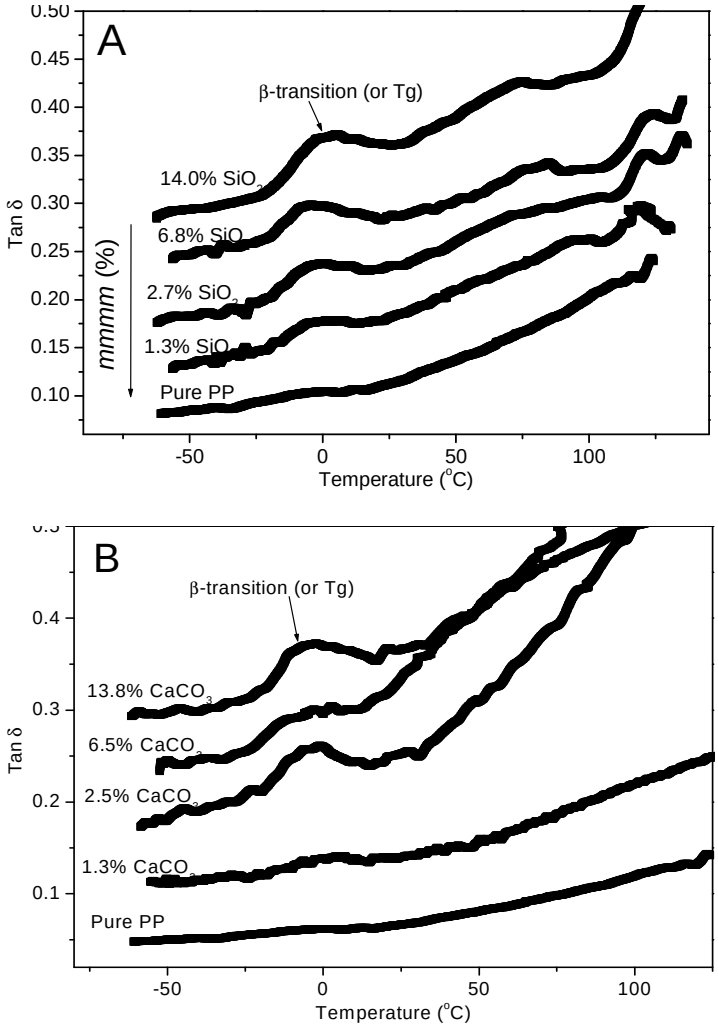

Figure 6.4: Tan δ of pure PP and in situ prepared PP/filler nanocomposites with different filler loads at 1 Hz.

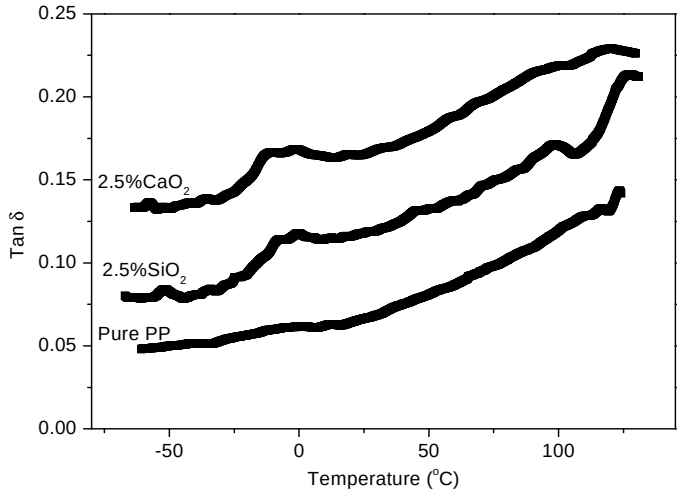

Figure 6.5: Tan δ of pure PP and melt-mixed PP/filler nanocomposites at 1 Hz.

The areas of the β-transition can be determined from the tan δ curve after subtraction of a linear baseline. Figure 6.6 shows a comparison of the

areas of the β-transition of the in situ polymerized and melt-mixed nanocomposite with similar filler load. The in situ polymerized nanocomposites have a larger area under the tan δ curve in the region of the β-transition than the melt-mixed nanocomposites (when nanocomposites with similar filler loads were compared). This result reveals that the synthesis technique plays an important role in determining the magnitude of the β-transition.

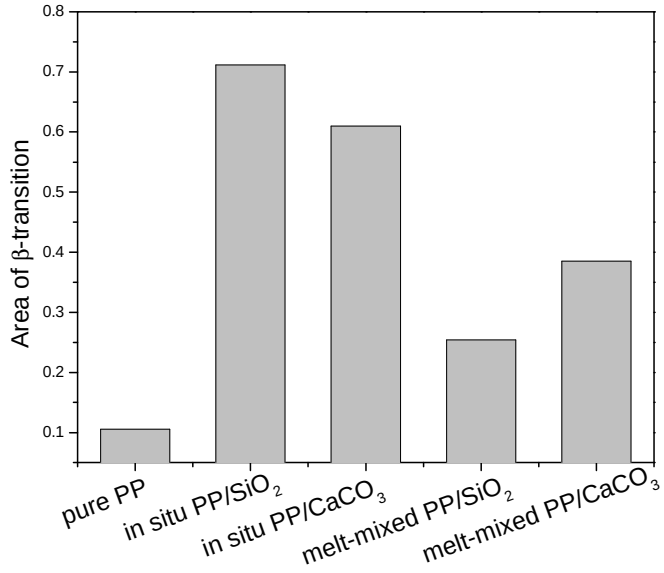

Figure 6.6: Magnitude of the area of the β-transition of pure PP and in situ and melt-mixed PP nanocomposites with similar filler loads of about 2.5%.

Since only the amorphous region undergoes this transition the difference in the intensity of the β-transition can be explained in terms of the differences in crystallinity. For melt-mixed PP/filler nanocomposites, Figure 6.6 illustrates that both melt-mixed nanocomposites show an increase in the β-transition intensity over pure PP. Furthermore, Figure 6.6 shows that the melt-mixed PP/$CaCO_3$ nanocomposite has higher β-transition intensity than melt-mixed PP/SiO_2. It was reported earlier (Section 5.3.2) that the addition of $CaCO_3$ filler to PP results in a substantial reduction in the degree of crystallinity, which might be the cause of the high intensity of the β-transition. However, in the case of SiO_2, where there was little decrease in the degree of crystallinity, the increase in the intensity of the β-transition might be due to a reduction of the crystal size.

For in situ polymerized nanocomposites, on the other hand, there are many other factors that might influence the intensity of the β-transition, as the systems presented in Figure 6.6 differ in matrix structure and dispersed phase morphology, and an explanation of these different factors is complex.

In order to clarify the effect of these factors on the intensity of the β-transition, the areas of the β-transitions of the in situ polymerized PP/$CaCO_3$ samples are given in Figure 6.7 as a function of the filler load. The PP microstructure and degree of crystallinity are also shown in the same figure.

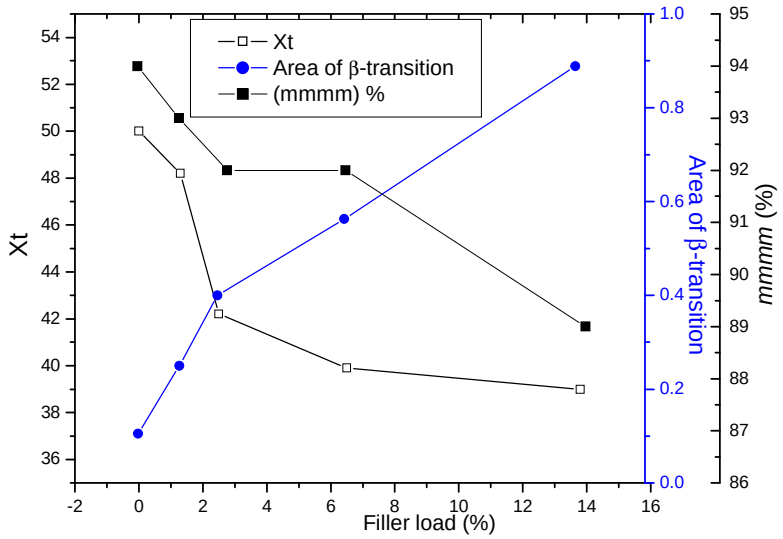

Figure 6.7: Magnitude of the β-transition of in situ polymerized PP/$CaCO_3$ nanocomposites as a function of filler load.

Figure 6.7 demonstrates that the tacticity and the degree of crystallinity of the PP matrix play major roles in determining the magnitudes of the β-transition. As the tacticity decreases, the percentage of the amorphous phase increases and consequently the magnitude of the β-transition increases. When comparing samples with similar tacticity (2.5% and 6.5% filler load in Figure 6.7), it is clear that with increasing filler content the degree of crystallinity decreases and the intensity of the β-transition increases. Thus it can be concluded that filler load plays an important role in determining the damping ability of the nanocomposites.

Thus, the differences between the magnitudes of the β-transitions of the in situ polymerized and melt-mixed PP/filler nanocomposite (See Figure 6.6) might be due to tacticity differences because the matrix of the in situ

polymerized nanocomposites has lower tacticity than that of the melt-mixed nanocomposites. The difference in the dispersed phase morphology is another important factor affecting the magnitude of the β-transition. A homogeneous distribution of filler in the PP matrix results in a smaller average crystal size and thus a larger β-transition, while poor filler dispersion results in non-homogeneous crystal regions and smaller β-transitions.

The Mw of the nanocomposite samples may also have an effect on the intensity of the β-transition. DMA analysis was performed on samples with different Mw to determine the influence of the Mw of the in situ polymerized nanocomposites on the intensity of β-transition. These two samples have comparable filler loads and tacticities. Results are shown in Figure 6.8.

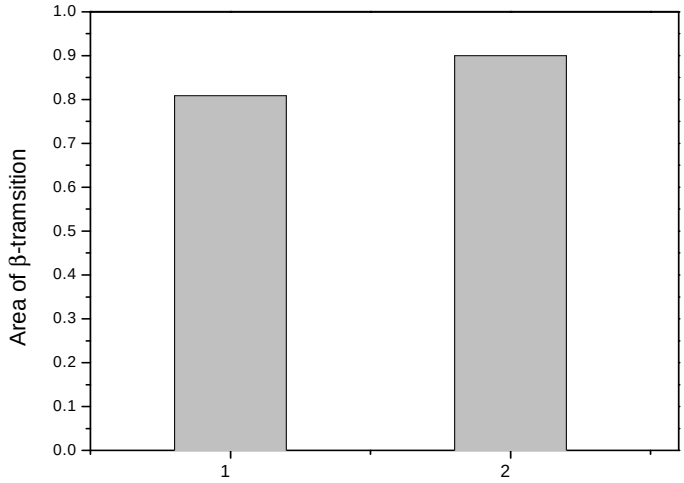

Figure 6.8: Effect of Mw on the magnitude of the area of the β-transition for in situ polymerized nanocomposites: 1) PP/$CaCO_3$ (13.8%) Mw 103; 2) PP/$CaCO_3$ (10.2%) Mw 190 kg/mol (see Table 5.1).

There is an increase in the magnitude of the β-transition of the in situ polymerized PP/$CaCO_3$ nanocomposites as the molecular weight increases. The increase in the magnitude of the β-transition of the high Mw sample could be due to a decrease in the degree of crystallinity caused by the higher molecular weight. This result is consistent with results reported by Stern and Weickert [7] who also found that the magnitude of the β-transition increased with increasing molecular weight.

The DMA results show that the Tg of PP is detected at about -18 ^{o}C, and that for both types of nanocomposites its position does not change with a

change in filler loading, as indicated by the fact that the peak in the tan δ curve did not change position. These results are consistent with results reported by Aso and Nazabal [8]. However, some authors have reported an increase in Tg with fillers which they attribute to the hindrance of the movement of the PP chains by the filler [6, 9, 10].

6.3.2 Microhardness

Hardness is a physical–mechanical characteristic of a material, defined as the local resistance against the penetration of a harder body under the pressure of a load. MH dependency upon structural parameters (molecular weight and degree of isotacticity) and thermal treatment is quite analogous to that observed for the modulus. Therefore, all the parameters that lead to an increase of crystallinity and crystallite sizes will provide higher MH values.

Figure 6.9 shows the MH of in situ polymerized PP/SiO_2 and PP/$CaCO_3$ nanocomposites. The tacticity and degree of crystallinity of the samples are also shown.

Generally, in PP composites the hardness increases as the filler concentration is increased [11]. However, Figure 6.9 shows that the MH follows the same trend as the tacticity and degree of crystallinity in spite of the increase in the filler content. These results are in agreement with the results obtained using DMA.

However, Figure 6.9 b shows that when the MH value of the in situ polymerized PP/$CaCO_3$ (1.3%) sample, which has a tacticity of 93% (MH 14.2 MPa), is compared with the MH value of pure PP, which has a tacticity of 94% (MH 13.0 MPa), one can see that the filler results in an increase in the MH of the in situ polymerized sample (when similar matrix tacticities are compared).

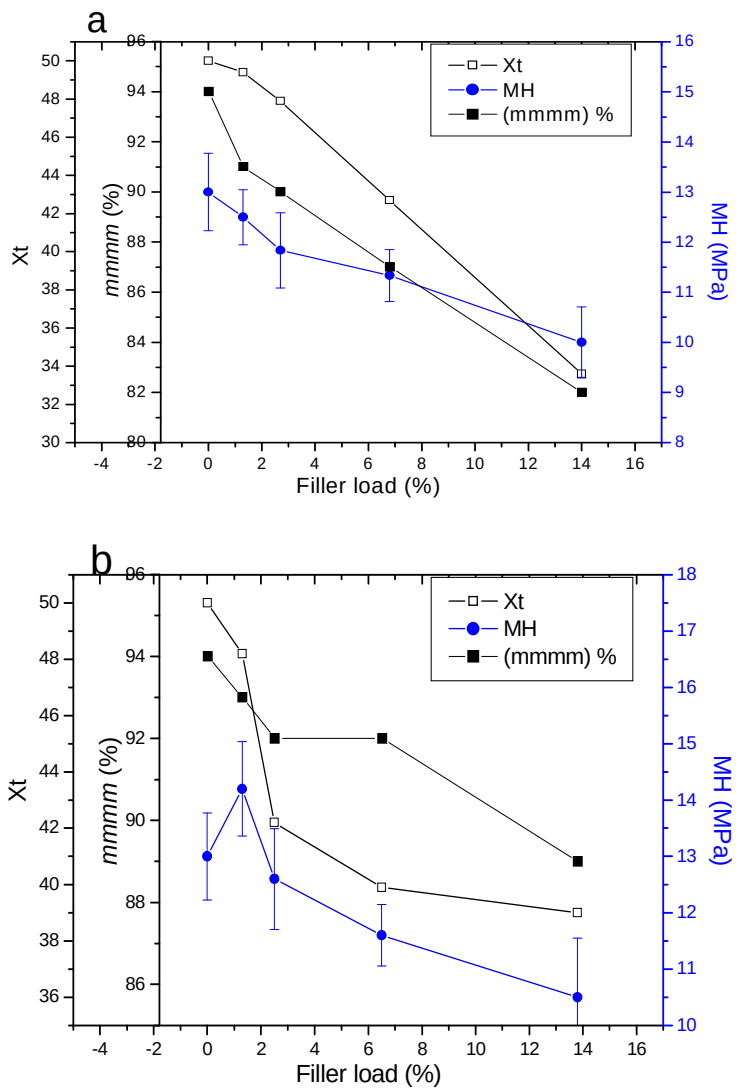

Figure 6.9: The MH values of in situ polymerized PP nanocomposites with different filler loads: a) PP/SiO_2 nanocomposites; b) PP/$CaCO_3$ nanocomposites.

Figure 6.10 illustrates the effect of the filler load on the MH of the melt-mixed PP/filler nanocomposites. The Xt of the respective samples are also included. The MH increases with filler content in spite of the decrease in the degree of crystallinity, especially in the case of PP/$CaCO_3$, where a substantial decrease in the crystallinity is observed.

Comparing the MH of the melt-mixed PP/$CaCO_3$ (1.5%) (MH 13.2 MPa) with the MH value of the in situ polymerized PP/$CaCO_3$ (1.3%) (MH 14.2 MPa), it is clear that the in situ polymerized nanocomposites show an improvement in the hardness of the sample when PP matrices with similar tacticities are compared.

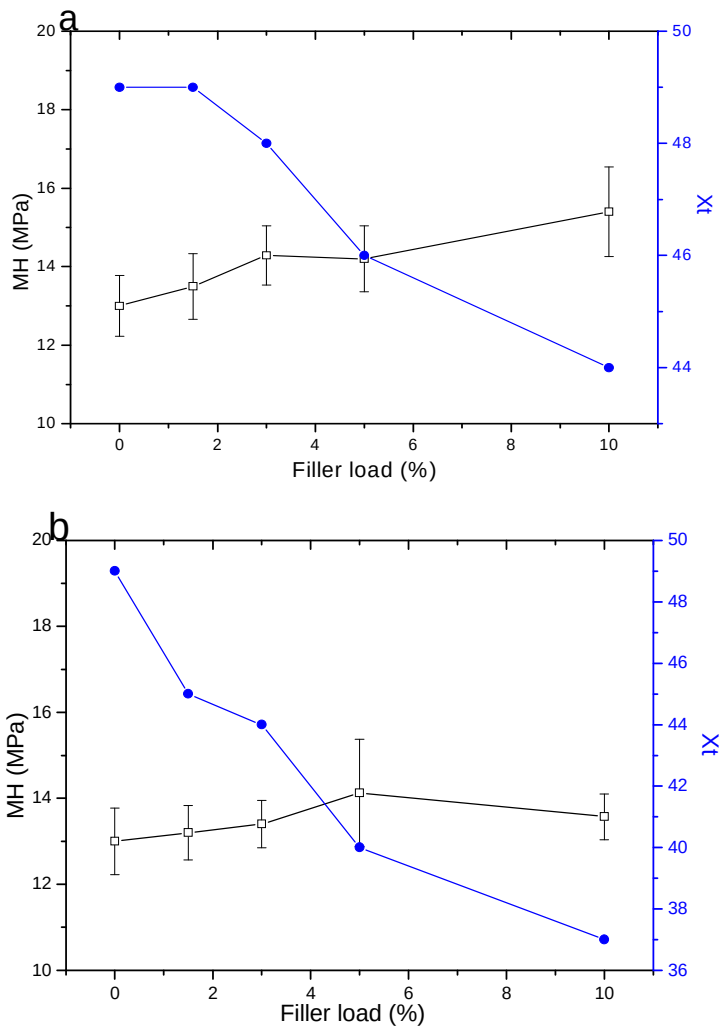

Figure 6.10: The MH values of melt-mixed PP nanocomposites with different filler loads: a) PP/SiO_2 nanocomposites; b) PP/$CaCO_3$ nanocomposites.

From the MH results of the melt-mixed nanocomposites (PP matrix having similar tacticity) and from results of in situ prepared nanocomposites it can be concluded that the filler content affects the hardness of the sample but the microstructure of the polymer matrix, and in particular the tacticity, is the main factor that determines the hardness of the composite.

6.3.3 Tensile properties of the nanocomposites

Tensile testing was carried out on PP/$CaCO_3$ nanocomposites to determine the effect of method of synthesis on the performance of the nanocomposites systems. PP nanocomposite samples with similar PP matrix microstructures and filler loads were selected for use. Since the synthesis of in situ polymerized PP nanocomposites with controlled PP microstructure and filler content is very difficult, it is not easy to obtain an in situ polymerized and

a melt-mixed nanocomposite with exactly the same PP matrix microstructures and filler contents. Therefore, two samples with comparable PP matrix microstructures and filler loads were chosen.

6.3.3.1 Tensile modulus

The effect of filler on the elastic modulus of a melt-mixed PP/$CaCO_3$ is shown in Figure 6.11. As expected, the tensile modulus of the system increases as the filler content increases.

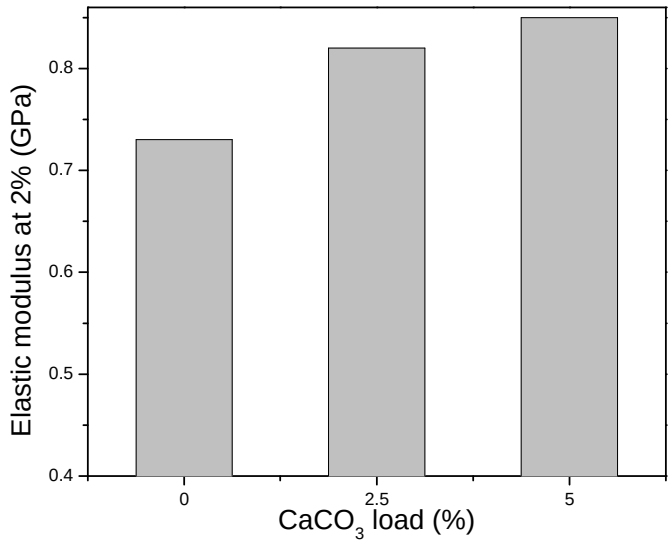

Figure 6.11: Effect of the filler content on the tensile modulus of melt-mixed PP/$CaCO_3$ nanocomposites.

In semicrystalline polymers, an increase in the crystallinity brings about an increase in the modulus [12]. The addition of inorganic fillers has long been known to increase the modulus of the products. The contribution of the stiffer inorganic filler to the modulus and the formation of a high modulus interfacial layer is the major reason for the increased modulus of the composites. During the crystallization of PP, the filler also acts as a nucleating agent, making the tie molecules drawn tight between spherulites, and resulting in an increased elastic modulus.

The tensile modulus of the in situ polymerized nanocomposites, however, is more dependent on the polymer matrix microstructure, in particular the tacticity, than on the filler content. To illustrate this, the experimental values of the tensile modulus of pure PP with an isotactic

content of 94% and in situ polymerized PP/$CaCO_3$ (13.8%) nanocomposites with an isotactic content of 89% are shown in Figure 6.12.

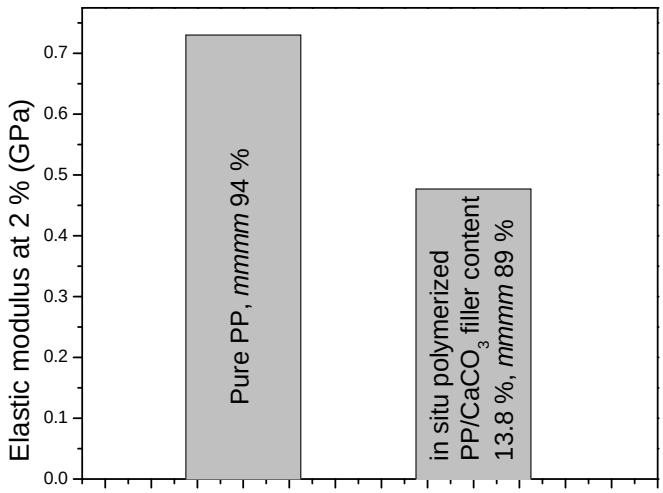

Figure 6.12: Effect of PP tacticity and filler content on the tensile modulus of pure PP and in situ polymerized PP/$CaCO_3$ nanocomposites.

Although the addition of filler is expected to increase the tensile modulus this effect is nullified by the effect of the tacticity of the PP matrix. This can clearly be seen by comparing the higher tensile modulus of high tacticity pure PP with the lower tensile modulus of the low tacticity PP/filler nanocomposite with the highest filler content. The tacticity is therefore the most important factor that determines the elastic modulus.

The tensile modulus of the various in situ polymerized nanocomposites was plotted as a function of the tacticity and is given in Figure 6.13. The tensile modulus increases with increasing tacticity regardless of the filler content and matrix molecular weight. Thus, for the in situ polymerized nanocomposites, the tensile modulus is determined mainly by the tacticity of the PP matrix, as opposed to the trend observed with the melt-mixed materials.

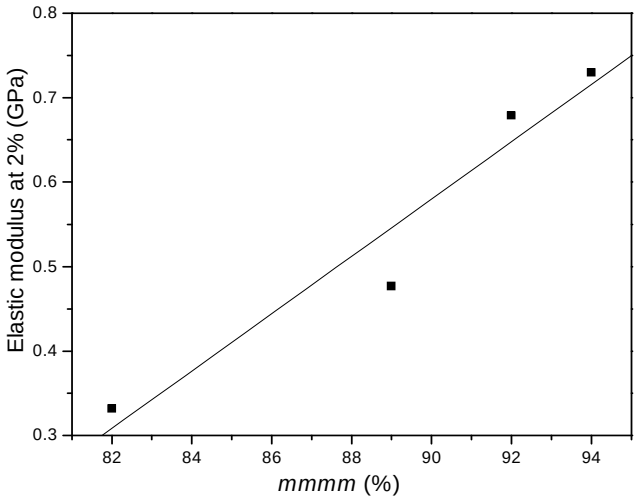

Figure 6.13: Dependence of elastic modulus on tacticity of PP matrix.

Figure 6.14 shows the tensile modulus of pure PP, an in situ polymerized PP/$CaCO_3$ (1.3%) sample, and a melt-mixed PP/$CaCO_3$ (1.5%) sample. The microstructures of these samples are given in Table 5.1.

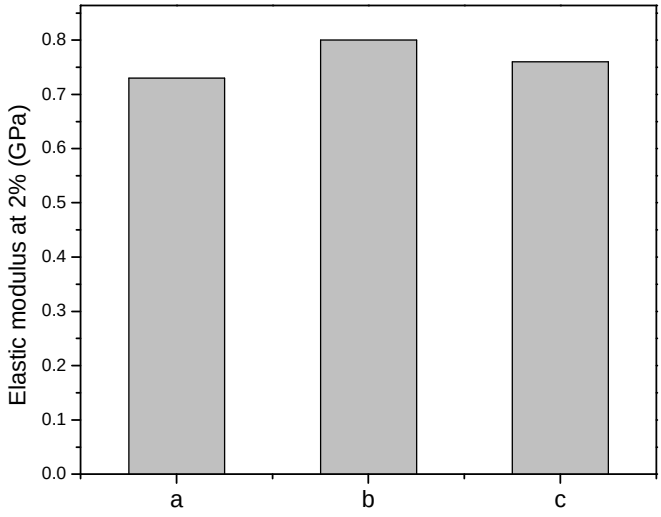

Figure 6.14: Tensile modulus of: a) pure PP, b) in situ polymerized PP/$CaCO_3$ (1.3%) sample, and c) melt-mixed PP/$CaCO_3$ (1.5%) sample with similar PP microstructures.

Figure 6.14 shows that, similar to the MH results, when samples with comparable tacticities are used the in situ polymerized sample has a higher tensile modulus than both pure PP and the melt-mixed PP nanocomposite at a similar filler loading. The improvement of the tensile modulus in the in situ polymerized sample over the melt-mixed PP nanocomposite at similar filler loading might be due to differences in the filler matrix interactions. The

polymer chains that were produced by the supported catalyst could result in an increased interaction between filler and matrix in the case of the in situ polymerized nanocomposite. The improved distribution of filler nanoparticles throughout the PP matrix in the in situ polymerized sample could be the cause of the higher tensile modulus.

6.3.3.2 Elongation at break

Results of the tensile tests generally revealed that all the samples break at relativity low strain. Most of sample exhibited a brittle fracture, and a cold deformation process or ductile fractures were not observed. This was despite the relatively low deformation rate during the tensile test (10 mm/min). This could be a result of a low concentration of tie molecules, due to the relativity low Mw and narrow MWD of the PP matrix. As a result of the possible low concentration of tie molecules the yield stress and crazing stress was greater than the stress needed for failure.

Figure 6.15 shows the effect of the addition of filler on the elongation at break of melt-mixed PP/filler nanocomposites.

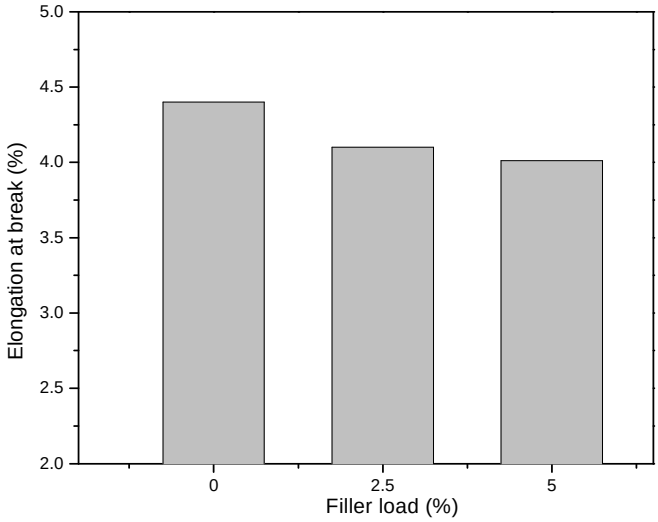

Figure 6.15: Effect of the filler content on the elongation at break of melt-mixed PP/$CaCO_3$ nanocomposites.

The elongation at break decreases with increasing filler content. Since no cold deformation process occurred, the decrease in the elongation at break with increasing filler content arises from the fact that the presence of filler restricts the movement or the stretching ability of the amorphous chains.

The effect of the filler content on the elongation at break for the in situ polymerized PP/filler nanocomposites was insignificant. Figure 6.16 shows the elongation at break for pure PP, in situ polymerized PP nanocomposite and melt-mixed PP nanocomposite. The systems shown in Figure 6.16 have comparable PP microstructure, with the exception that the in situ polymerized nanocomposite has a slightly lower tacticity. Both nanocomposites were chosen due to their similar filler content.

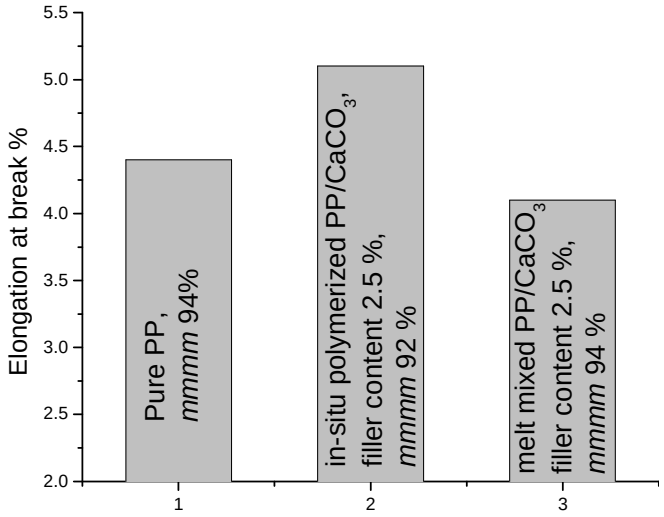

Figure 6.16: Effect of the synthesis method on the elongation at break.

Although the incorporation of filler into the polymer matrix decreases the elongation at break, Figure 6.16 shows that the in situ polymerized nanocomposite has a higher elongation at break than both the pure PP and the melt-mixed nanocomposite. The synthesis method clearly has an effect on the elongation at break. The homogeneous dispersion of the nanoparticles in the PP matrix results in better distribution of crystallinity and thus an increased elongation at break.

The slight lower tacticity of the in situ polymerized sample might be a major factor for the higher elongation at break of the in situ polymerized sample. The effect of the tacticity on the elongation at break is shown in Figure 6.17. The elongation at break increases with decreasing tacticity, regardless of the filler content.

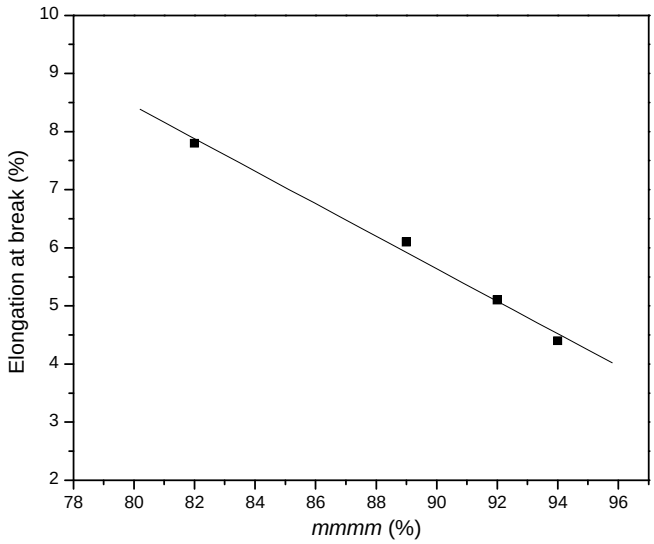

Figure 6.17: Dependence of elongation at break on tacticity of PP matrix.

The increase in the elongation at break of the low tacticity sample was not due to a cold deformation process, but rather to the increasing elasticity of the PP matrix. As a result of the low tacticity the polymer chains are not perfectly packed during the crystallization. For this reason, tie-molecules are not drawn tightly between spherulites. In other words, when force is applied the tie-molecules orient in the direction of the applied stress without any yield occurring in the crystalline structure.

6.3.3.3 Tensile strength

The results of the tensile strength tests presented in this chapter are the ultimate tensile strengths or stress at break.

Figure 6.18 shows the tensile strengths of pure PP, in situ polymerized PP/CaCO3 (2.5%), and melt-mixed PP/$CaCO_3$ nanocomposites (2.5%). The microstructures of these samples are given in Table 5.1.

Comparing the tensile test results of the melt-mixed PP/filler nanocomposite with that of the in situ polymerized PP nanocomposites, it can be concluded that much improved tensile properties (tensile strength) were obtained for the in situ polymerized PP/filler nanocomposites when PP matrices with comparable Mw were used. This result indicates that the synthesis method has a huge impact on the performance of the PP nanocomposites. This might be attributed to the much better distribution of the

nanoparticles in the case of the in situ polymerized PP nanocomposite (as was shown by TEM results, Section 4.3.6). The homogeneous dispersion of nanoparticles produces a homogeneous stress concentration in the PP matrix under the influence of an external load. The homogeneous dispersion of nanoparticles also results in very small homogeneous spherulites, which in turn results in a higher density of tie molecules.

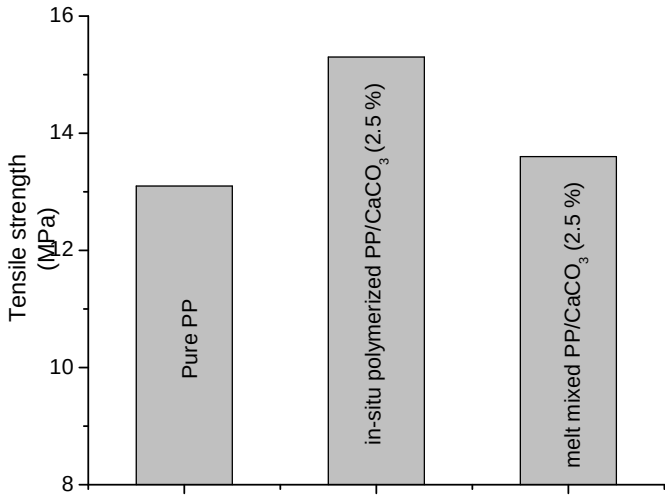

Figure 6.18 Effect of the synthesis method on the tensile strength at break of PP nanocomposites (see Table 5.1 for details on the microstructures of the samples).

Enhanced interactions between the filler nanoparticles and PP matrix could also be a possible reason for the improvement in the performance of the in situ polymerized PP nanocomposites, as some PP chains are produced on the surface of the particle.

In order to investigate the effect of the polymer matrix Mw on the tensile strength, a tensile test was performed on two samples with different Mw, and comparable filler content and tacticities. The tensile strengths of PP/$CaCO_3$ (10.2%) (Mw 190 kg/mol) and PP/$CaCO_3$ (13.8%) (Mw 103 kg/mol) are shown in Figure 6.19.

The PP/filler nanocomposite with the higher Mw has a tensile strength that is about double that of the PP/filler nanocomposite with the lower Mw. Hence the polymer matrix Mw is the most important factor that determines the tensile strength of the composites. This is attributed to an increase in the number of tie molecules. An increase in the Mw causes an increase in the number of tie molecules [13].

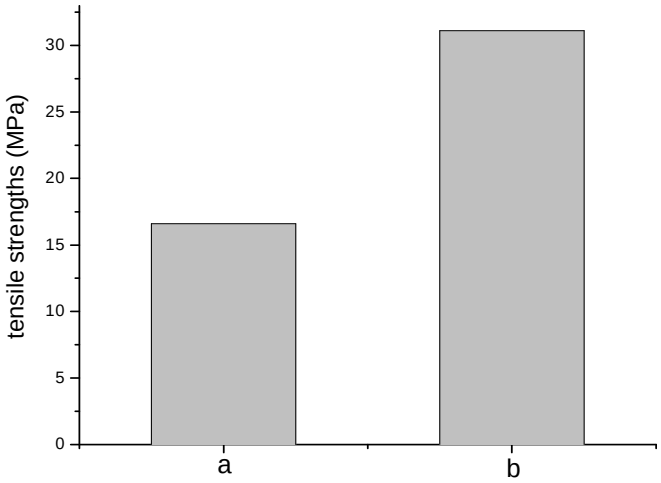

Figure 6.19: Effect of Mw on tensile strength for in situ polymerized PP/$CaCO_3$ nanocomposites: a) Mw=103; b) Mw=190 kg/mol.

The importance of tie molecules of semicrystalline polymers on the deformation process is well documented and is illustrated in Figure 6.20. A high percentage of tie molecules results in sufficient stress transferred between the crystalline lamellae. This will force the polymer chains to be drown as a fiber from the crystal part.

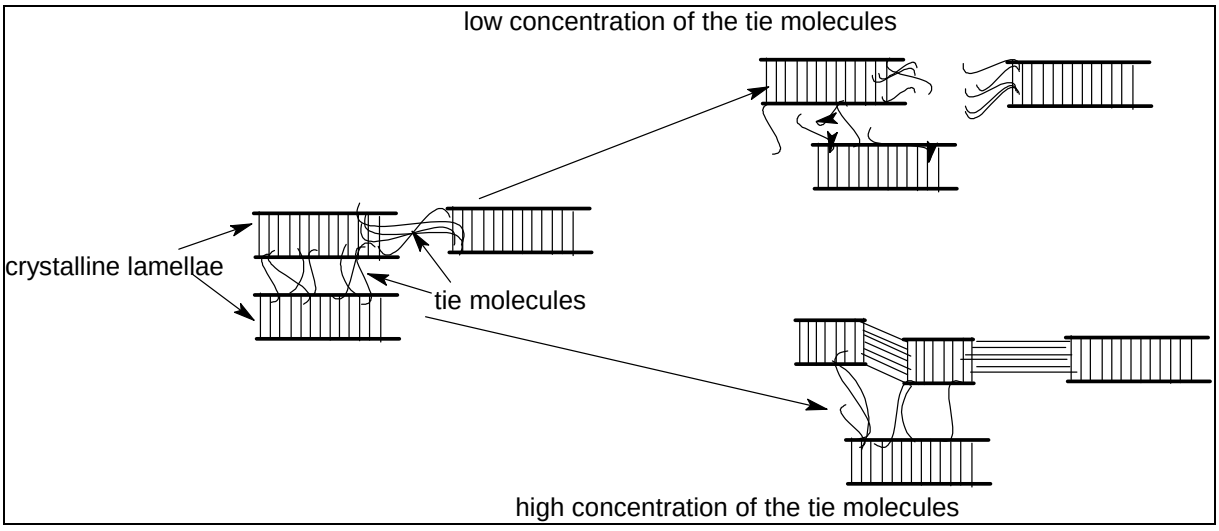

Figure 6.20: Effects of tie molecules on the deformation process during a tensile testing.

6.3.4 Impact strength

Results of impact tests performed on in situ polymerized and melt-mixed PP nanocomposite as well as pure PP, with comparable Mw values are shown in Figure 6.21. Generally, very low impact energies were recorded. This is due to the relatively low Mw of the tested samples, which affects the

density of chain entanglement and, consequently, the brittle to ductile transition. The in situ polymerized PP/filler nanocomposite has a higher impact strength than both the pure PP and the melt-mixed PP nanocomposite.

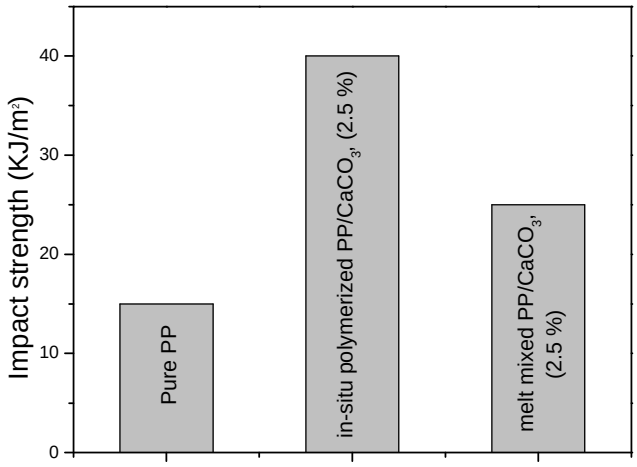

Figure 6.21: Impact strength of pure PP and PP/filler nanocomposites prepared using different synthesis methods.

The impact toughness reflects the degree of energy absorption from the beginning of mechanical loading to final fracture. It appears that the in situ polymerization method plays an important role in generating a process or a response in which the PP matrix has the ability to disperse energy.

The impact strength depends on several parameters, such as the inherent deformation behaviour, the entanglement density (which affects plasticity), and flow-induced orientation. In PP nanocomposites the impact strength is further affected by the stress distribution around the nanoparticles, interfacial debonding, plastic deformation of interparticle ligaments and crack deflection. The results show that both the in situ prepared and the melt-mixed nanocomposites have higher impact strength than pure PP. A possible explanation for the improvement of the impact strength of both nanocomposites is the enhancement of the density of chain entanglement, which generates shear yielding in the PP matrix.

The improvement of impact strength of the in situ polymerized PP nanocomposites might be due to the better nanoparticle distribution (as proved in Section 4.3.6). The possible enhancement of interfacial debonding

in the in situ polymerized composite due to the close contact of polymer and filler during synthesis is another reason for the improvement of its impact strength. More details will be provided on this issue when the mechanism of failure is discussed (Section 6.3.5).

6.3.5 Investigation of the fracture mechanisms

The SEM micrographs of the fractured surfaces obtained during the impact tests on pure PP, melt-mixed PP nanocomposite, and in situ PP nanocomposites are shown in Figures 6.22, 6.23, and 6.24, respectively.

The fracture surface morphology of all specimens shows the same features, in which the crack propagation generates two different morphologies: the rough zone (close to the crack edge) where the crack propagates and generates crazes at the surface, and the smooth zone where the crack grows without any plastic deformation.

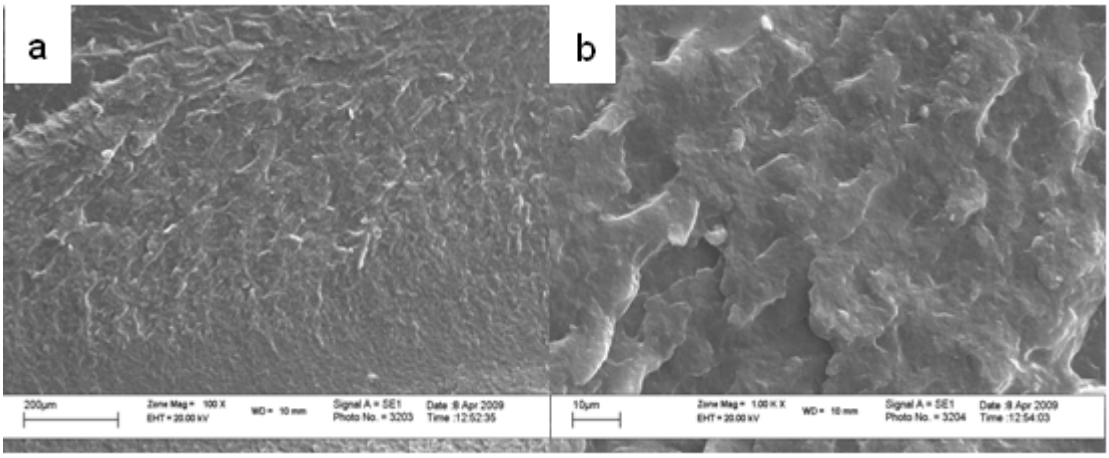

Figure 6.22: SEM micrographs of: a) an impact fracture surface at the initial crack roots in a pure PP sample; b) an enlarged view at the rough zone.

Figure 6.22 shows that the extension of rough zones in pure PP is limited and most of the fractured surface was smooth. It is also clear that pure PP exhibits no signs of plastic deformation or drawing (Figure 6.22 b). The breaking of the -C-C- bonds of the tie molecules is the dominating mechanism for energy dispersion. The tie molecules do not have the strength required to force the crystallized chains to be withdrawn from the spherilite structure to form a fiber or craze zone.

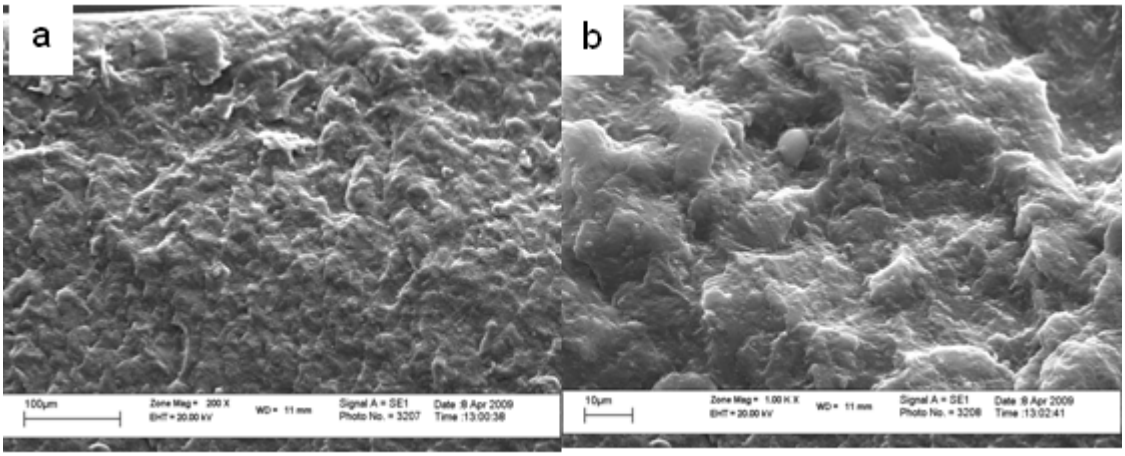

Figure 6.23: SEM micrographs of: a) an impact fracture surface at the initial crack roots in a melt-mixed PP nanocomposite; b) an enlarged view at the rough zone.

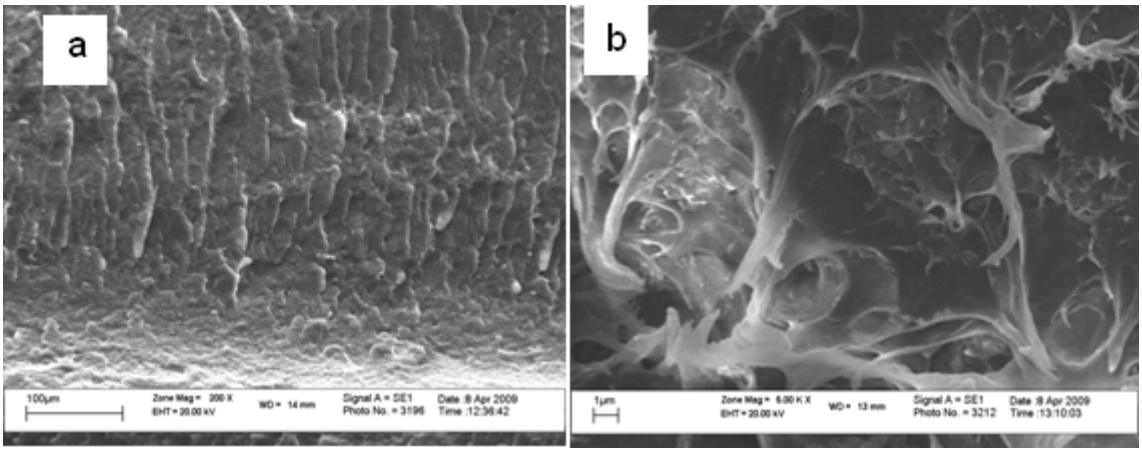

Figure 6.24: SEM micrograph of: a) an impact fracture surface at the initial crack roots in an in situ prepared nanocomposite; b) an enlarged view at the rough zone.

On the other hand the fracture surface morphology of the melt-mixed PP nanocomposite (Figure 6.23) shows that the extent of the rough zones is large. The figure also illustrates that the fracture surface becomes rougher than that of the pure PP, indicating the start of the formation of crazes. However, some agglomerated nanoparticles can be seen in Figure 6.23 b. These agglomerated nanoparticles cause stress concentrations in the PP matrix and premature failure will occur before the yielding stress reached.

In contrast with the previous systems the fracture surface morphology of in situ polymerized PP shows clear evidence of plastic deformation (Figure 6.24 b). This may be because the interfacial debonding between the filler nanoparticles forces the polymer chains to be pulled from the matrix

generating shear yielding in the PP matrix. The good nanoparticle distribution also creates much better stress distribution around the nanoparticles.

6.4 Conclusions

The relationships between synthesis–structure–morphology-properties have been investigated for PP/filler nanocomposites. The results revealed that incorporation of inorganic filler into the PP matrix via melt-compounding increases the modulus related properties. However, the modulus and its related properties, in the case in situ polymerized nanocomposites, were mainly determined by the PP matrix microstructure. On the other hand tensile and impact strength were greatly improved for the in situ polymerized nanocomposites compared to the melt-mixed nanocomposites, and this was attributed to improvement in both nanoparticle dispersion and interfacial adhesion. The results also revealed that the Mw of the PP matrix is the main factor affecting the tensile and impact strengths. Finally the fracture mechanisms showed that matrix deformation and the formation of multiple crazes were the major energy absorbing mechanisms.

6.5 References

1. Edward, P.; Moore, J, *Polypropylene Handbook*. 1996, Munich: Hanser.
2. Karger-Kocsis, J, *Polypropylene: structure, blends and composites*. Vol. 3. 1995.
3. Tjong, S., *Mater. Sci. Eng., R*, 2006. **53**: p. 73.
4. Jordan, J.; Jacob, K.; Tannenbaum, R.; Sharaf, M.; Jasiuk, I., *Mater. Sci. Eng., A*, 2005. **393**: p. 1.
5. Arranz, J.; Pena, B.; Benavente, R.; Perez, E.; Cerrada, M., *Eur. Polym. J.*, 2007. **43**: p. 2357.
6. Lee, G.; Jagannathan, S.; Chae, H.; Minus, M.; Kumar, S., *Polymer*, 2008. **49**: p. 1831.
7. Stern, C.; Frick, A.; Weickert, G., *J. Appl. Polym. Sci.*, 2007. **103**: p. 519.
8. Aso, O.; Eguiazabal, J.; Nazabal, J., *Compos. Sci. Technol.*, 2007. **67**: p. 2854.

9. Tjong, S.; Meng, Y.; Hay, A., *Chem. Mater.*, 2002. **14**: p. 44.
10. Zhang, T.; Ruan, W.; Yang, J.; Rong, M, Zhang, Z., *Compos. Sci. Technol.*, 2007. **67**: p. 2279.
11. Dasari, A.; Rohrmann, J.; Misra, R, *Mater. Sci. Eng., A*, 2004. **364**: p. 357.
12. Dario Del Duca.; Edward, P. Moore, J, *End-Use Properties*, in *Polypropylene Handbook*, P.M. Edward, J, Editor. 1996, Hanser: Munich. p. 240.
13. Nitta, K.; Takayanagi, M., *J. Polym. Sci., Part B: Polym. Phys.*, 1999. **37**: p. 357.

Chapter 7: The effects of the filler characteristics on the properties of PP nanocomposites

7.1 Introduction

The effects of fillers on the mechanical and other properties of polymer composites depends strongly on their shape, size and size distribution of the primary particles and their aggregates, surface characteristics, and the degree of dispersion and distribution.

In terms of the size, when the filler is very large then high filler loadings (20–40%) are required to achieve markedly improved properties. High filler loadings may, however, adversely affect the processability.

The adhesion between the filler and the matrix is very important for PP composites. The two major factors that determine the particle–particle interactions are particle size and surface free energy [1].

$CaCO_3$ and SiO_2 are inorganic materials that do not exhibit good adhesion to thermoplastic matrices. Therefore, surface modification of filler particles with suitable coupling agents is often recommended to enhance the filler–particle dispersion into PP matrices, to improve strong bonding with the matrix.

Although the effects of the filler particles' parameters such as type [2, 3], size [4] and surface function [5], on the mechanical properties of PP/$CaCO_3$ have been extensively examined, the balance between these parameters on the one hand and the mechanical properties and processability of the composites on the other hand is not yet fully understood. This chapter therefore describes an investigation into the influence of the particles parameters on the mechanical properties and processability of PP composites.

7.2 Experimental

7.2.1 Materials

PP homopolymer (Moplen–Himont, Italy) with Mw 690 kg/mol and a MWD 5.2 was used in this study. Nanosilica (15 nm) was obtained from Sigma-Aldrich. Four different types of precipitated calcium carbonate were kindly donated by Solvay. The coated calcium carbonates were treated with fatty acid by the manufacturer. Material specifications are listed in Table 7.1.

Table 7.1: Characteristics of filler particles

code	trade name	Specific surface (m^2/g)	Mean particle diameter (nm)
SiO2	Silica	150	15
Uncoated CC0.07	SOCAL® 31	20	70
Uncoated CC0.25	SOCAL® P2	8	250
Coated CC0.07	SOCAL® 311	19	70
Coated CC0.1	SOCAL® U1S2	16	100

7.2.2 Preparation of nanocomposites

The filler particles were dried before melt-compounding, by heating to 100 ℃ under vacuum for 6 h. The compounding was ca rried out for 15 min using a mechanical stirrer. The mixing temperature was 230 ^{o}C and the rotor speed was 60 rpm. In a typical experiment, 4 g of PP was charged into the mixer and then antioxidant and the predetermined quantity of filler were added. After mixing, the nanocomposites were ground into powder.

7.2.3 Characterization techniques

7.2.3.1 SEM

To evaluate the dispersion quality of the $CaCO_3$ nanoparticles, freeze-fractured surfaces of the PP/$CaCO_3$ nanocomposites obtained at liquid nitrogen temperature were examined. The SEM analysis procedure was described in Section 4.2.4.5.

7.2.3.2 DSC

As described in Section 4.2.4.3.

7.2.3.3 MFI

The processability of the filled PP composites was determined with a CEAST melt flow indexer, according to a standard procedure. A load of 2.16 kg at 230 ^{o}C was used.

7.2.3.4 MH

As described in Section 6.2.3.2.

7.2.3.5 Tensile test

As described in Section 6.2.3.4.

7.2.3.6 Impact strength

As described in Section 6.2.3.5.

7.3 Results and discussion

7.3.1 Dispersion of filler nanoparticles

The main purpose of treatment of the filler is the reduction of the surface free energy, which results in a decrease of particle–particle interactions. Weaker interaction leads to a dramatic decrease in aggregation, improved dispersion, and better mechanical properties.

Figure 7.1 shows SEM micrographs of the fractured surfaces of the various PP/filler nanocomposites at a filler load of 20%.

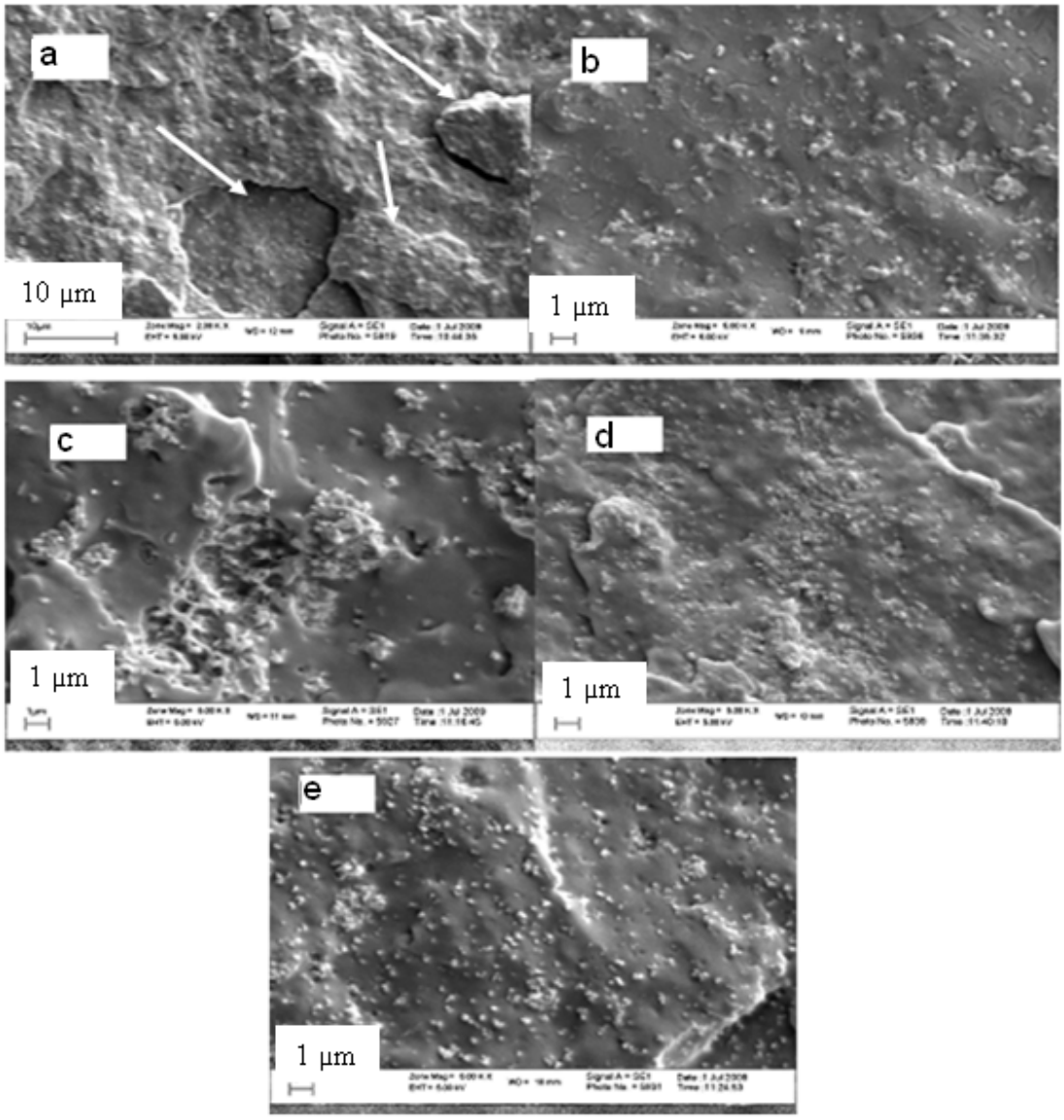

Figure 7.1: SEM images of fracture surfaces of various PP/filler nanocomposites with 20% filler: a) untreated SiO_2 nanoparticle, b) uncoated CC0.07, c) uncoated CC0.25, d) coated CC0.07, and e) coated CC0.1.

Figure 7.1 (a) shows that there are many large aggregated particles in the PP composites filled with SiO_2 nanoparticles. This is due to the high surface tension of SiO_2 (257.7 mJ/m^2) and the small particles size [6]. The particle

aggregations were also observed in the case of the PP composites filled with uncoated CC0.07 (Figure 7.1 (b)) and uncoated CC0.25 (Figure 7.1 (c).

The size of the aggregated particles in all PP/$CaCO_3$ nanocomposites is smaller than that of the PP/SiO_2 nanocomposites. The lower surface tension of the $CaCO_3$ (207.9 mJ/m^2) compared to the SiO_2 allows the shear forces during compounding to break down all the large $CaCO_3$ aggregates.

Figure 7.1 (d) and (e) show SEM images of the fractured surface of PP filled with coated CC0.07 and coated CC0.1. Better dispersion with a lower degree of agglomeration of the filler was observed when the surface of the $CaCO_3$ particles was coated with a fatty acid.

When the fractured surfaces of the PP/filler nanocomposites with similar surface characteristics but with different filler particle sizes are compared (CC0.07 and CC0.1), it is clear that the larger the particle size the less aggregation occurs. This is because larger filler particles have a lower surface tension compared to small filler particles.

7.3.2 Crystallization behaviour

The different nanocomposites were examined according to their crystallization behaviour. The effect of the filler size, filler content, and surface treatment on the crystallization temperatures are shown in Figure 7.2.

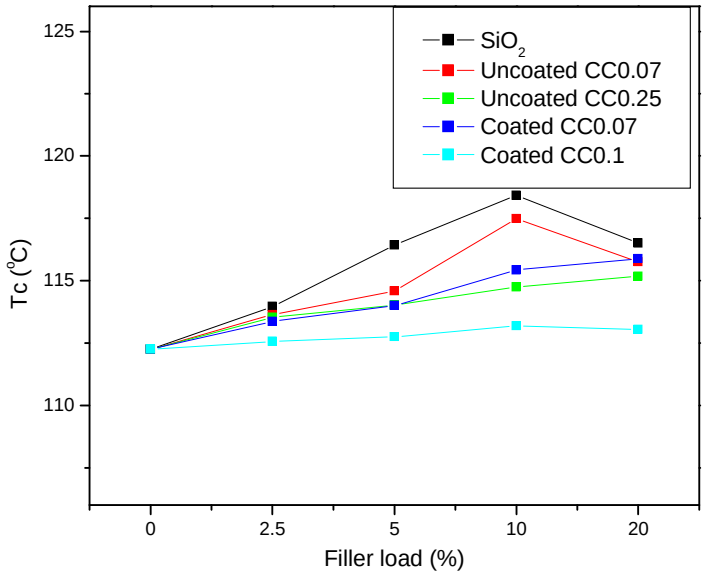

Figure 7.2: Crystallization temperature of PP as a function of filler content for various types of filler.

Figure 7.2 shows that pure PP has a Tc at about 112.3 ^{o}C and that the Tc value of all nanocomposites are higher than that of pure PP. The increase in the Tc upon increasing the filler content illustrates the nucleating effect of these fillers on PP crystallization up to 10% filler. At higher concentrations, Tc decreases slightly due to the restricted mobility of polymer chains by the fillers.

It is also clear that the various fillers affect the Tc of PP differently. The Tc values for the nanocomposites made with SiO_2 nanoparticles were higher than those of the other nanocomposites. This might be due to either the difference in inherent characteristics of the surface of the fillers or differences in particle sizes of the different fillers. The high tendency of SiO_2 to interact with other surfaces due to the high surface tension of SiO_2 might be the cause of the highest Tc. The PP nanocomposite made with the uncoated CC0.07 nanoparticles shows a higher Tc than that made with uncoated CC0.25, for all filler contents. This means that the size of the filler particles, if homogenously dispersed, has an influence on the crystallization behaviour. It is reported that reducing the particle size of $CaCO_3$ leads to the appearance of a second crystallization peak, and then to the shift of the complete crystallization peak to higher temperatures [7].

The Tc of the PP/uncoated CC0.07 nanocomposites is higher than that of the coated CC0.07 based nanocomposites regardless of the $CaCO_3$ content. Nanocomposites made with coated CC0.1 show the lowest Tc. The results clearly suggested that the treatment of the surface of $CaCO_3$ particles with fatty acid reduced the nucleating ability of these particles towards PP. Similar results were reported by Rungruang et.al [8], where the Tc value of PP filled with untreated $CaCO_3$ particles was higher than that of PP filled with stearic acid coated $CaCO_3$.

A possible explanation for this behaviour is that, unlike the surface of neat $CaCO_3$, the chains of the fatty acids on the coated $CaCO_3$ are wavering during the crystallization process and as a result a delay in the crystallization process of PP will occur. Another possible explanation is that when the filler surface is coated with fatty acids the free surface tension is decreased, thus reducing its wettability.

The effects of the various filler types and the filler loading on the Xt of the PP matrix are shown in Figure 7.3. Generally, there is a decrease in the Xt with an increase in filler load for SiO_2, coated CC0.07 and uncoated CC0.07 filled PP nanocomposites, regardless their filler loads.

However, nanocomposites made with larger fillers (coated CC0.1 and uncoated CC0.25) show an increase in the Xt at low filler loading (2.5%), after which the Xt decreases as the filler load increases. It is worth mentioning here that, at high filler load, the weight fraction of filler will affect the value of the Xt. However, the decreases in the Xt were obtained even after subtraction of the filler portion.

From these results it seems that the size of the filler particles is the main factor that influences the Xt despite the surface characteristic of the fillers.

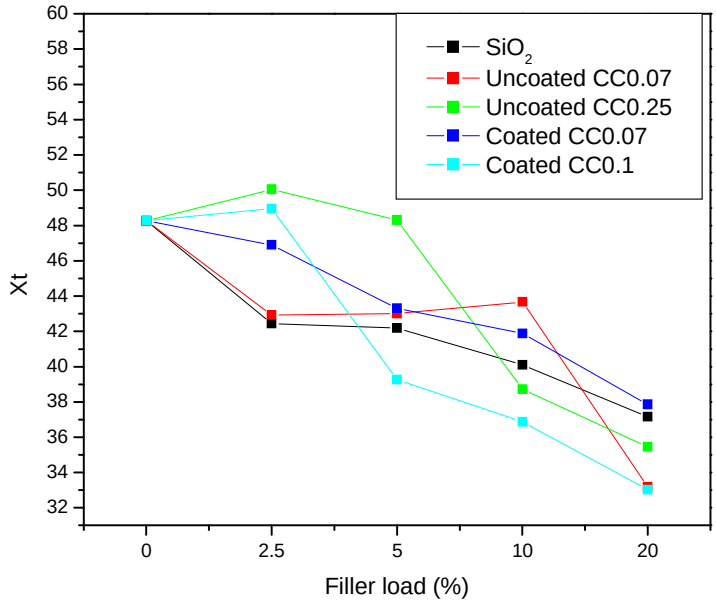

Figure 7.3: The effects of filler types and loading on the Xt of PP.

The decrease in the degree of crystallinity, as explained in Chapter 5, is due to the presence of an excessive number of filler particles which can hinder the motion of the polymer chain segments and thus retard crystal growth.

The increase in the Xt at low filler loading (2.5%) for coated CC0.1 and uncoated CC0.25 based nanocomposites might be due to large interparticle distances. At the same filler loads, as the filler size increase, the average distance between adjacent particles increases, thus allowing the polymer chains to move freely without any retardation by the filler. The addition of filler particles generally causes a reduction of the average distance between adjacent particles. Another possible reason is that the production of low Mw polymer chains by chain scission during compounding will result in high crystallinity.

7.3.3 Effect of filler type on MFI

In the thermoplastic processing industry, the MFI is an important parameter that is widely used to characterize the flow property of resins due to its ease of measurement. Generally, an increase in MFI value indicates better molecular motion between polymer chains.

The MFI values of various composites are shown in Figure 7.4. The MFI values for PP nanocomposites filled with SiO_2, coated CC0.07, uncoated CC0.07, and coated CC0.1 decrease with increasing filler content.

The incorporation of fillers hinders the flow of polymer and increases the viscosity of the polymer melt, thus a reduction of the MFI with increasing filler loading is expected. The MFI values of SiO_2 filled PP were lower than those of the neat PP and $CaCO_3$ filled PP nanocomposites.

When comparing the MFI values of the uncoated CC0.07 filled PP composites with those of the coated CC0.07 filled PP composites at all filler loading it is clear that the coated CC0.07 filled PP has improved processability compared to the uncoated CC0.07. This result was in agreement with the results of other related studies reported by several authors [9-11].

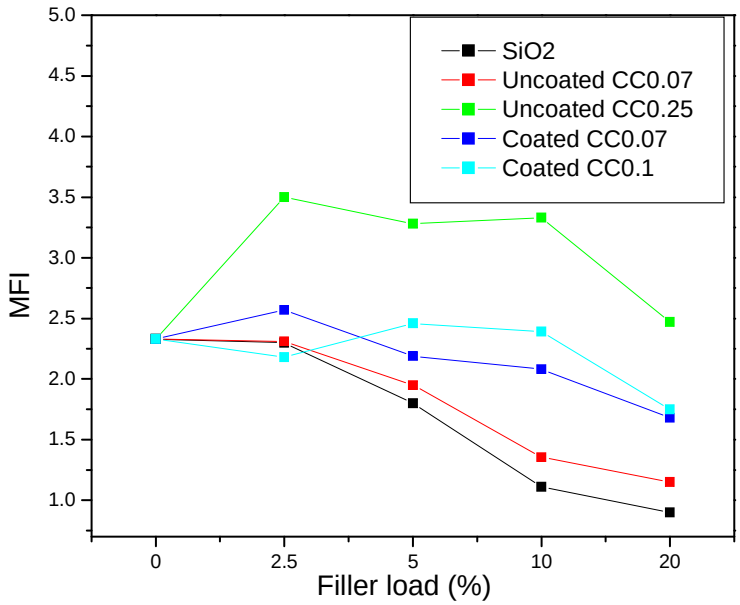

Figure 7.4: The effect of filler types and loading on the MFI values of PP nanocomposites.

This increase in melt flow may have been due to the lubricating/plasticizing effect induced by the coupling agent. According to Han et al. [11] the reduction in melt viscosity with the presence of a coupling agent may result from the surface modification of the filler particles. Thus, under shear

stresses, there could be far less frictional resistance to flow with treated filler particles than would be possible with untreated filler particles.

The MFI values for the PP composites filled with uncoated CC0.25 fillers, however, increased slightly compared to that of the pure PP. This trend agreed with the work of Ai Wah et al. [12], who reported an increase in MFI with the incorporation of filler into PP. Since this filler was uncoated, the lubricating effect is not possible and thus the possible reasons for this phenomenon could be molecular chain scission or change in MWD.

7.3.4 MH

The microhardness results of various nanocomposites are shown in Figure 7.5.

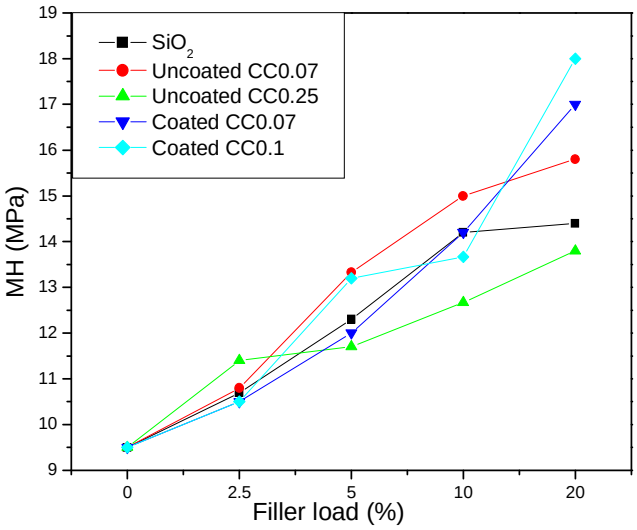

Figure 7.5: The influence of filler types and loading on the MH values of PP nanocomposites.

As demonstrated in the previous chapter, the MH results show an increase in the MH values with increasing the filler content for all types of fillers. Although Figure 7.5 shows that there are no major differences regarding the effect of filler type on the MH results of the nanocomposites at low filler load, at high filler load (e.g. 20%) the coated filler samples have higher MH values than those containing the uncoated filler. At filler loads of 20%, comparing fillers with

the same surface characteristics but differences in the particle sizes, it seems that the smaller the particle size the higher the MH value. Taking into account the effect of the fillers on the Xt, which is known to have a significant effect on the MH value, it is clear that this effect was a result of differences in the interaction between the filler and the matrix and not a result of differences in Xt. The size of the interfacial layer is also very significant in determining the MH value as this layer has a higher modulus and MH value than the PP matrix. Increasing the $CaCO_3$ particle size and treatment of $CaCO_3$ with fatty acid decreases the thickness of this layer [13]. Thus, PP filled with small $CaCO_3$ particles and uncoated $CaCO_3$ should have higher MH. The contradictory results might be due to the differences in filler dispersion.

7.3.5 Tensile properties

Figure 7.6 shows the tensile modulus of the various filled PP composites. A significant improvement in the modulus of PP can be observed for all types of filled PP. Due to the fact that the modulus is measured before any significant plastic deformation takes place in the crystalline phase, the differences in the values of the tensile modulus of the various composites is due to differences in the interaction between the fillers and the polymer matrix. The changes in crystallinity, the thickness of the interfacial layer, and level of chain tightening in the amorphous phase are also factors that influence the tensile modulus of PP composites.

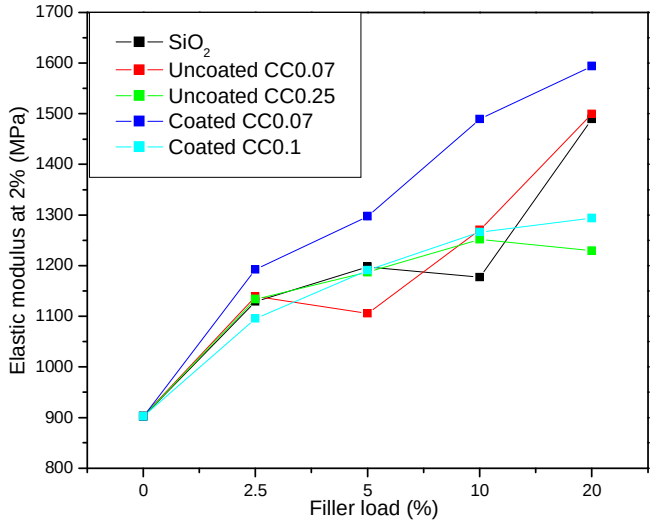

Figure 7.6: Effects of the different filler types and loadings on the tensile modulus of PP nanocomposites.

Figure 7.6 illustrates that the coated CC0.07 filled PP shows the highest tensile modulus. Comparing the tensile modulus of coated CC0.07 filled PP with that of uncoated CC0.07, it can be concluded that although the coated filler reduces the thickness of the interfacial layer, the homogenous dispersion of coated CC0.07 in the matrix produces a smaller crystal size with tighter chains in the amorphous phase.

Furthermore, when the tensile modulus of coated CC0.07 filled PP is compared with that of coated CC0.1 based nanocomposite it is clear that the size of the filler has an effect on the restriction of the polymer chains in the amorphous phase. The smaller the filler size the more restriction of the polymer chains and thus the higher the modulus.

The results of the elongation at break of the various filler filled PP nanocomposites are shown in Figure 7.7. It can be seen that pure PP has the highest elongation at break and that the incorporation of fillers into PP resulted in a drop in the elongation at break. The high elongation at break of pure PP originates from the cold drawing of the large spherulite structures to form fibres. Incorporation of the fillers reduces the size of the spherulites. The presence of the fillers also suppresses the ability of the PP matrix to undergo plastic

deformation. It appears that at the highest filler load the failure mode of the PP matrix shifts from ductile to brittle and that no cold deformation has occurred.

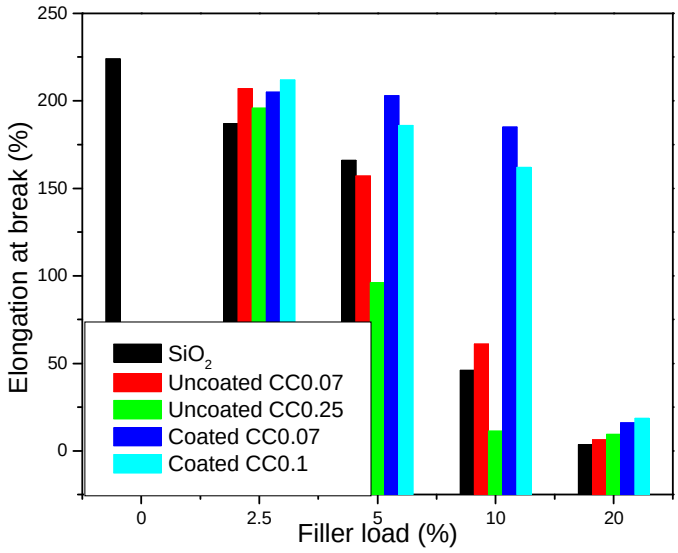

Figure 7.7: Effects of the different filler types and loadings on the elongation at break of PP nanocomposites.

Furthermore, Figure 7.7 shows that the elongation at break of coated CC0.07 and coated CC0.1 filled PP composites has improved drastically compared to that of the other PP composites and that this could be attributed to the improved dispersion of the filler in the PP matrix. The improved dispersion of the filler in PP matrix results in a homogenous stress concentration and thus cold drawing of the small spherulites occurs evenly.

Figure 7.8 shows the tensile strength of various filler filled PP nanocomposites. Only the coated CC0.07 filled PP shows a slight improvement in the tensile strength compared to pure PP at filler loads of less than 10%. A decrease in the tensile strength was observed for most of the other nanocomposites. SiO_2 filled PP showed the lowest tensile strength followed by uncoated CC0.25 then uncoated CC0.07.

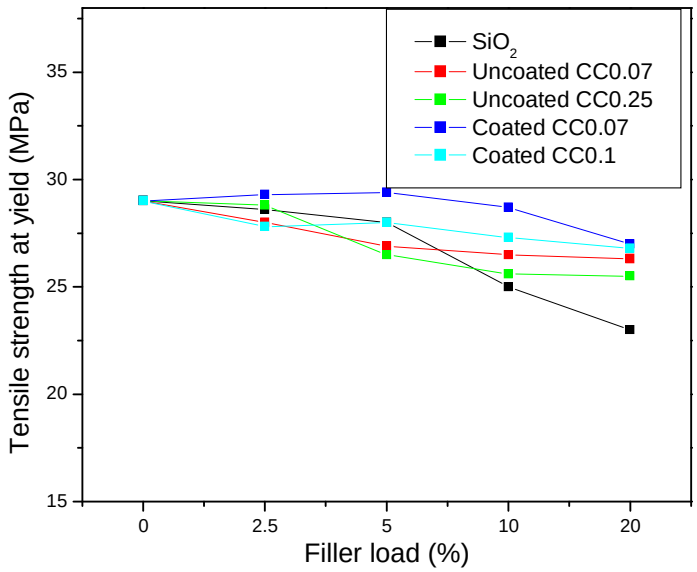

Figure 7.8: Effects of the different filler types and loadings on the tensile strength of PP nanocomposites.

It is worth mentioning here that the results presented are the yield tensile strengths, which is the strength that is required in order to destroy the crystalline structure to form a fibre structure through the drawing or the crystal-slips of polymer chains from the crystalline structure. Therefore, a possible explanation for the slight increase in the yield tensile strength after addition of coated CC0.07 is that it reduces the local stress on the crystalline structure by forming a homogenous stress distribution in the PP matrix. Thus, enhancement of the tensile strength requires a homogenous distribution of the filler particles in the PP matrix.

The decrease in strength of SiO_2 filled PP composites was mainly due to poor filler distribution, as shown in Section 7.3.1, which was largely due to the high surface energy of SiO_2.

Tensile test results show that the tensile strength of all PP nanocomposites diminished at high filler content (≥10%). At filler loadings higher than 10%, agglomeration occurs resulting in decreased tensile strength.

7.3.6 Impact strength

The results of impact strength of pure PP and PP filled with various fillers of various sizes and surface characteristics are presented in Figure 7.9. It is evident that the impact strengths of PP filled with coated CC0.07 and coated CC0.1 particles were higher than those of PP filled with SiO_2, uncoated CC0.07, and uncoated CC0.25 at all filler loadings.

The impact strengths of uncoated CC0.25 filled PP were the worst compared to pure PP and other PP composites over the whole range of filler loads. The drastic decrease in the impact strength of uncoated CC0.25 filled PP can be attributed to the decrease in the Mw of the PP matrix and the change in MWD which is a result of molecular chain scission during compounding. Another possible reason for the low impact strength of this sample is that the low Mw chains increase the degree of crystallinity (see Section 7.3.2). The high degree of crystallinity in turn enhances the immobilization of the PP chains, which limits their ability to adapt to the deformation and, therefore, makes the composite more brittle.

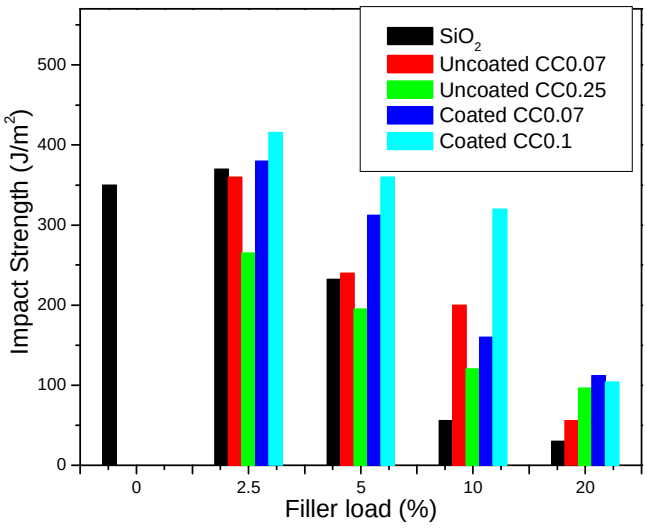

Figure 7.9: Effects of the different filler types and loadings on the impact strength of PP nanocomposites.

For the SiO_2 and uncoated CC0.07 filled PP, the agglomeration of the filler particles results in a decreased impact strength because of the low strength of the agglomerates themselves, particularly at high filler loads.

The improvement of the impact strengths of PP filled with coated CC0.07 and coated CC0.1, especially for lower filler contents was the result of the homogeneous distribution of $CaCO_3$ in the matrix as shown in Section 7.3.1.

7.4 Conclusions

It has been shown that during the melt-mixing the filler type, size, and applied surface coating significantly influence the flow, thermal, and mechanical properties of filled PP. SEM studies revealed that better distribution with decreased agglomeration of the $CaCO_3$ particles within the PP matrix was found for the fatty acid coated fillers. Study of the crystallization of the various PP nanocomposites revealed that both the size and the surface characteristic of the filler can influence the Tc while the Xt was affected mainly by the size of the filler particle independent of the surface characteristic of the fillers. Examination of the flow behaviour of the various PP composites shows that the incorporation of the filler in PP adversely affected the processability. However, PP filled with coated filler shows improvement in the processability compared to PP filled with uncoated filler. This effect was explained by the lubricating effect of the fatty acid. Study of the mechanical properties showed that for all PP nanocomposites the MH and tensile modulus of the PP nanocomposites increased with increasing filler content. Finally, the results show that a homogenous dispersion of nanoparticles is essential in order to obtain PP nanocomposites with improved performance. A homogenous dispersion of nanoparticles can be achieved by coating the nanoparticles with fatty acids.

7.5 References

1. Pukanszky, B., *Polypropylene: structure, blends and composites*. Composites, ed. J. Karger-Kocsis. Vol. 3. 1995, London: Chapman and Hall. p. 8.

2. Leong, Y.; Ishak, Z.; Ariffin, A., *J. Appl. Polym. Sci.*, 2004. **91**: p. 3327.
3. Supaphol, P.; Thanomkiat, P.; Junkasem, J.; Dangtungee, R., *Polym. Test.*, 2007. **26**: p. 20.
4. Zuiderduin, W.; Westzaan, C.; Huetink,J.; Gaymans, R., *Polymer*, 2003. **44**: p. 261.
5. Alexandre, M.; Dubois, P., *Mater. Sci. Eng., R*, 2000. **28**: p. 1.
6. Karger-Kocsis, J, *Polypropylene: structure, blends and composites*. Vol. 3. 1995. p. 26.
7. Karger-Kocsis, J, *Polypropylene: structure, blends and composites*. Vol. 3. 1995. p. 5.
8. Rungruang, P.; Grady, B.; Supaphol, P, *Colloids Surf., A*, 2006. **275**: p. 114.
9. Leong, Y.; Abu Bakar, M.; Ishak, Z.; Ariffin, A., *J. Appl. Polym. Sci.*, 2005. **98**: p. 413.
10. Doufnoune, R.; Haddaoui, N.; Riahi, F., *Int. J. Polymer. Mater.*, 2007. **56**: p. 977.
11. Han, D.; Van Den Weghe, T.; Shete, P.; Haw, R., *Polym. Eng. Sci.*, 1981. **21**: p. 196.
12. Ai Wah, C.; Leong, Y.; Gan, N., *Eur. Polym. J.*, 2000. **36**: p. 789.
13. Karger-Kocsis, J, Polypropylene: structure, blends and composites. Vol. 3. 1995. p. 21.

Chapter 8: Conclusions and recommendations

8.1 Conclusions

The aim of this dissertation was to broaden the current understanding of the structural and morphological changes in the polymers induced by nanofillers, for nanocomposites prepared by melt-blending and by in situ polymerization. In particular the in situ polymerization which is proven to be a successful approach to obtain a homogenous dispersion of filler in polymer matrix.

In this dissertation, in situ polymerizations of propylene with metallocene/MAO catalysts in the presence of the fillers were used successfully for the synthesis of in situ polymerized PP/filler nanocomposites. The synthesis of melt-mixed PP/filler nanocomposites was also performed in order to have a base case with which to correlate the synthesis–structure–property relationships.

In Chapter 3, two filler types (silica and calcium carbonate nanoparticles) were examined as a carrier for a metallocene catalyst. Different immobilization methods were investigated and the main aim of this chapter was to achieve a supported catalyst with high activity, relative to that of a homogeneous polymerization.

FTIR result revealed that the concentration of the hydroxyl groups on the SiO_2 is higher than that on the $CaCO_3$. The FTIR results also illustrated that the surface of $CaCO_3$ filler is characterized by the presence of hydrocarbon groups as indicated by the band at 3000 cm^{-1}. FTIR results also demonstrated that the thermal treatment of the fillers is essential in order to get rid of the adsorbed water molecules.

EDX results revealed that a metallocene catalyst could be successfully supported on both fillers. It was also shown that the concentration of the OH groups, which can be adjusted via thermal treatment, affects the catalyst and the cocatalyst loading on the filler. For example, in the case $CaCO_3$ filler, Al and Zr loading increased as the treatment temperature increased from 25 to 100 ^{o}C and then decreased.

EDX analysis also revealed that the catalyst and cocatalyst loading on the SiO_2 filler is much higher than that on $CaCO_3$ filler. This is attributed to the

higher intensity of the OH group on the SiO_2 than on $CaCO_3$ and also to the hydrophobic characteristic of the $CaCO_3$ surface.

This chapter also demonstrated that the impregnation of MAO on filler prior to metallocene immobilization is important, which led to higher catalyst contents on the filler, and thus higher activity than directly grafting the metallocene onto the fillers. The results of this chapter concluded that a supported catalyst prepared with preactivated catalyst pre-Zr-MAO-filler (method 3) shows a huge improvement in polymerization activity and should be used in the synthesis of in situ nanocomposites.

In Chapter 4 the effect of the presence of filler particles on the polymerization rate and consequently on the produced polymer microstructure was investigated. It was shown that at low polymerization time the in situ polymerization has lower R_p than that of the homogenous polymerization. However, as the polymerization time proceeds, the decay in the R_p of the homogenous polymerization was faster than that of the in situ polymerization. The difference in the R_p was attributed to a steric hindrance of the available active sites by filler particles, change in the catalyst concentration, and differences in monomer diffusion. Due to the changes in the polymerization kinetics, the in situ polymerization produces PP matrices having microstructure different from that of the homogenous polymerization.

^{13}C-NMR analysis showed that the *mmmm* (%) of the PP matrix decreased with increasing the quantity of MAO-filler in the polymerization. CRYSTAF analysis illustrated that the decrease in the *mmmm* (%) of the PP matrix was due to stereoerrors along the PP chains backbone. HT-GPC analysis showed that the homogeneous polymerization produces PP with Mw which is slightly higher than that of PP produced via in situ polymerizations. However, increasing the filler content has no effect on the Mw of produced PP matrix.

Comparing the in situ polymerizations using different filler types, it was evident that the type of the filler affects both the polymerization activity and the produced PP microstructure. For example it was shown that the in situ polymerization performed with SiO_2 nanoparticles yields an activity and PP

microstructure that is slightly different from that of the in situ polymerization performed with $CaCO_3$ nanoparticles.

TEM and SEM results showed that the filler dispersion in the PP matrix was improved in the in situ polymerized nanocomposites compared to that of melt-mixed nanocomposites.

In Chapter 5, the crystallization behaviour and the morphology of the various nanocomposites were investigated and compared. It was found that both fillers have a nucleating effect on the crystallization of PP. This effect was more pronounced for the in situ polymerized nanocomposites than the melt-mixed nanocomposites. It was also found that for the in situ prepared nanocomposite, the tacticity of the PP matrix plays the major role in determining the Xt while the Tc was more affected by the filler content.

The results of isothermal crystallization experiment show that at all crystallization temperatures, the crystallization rates of the in situ PP nanocomposites were higher than both pure PP and melt-mixed PP nanocomposite of the same filler load and matrix structure. XRD results show that the incorporation of nanofiller into low tacticity PP results in the dramatic enhancement of the formation of the γ-phase.

In Chapter 6 the relationships between synthesis-structure-morphology-properties for PP/filler nanocomposite were investigated. The results show that the modulus and its related properties, in the case of the in situ polymerized nanocomposites, were mainly determined by the PP matrix microstructure and in particular the tacticity, while in the case of melt-mixing, incorporation of inorganic filler into the PP matrix increase the modulus and its related properties. However, when samples with similar microstructures were used an improvement in the tensile modulus and in the hardness of the in situ polymerized sample compared to the melt-mixed sample was obtained.

The results also show that the tensile and impact strength were greatly improved for the in situ polymerized nanocomposites compared to the melt-mixed nanocomposites and this was attributed to improvement in both nanoparticle dispersion and interfacial adhesion. The results also reveal that

the Mw of the PP matrix is the main factor affecting the tensile and impact strength.

In Chapter 7, is shown that the filler type, size, and applied surface coating may influence the processability, and mechanical properties of filled polypropylene. The results show that coating the $CaCO_3$ filler with a fatty acid can bring about a good balance between the processability and mechanical properties. A homogenous dispersion of nanoparticles can be achieved by coating the nanoparticles with fatty acids. The improvement of the processability was a result of a lubricating effect of the fatty acid and the improvement of the mechanical properties was driven by the homogenous dispersion of nanoparticles in the PP matrix.

8.2 Suggestion for further investigation

Although the research objectives of this study were accomplished, a number of recommendations can be made. These recommendations can contribute to future research based on this work and lead to an increase in the commercial value of the project.

It has been shown in Chapter 4 that the presence of the fillers in the polymerization media alters the polymer microstructure, thus polymer with different microstructures and consequently new inherent properties could be obtained. The effect of the filler types, sizes, and amount on the properties of the formed polymer is well investigated.

This can be expanded to investigate the effect of the presence of the fillers in the polymerization media during the syntheses of various polyolefins and polyolefin copolymers. This includes the effect of the presence of fillers on the reactivity ratio of two monomers.

The effect of the nanofiller incorporation into low tacticity PP, enhancing the formation of the γ-phase, could also be investigated by optical analysis.

In Chapter 7 it is demonstrated that under similar compounding condition some fillers enhance the degradation of PP. The effect of the filler types, sizes and applied surface coating on the degradation of PP, under harsh compounding conditions needs to be investigated further.